Class-E Power Amplifiers in Modern RF Transmitters

Pavel Afanasyev

Department of Electronic Engineering

Maynooth University
Ireland

Supervisors of the Research: Dr John Dooley, Prof Ronan Farrell

Head of the Department: Prof Subhrakanti Dey

This dissertation is submitted for the degree of
Doctor of Philosophy

Maynooth University   February 2021

I would like to dedicate this thesis to the ones who motivated me through my life and my research.

Declaration

I have read and understood the Departmental policy on plagiarism.

I declare that this thesis is my own work and has not been submitted in any form for another degree or diploma at any university or other institution of tertiary education.

Information derived from the published or unpublished work of others has been acknowledged in the text and a list of references is given.

Signed:

_____

Pavel Afanasyev

Pavel Afanasyev

February 2021

Abstract

Power amplifiers have been playing a vital role in most wireless communication systems. In order to improve efficiency of wireless systems, advanced transmitter architectures, such as Doherty amplifiers, outphasing amplifiers, supply voltage modulation techniques are widely used. The goal of this work is to develop novel techniques for building load modulation transmitters based on class-E power amplifiers.

The first contribution is an analytical model for derivation load network parameters. The proposed model derives the parameters for both the peak and back-off power levels providing high efficiency. The proposed model demonstrates, that class-E PA with shunt capacitance and shunt filter is capable of providing high drain efficiency for back-off output power levels.

The second contribution is a design of a wideband class-E power amplifier (PA) with shunt capacitance and shunt filter. The broadband operation has been achieved by application of the double reactance compensation technique. Simulated and experimental results are presented. The performance of the fabricated PA is compared with existing wideband PAs.

The third contribution is application of the proposed technique to outphasing PA design. The designed outphasing PA was optimized, fabricated and tested. A possibility to extend the operational bandwidth of the PA is considered. Also the application of the proposed technique to Doherty PA design is demonstrated.

The fourth contribution is linearization of outphasing PA. Firstly, an analytical model describing the nonlinearity of nonisolated combiners under amplitude imbalance is presented. Secondly, a novel phase-only predistortion technique for class-E outphasing PAs is proposed. Thirdly, linearization of the fabricated outphasing

PA based on memory polynomial model is demonstrated using a 64QAM OFDM modulated signal with 20 MHz bandwidth.

Overall, this work provides novel techniques for load modulation transmitter design based on class-E power amplifiers with shunt capacitance and shunt filter.

Acknowledgements

Table of contents

List of figures

List of tables

Notations and Abbreviations

Throughout the thesis, matrices, vectors and scalar quantities are denoted by boldface uppercase, boldface lowercase and normal letters, respectively.

Notations

j	Unit imaginary number $\sqrt{-1}$
$(\cdot)^{\mathrm{T}}$	Transpose of a matrix
$(\cdot)^{\mathrm{H}}$	Conjugate transpose of a matrix
$(\cdot)^{*}$	Conjugate
$|\cdot|$	Absolute value operator

Acronyms / Abbreviations

3GPP	3rd Generation Partnership Project
4G	Fourth generation of wireless communication systems
5G	Fifth generation of wireless communication systems
ACLR	Adjacent Channel Leakage Ratio
ADC	Analogue-to-Digital Converter
AM	Amplitude Modulation
APSK	Amplitude and phase shift keying

BER   Bit Error Rate

BJT   Bipolar Junction Transistor

CPW   Coplanar Waveguides

DAC   Digital-to-Analogue Converter

dB   Decibels

DC   Direct Current

DE   Drain Efficiency

DPD   Digital Predistortion

EER   Envelope Elimination and Restoration

ET   Envelope Tracking

EVM   Error Vector Magnitude

FET   Field Effect Transistor

FPGA   Field-Programmable Gate

FR1   Frequency range 1 for 5G communications systems

FR2   Frequency range 2 for 5G communications systems

GaN   Gallium nitride

Gbps   Gigabits per second

GHz   Gigahertz

GMP   Generalized Memory Polynomials

HEMT   High Electron Mobility Transistor

IF   Intermediate Frequency

I	In-phase
ILA	Indirect Learning Algorithm
IoT	Internet-of-Things
ISI	Intersymbol interference
LDMOS	Laterally-Diffused Metal-Oxide Semiconductor
LINC	Linear amplification with Nonlinear Components
LNA	Low-Noise Amplifier
LO	Local Oscillator
LS	Least Square
LTE	Long Term Evolution
Mbps	Megabits per second
MHz	Megahertz
MIMO	Multiple Input Multiple Output
MP	Memory Polynomial
MSE	Mean Squared Error
NMSE	Normalized Mean Square Error
OFDM	Orthogonal Frequency Division Multiplexing
PAE	Power Added Efficiency
PA	Power Amplifier
PAPR	Peak to Average Power Ratio
QAM	Quadrature Amplitude Modulation

Q	Quadrature-phase
RFC	Radio Frequency Choke
RF	Radio Frequency
Rx	Receiver
SCS	Signal Components Separator
SMA	SubMiniature version A
SNR	Signal-to-Noise Ratio
SoC	System-on-Chip
TEM	Transverse Electro-Magnetic
TV	Television
Tx	Transmitter
VNA	Vector Network Analyzer
WCDMA	Wideband Code Division Multiplexing
ZVDS	Zero Voltage Derivative Switching
ZVS	Zero Voltage Switching

Chapter 1

Introduction

1.1 Motivation

Since the in the end of 19th century, wireless transmission technologies have transformed life immensely. The invention of radio telegraphy enabled the transatlantic transmission of information without long and expensive cables. Besides, the wireless transmitter systems provided maritime communication which was extremely important for rescue services. Nowadays, radio communication systems have numerous applications incluing voice and video communication, radio and TV broadcasting, internet access, emergency services, remote health-care systems, car-to-car communication, etc. With the development of the 5th generation of cellular communications (5G) and the internet-of-things (IoT) systems, the demand for wireless data transmission is going to further increase.

According to the 3rd Generation Partnership Project (3GPP) standalone specification, 5G systems must provide peak data rates of 20 Gbps for downlink and 10 Gbps for uplink, whereas the user expected data rate should be 100 Mbps and 50 Mbps for downlink and uplink respectively [1]. Besides, they should have low latency, high energy efficiency, improved spectral efficiency compared to 4G and capability to support a large number of connected devices. In order to cope with these requirements, a number of techniques have been proposed for 5G systems [2].

The first way to improve the general throughput is to use wider bandwidth. For this reason, several new bands have been allocated for 5G applications at two frequency ranges - Frequency Range 1 (FR1) (410 MHz - 7125 MHz) and Frequency Range 2 (FR2) (24.25 GHz - 52.6 GHz).

Another way of improving channel capacity is to use multiple-input-multiple-output technology (MIMO) [3]. Although multiple antenna transmitters have been widely used for LTE systems, very large MIMO arrays have been proposed for 5G standard [4]. Each base station uses a number of antennas much larger than the number of terminals. Using beamforming technology along with time- and frequency-division multiplexing enables to serve many terminals with relatively low transmitted power. Analog, fully digital and hybrid beamforming have been proposed [5]. The fully digital beamforming provides the highest level of flexibility and, therefore, the best performance. However, increasing the number of RF chains in very dense antenna arrays imposes additional challenges on the transmitter design.

1.2   RF transmitter architectures

A block-diagram of a typical RF transmitter is shown in Fig. 1.1. Information represented as a bitstream is modulated with one of the types of modulators. The outputs of the modulator are in-phase and quadrature components of the transmitted signal in the digital domain. These two components are transformed into the analogue domain with digital-to-analogue converters (DAC). The two components of the baseband signal are upconverted to an RF frequency with a local oscillator (LO) signal with 90° phase shift as shown in Fig. 1.1. In order to travel over a long distance the signal is amplified with the power amplifier (PA) before the transmitting antenna.

Different types of modulator can be used depending upon the application and the requirements to the system. High-order modulation schemes, such as quadrature amplitude modulator (QAM) or amplitude and phase shift keying (APSK) enable the transmission of high number of bits per symbol, which in turn increases the channel
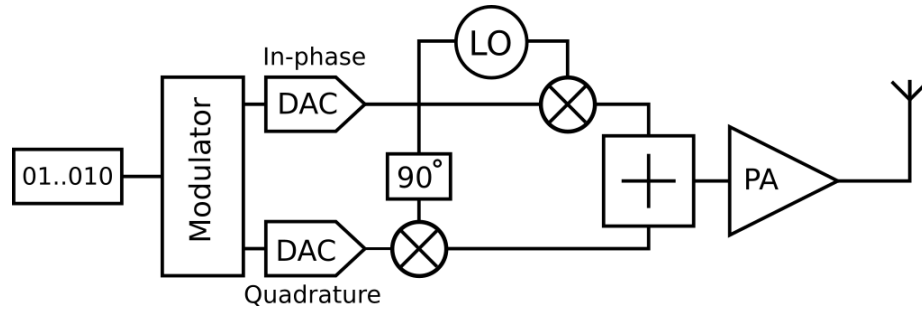
Fig. 1.1 Block-diagram of RF transmitter.
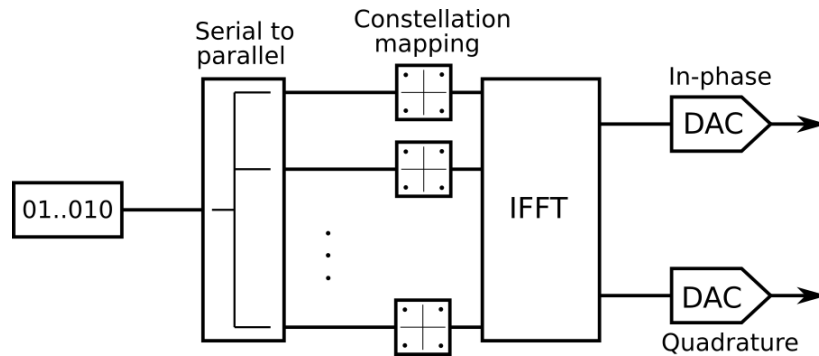
Fig. 1.2 Diagram of OFDM modulator.

capacity. In order to eliminate intersymbol interference (ISI), raised cosine filtering can be used, which widens the occupied bandwidth [6]. In orthogonal frequency-division multiplexing (OFDM) the binary data is split into several parallel streams as shown in Fig. 1.2. Each stream is modulated with a conventional constellation mapping scheme such as QAM or APSK. The modulated streams are transmitted at a number of orthogonal subcarriers. Since the bandwidth of each subcarrier is relatively small, the duration of each symbol is long which significantly reduces ISI caused by multipath propagation in wireless systems. Reduced ISI allows to simplify the equalization filters at the receiver side and achieve low bit error rate (BER) [7]. Due to aforementioned advantages, OFDM has been widely used for LTE and 5G systems [8].

A typical RF transmitter is designed to provide high spectrum efficiency, high energy efficiency and low signal distortion. As it will be discussed in the following chapters, the last two requirements are often in contradiction with each other. For most applications the required output power is much higher than a typical modulator

can provide and therefore, a PA is required. Any PA, regardless of the structure and type of the device, transforms the power of the direct current (DC) supply into the power of the output RF signal. Depending upon the operation point, the PA can provide either high efficiency or high linearity [9]. Switchmode PAs (e. g. class-D, class-E, class-F) provide the highest efficiency, however, they introduce significant nonlinear distortion. In order to provide both linearity and efficiency requirements several techniques have been proposed: outphasing PA [10], Doherty PA [11], envelope tracking [12]. However, since these types of PA introduce nonlinear distortion, digital predistortion (DPD) techniques are used in modern base station transmitters [13, 14].

1.3 Contribution

The work presented in this thesis focuses on theoretical analysis, design and practical implementation of load modulation techniques based on class-E PA. New solutions are proposed in both circuit design and linearization algorithms. The suggested solutions enable high efficiency wideband RF transmitters along with low level of nonlinear distortion.

The first contribution is the novel analysis of class-E PA with shunt capacitance and shunt filter for back-off power level. Since switchmode PAs are usually used as part of more complicated PAs, such as Doherty or outphasing, most of the time they operate under back-off power conditions. In these cases, the back-off operation is achieved by modulating the load presented to the transistors' outputs. It this thesis it is shown that the class-E PA with shunt capacitance and shunt filter can provide high drain efficiency for any back-off power level. Furthermore, it is shown that a necessary output power level can be provided by variation of the impedance of the output load, which is important for load modulation structures. The proposed solution provides a new method to calculate the value of the load that provides the highest drain efficiency for a specified back-off power level.

The second contribution is the design of wideband class-E power amplifier with shunt capacitance and shunt filter. It is shown that by applying the double reactance compensation technique it is possible to achieve broad band class-E operation. Compared to other wideband switchmode PA structures, the proposed PA has a very compact load circuit. The designed PA structure has been implemented and experimental results are presented.

The third contribution is the design of load modulation PA structures based on the class-E PA with shunt capacitance and shunt filter. Based on the proposed model the optimum impedance values for both peak and back-off output power were calculated. In order to build an outphasing PA, a Chireix combiner that provides the required values of peak and back-off impedance is designed. The designed outphasing PA was implemented and tested. Based on the same model a Doherty PA has been designed, where optimum peak and back-off impedance values are provided for carrier PA.

The fourth contribution is the linearization technique for outphasing PAs. Firstly, an ideal case when the two branches of the outpasing PA have the same magnitudes is studied. It is shown, that a simple memoryless predistortion technique can be applied in order to improve linear performance of the PA. Secondly, the nonlinear behaviour of the outphasing PA is studied. Finally, the application of the memory polynomial technique to the outpasing PA has been demonstrated.

1.4   Thesis Outline

This thesis is organized as follows: In Chapter II the operation of different classes of PAs is reviewed. In Chapter III the analysis of the class-E PA with shunt capacitance and shunt filter is presented. Special attention is paid to the load modulation properties of this type of the PA. Design examples are presented. The results from this chapter are published in the journal paper 1. In Chapter IV the wideband operation of the class-E PA with shunt capacitance and shunt filter using the double reactance compensation technique is demonstrated. The achieved

results are published in the conference paper 3. In Chapter V the application of the analytical technique described in Chapter III to the load modulation transmitter design is demonstrated. The design of outphasing and Doherty PA is demonstrated. The designed outphasing PA has been presented in the journal paper 1. In Chapter VI the analysis of nonlinearity of a Chireix combiner under amplitude imbalance is proposed. The results have been presented in conference paper 2. The linearization of the class-E outphasing PA is demonstrated. The memoryless phase+only digital predistortion technique has been presented in conference paper 1. The linearization of a GaN HEMT class-E PA has been presented in the conference paper 1. Finally, in Chapter VII conclusions and some prospects for the future work are outlined.

1.5 List of publications

The following publications are directly related to this thesis:

1.5.1 Peer-Reviewed Journal Papers

1. P. Afanasyev, A. Grebennikov, R. Farrell, J. Dooley, "Analysis and Design of Outphasing Transmitter Using Class-E Power Amplifiers with Shunt Capacitances and Shunt Filters", *Submitted to IEEE Access Journal.*

1.5.2 Conference publications

1. P. Afanasyev, P. Ramabadran, S. Mohammady, R. Farrell and J. Dooley, "Phase-Only Digital Predistortion Technique for Class-E Outphasing Power Amplifiers," 2019 *European Microwave Conference in Central Europe (EuMCE)*, Prague, Czech Republic, 2019, pp. 14-17.

2. P. Afanasyev, P. Ramabadran, R. Farrell and J. Dooley, "Nonlinearity Modeling of Chireix Outphasing Power Combiner Under Amplitude Imbalance," 2019 *17th IEEE International New Circuits and Systems Conference (NEWCAS)*, Munich, Germany, 2019, pp. 1-4.

3. P. Afanasyev, A. Grebennikov, R. Farrell and J. Dooley, "Broadband Operation of Class-E Power Amplifier with Shunt Filter," 2020 *18th IEEE International New Circuits and Systems Conference (NEWCAS)*, Montréal, QC, Canada, 2020, pp. 54-57.

Chapter 2

Power amplifier operation principles

Since the beginning power amplifiers have been an essential part of wireless communication systems that has huge impact on the transmitter performance. In this chapter general power amplifiers operation principles are presented. Firstly, the operation of the class-A,B,C power amplifiers is demonstrated. Secondly, switchmode PA classes (class-D,E,F) are reviewed. Finally, some existing efficiency enhancement techniques, such as Doherty PA, outphasing PA, envelope tracking transmitter, are explained. A special attention is given to the class-E PAs and their application to load modulation techniques.

2.1 Power amplifier classes of operation

Generally, all types of PAs are based on a nonlinear device that transforms the energy of a power supply into the energy of the output RF signal. The amplitude of the output RF signal (i_{out}) is manipulated by the small input signal (see Fig. 2.1(a)). Regardless of what type of the device is used (vacuum tube, BJT transistor, FET transistor), it has a minimum level of the input signal when the current starts flowing through the output circuit. In the case of FET transistor it is called the pinch-off voltage V_{p} as shown in Fig. 2.1(b). Therefore, in the simplest case the I-V curve of

(a)   **(b)**
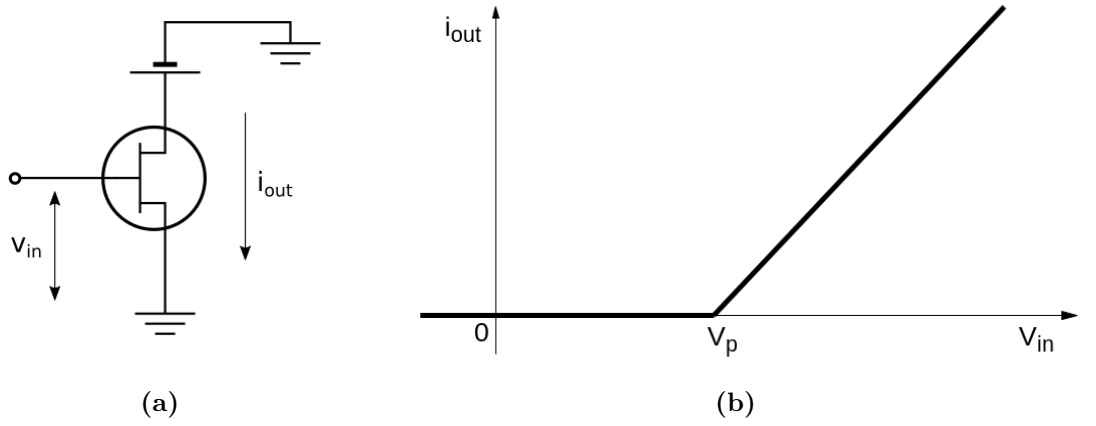
Fig. 2.1 Active device operation: (a) - nonlinear active device; (b) - I-V curve approximated by a piecewise-linear function.

such a device can be approximated with a piecewise-linear function [15]:

$$i_D = \begin{cases} 0, & v_{in} < V_p \\ g_m(v_{in} - V_p), & v_{in} \geq V_p \end{cases} \tag{2.1}$$

where v_{in} is the input voltage, i_D is the output current, g_m is the device transconductance. Let's assume that the input signal consists of bias voltage V_b and harmonic voltage with magnitude V_{in}:

$$v_{in} = V_b + V_{in} \cos \omega t \tag{2.2}$$

then the output current will be zero when the phase of the phase of the input signal takes on the value θ_0:

$$\cos \theta_0 = -\frac{V_b - V_p}{V_{in}} \tag{2.3}$$

Therefore, if the bias voltage $V_b > V_p - V_{in}$ then the output current will never reach the zero value, and the output current will be a pure harmonic oscillation with significant DC-component. Otherwise, the output current can be expressed as:

$$i_D = \begin{cases} 0, & -\theta \leq \omega t < \theta \\ I_q + I_a \cos \omega t, & \theta \leq \omega t < 2\pi - \theta \end{cases} \tag{2.4}$$

9
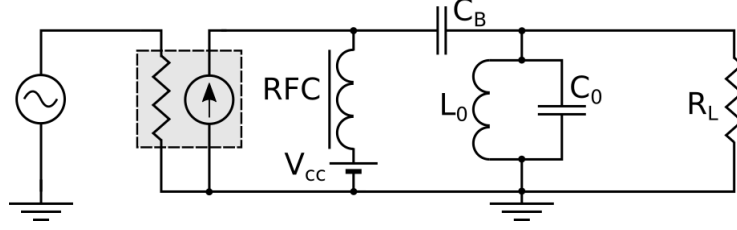
Fig. 2.2 General structure of power amplifier.

where I_q is the quiescent current and I_a is the magnitude of the output current. From (2.4) one can see that the output current of the active device is a periodic function and therefore, can be represented using Fourier-series expansion, as was demonstrated in [16, 17]:

$$i_D(\omega t) = I_0 + I_1 \cos \omega t + I_2 \cos 2\omega t + ... + I_n \cos n\omega t =$$
$$= I\Big(\gamma_0(\theta) + \gamma_1(\theta) \cos \omega t + \gamma_2(\theta) \cos 2\omega t + ... + \gamma_n(\theta) \cos n\omega t\Big) \tag{2.5}$$

where I is the magnitude coefficient, and $\gamma_n(\theta)$ are the coefficients of expansion of the output current waveform [18, 19].

The detailed analysis of the PA waveforms can be found in [19, 20]. Particularly, it is shown that the coefficients γ_0 and γ_1 can be found from the expressions [19]:

$$\gamma_0 = \frac{1}{\pi}\Big(\sin \theta - \theta \cos \theta\Big) \tag{2.6}$$

$$\gamma_1 = \frac{1}{\pi}\Big(\theta - \sin \theta \cos \theta\Big) \tag{2.7}$$

$$\gamma_n = \frac{1}{\pi}\left(\frac{\sin(n-1)\theta}{n(n-1)} - \frac{\sin(n+1)\theta}{n(n+1)}\right), \quad n \geq 2 \tag{2.8}$$

It order to analyze the properties of power amplifiers, we assume, that the load network consists of a DC-blocking capacitance, ideal shunt resonator L_0C_0 tuned to the fundamental frequency and an active load R_L (see Fig. 2.2). Drain supply voltage V_{cc} is supplied to the device through an ideal RF choke. The drain current will be defined by the expression (2.5). Since the shunt resonator provides short circuit conditions for all the harmonics, the current through the output load can be

expressed as:

$$i_{\text{out}} = \gamma_1(\theta) I \cos \omega t \tag{2.9}$$

At the same time the voltage across the active device is a sum of the DC supply voltage and fundamental voltage:

$$v_{\text{D}} = V_{\text{cc}} + \gamma_1(\theta) I R_{\text{L}} \cos \omega t \tag{2.10}$$

When the magnitude of the fundamental frequency reaches the point where $\gamma_1(\theta) I R_{\text{L}} = V_{\text{cc}}$, the drain voltage swings from 0 to $2V_{\text{cc}}$. In this case the device reaches saturation.

The DC power that the PA consumes, can be defined as:

$$P_{\text{DC}} = \gamma_0(\theta) V_{\text{cc}} I, \tag{2.11}$$

whereas the output power dissipated in the load is:

$$P_{\text{out}} = 0.5 \gamma_1^2(\theta) I^2 R_{\text{L}}. \tag{2.12}$$

Therefore, the drain efficiency is:

$$\eta = 0.5 \frac{\gamma_1}{\gamma_0} \cdot \frac{\gamma_1 I R_{\text{L}}}{V_{\text{cc}}} \tag{2.13}$$

From the last expression one can see, that the drain efficiency of the PA is maximized if the active device is driven into saturation. The saturation is achieved when the following expression is fulfilled:

$$R_{\text{L}} = \frac{V_{\text{cc}}^2}{2P_{\text{out}}} \tag{2.14}$$

As it is demonstrated, the power generated at each harmonic depends on the conduction angle θ. In order to achieve the maximum power at the n-th harmonic, the conduction angle of $\theta = \pi/n$ must be provided. Therefore, the ratio of the
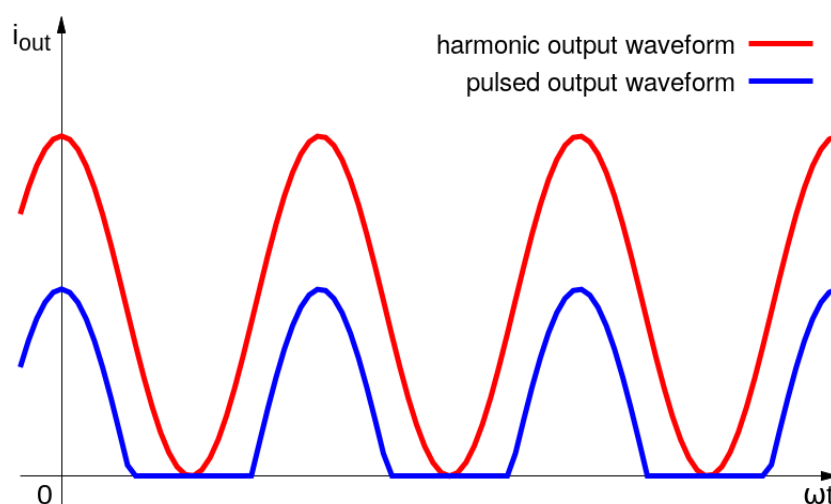
Fig. 2.3 Output current waveforms for different conduction angle values.

fundamental harmonic amplitude to the DC component amplitude can be tuned by the variation of the conduction angle.

The possibility to manipulate the PA operation by tuning the bias voltage was experimentally studied in [21, 22]. It was shown, that for a pure sinusoidal input signal it is possible to achieve a pure sinusoidal output current by adjusting the voltage at the grid of the vacuum tube. However, in this case the current in the anode-to-cathode circuit will have significant DC component, and the anode efficiency cannot exceed 50%. The efficiency of the PA can be significantly improved by reducing the output DC current, however, the anode-to-cathode current will have a pulsed shape, as shown in Fig. 2.3, and consequently contain high-order harmonics. It was also shown, that at a certain level of grid voltage the conduction angle reduces to zero, and the anode efficiency approaches 100% [22].

Initially, the PAs were classified according to the level of distortion caused either by tube nonlinear characteristic or by the pulse shaped anode-to-cathode current [9]. Since the 1930s the PAs are usually classified according to the conduction angle 2θ into following classes:

- **Class A**: $2\theta = 360°$

- **Class AB**: $180° < 2\theta < 360°$

- **Class B**: $2\theta = 180°$

- **Class C**: $2\theta < 180°$

The theoretical limit for drain efficiency for class-A PAs is 50% whereas drain efficiency of a class-B PA cannot exceed 78.5%. Recently it has been shown the efficiency of the class-B can be improved by adding a parallel capacitance to the load network along with complex load. This type of operation is referred to as class-J PA [23–25]. As it was demonstrated, if a certain complex load impedance is provided for the first and second harmonics, the voltage and current waveforms can be shaped as half-sinusoid waves with minimum overlap in the time domain. However, compared to switchmode PAs, the class-J PA provides higher level of linearity [24].

The choice of the type of operation depends on requirements to the PA. The bigger values of the conduction angle demonstrate lower level of nonlinear distortion at the cost of drain efficiency. At the same time, reducing the conduction angle improves the drain efficiency, however, it reduces the amplitude of the fundamental harmonic of the output current, which in turn reduces gain and power added efficiency (PAE).

2.2 Switchmode power amplifiers

As it was shown in Section 2.1, the drain efficiency of a PA can be significantly improved by reducing the conduction angle. In the extreme case the conduction angle is minimized and the PA device (either a vacuum tube or a transistor) switches between the saturation and cutoff points. In the saturation state the switch is turned on and its resistance is zero, whereas in the cutoff state the switch is off and has infinitely large resistance. In this section several classes of the switchmode PAs are considered: class-D, class-F and class-E.

2.2.1 Class-D power amplifiers

The class-D PA was initially proposed in [26] as a way to efficiently convert DC energy to AC energy. Since then this type of PA has been widely used for numerous
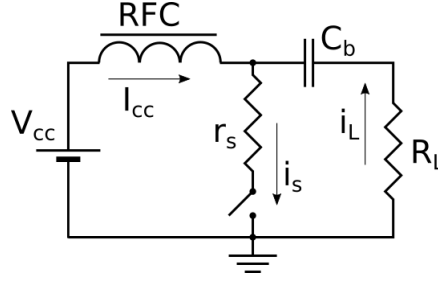
Fig. 2.4   Ideal model of a class-D PA.

applications, such as dc-dc converters, fluorescent lamps, induction welding, soldering, wireless transmitters, etc. The main advantage of using class-D PAs for RF applications is high drain efficiency compared to class-B,C PAs, due to the switch operation of the PA devices. Depending upon the type of the DC power supply, two main groups of the class-D PA can be distinguished: voltage-switching class-D PA and current-switching class-D PA. In the former case the drain (collector, anode) of the device is fed by a voltage source and in the latter case it is fed by a current source usually made by series connection of a voltage source and an RF choke.

The operation principle of the class-D PA can be demonstrated using a simplified model shown in Fig. 2.4. The transistor is represented as an ideal switch with saturation resistance r_s. The DC current is supplied from a voltage source V_cc via an RF choke RFC. The output circuit consists of an active output load R_L connected to the device via a DC block capacitor C_b. It is assumed that the input of the PA is fed by a square-wave signal with 50% duty ratio. Therefore, the operation of the PA can be described separately in two state: when the switch is closed ($0 \leq \omega t < \pi$) and when the switch is open ($\pi \leq \omega t < 2\pi$).

When the switch is turned on, the circuit can be described by Kirchoff's law in the time domain:

$$i_\mathrm{s}(\omega t) = i_\mathrm{L}(\omega t) + I_\mathrm{cc} \tag{2.15}$$

$$V_\mathrm{cc} = i_\mathrm{L}(\omega t)R_\mathrm{L} + i_\mathrm{s}(\omega t)r_\mathrm{s} \tag{2.16}$$

Here it is assumed that the DC-block capacitor C_b has an infinite capacitance and therefore immediately charges to the voltage V_{cc}. Solving the system of two equations (2.15) and (2.16) an expression for the switch current can be derived:

$$i_s(\omega t) = \frac{V_{cc} + I_{cc}R_L}{R_L + r} \tag{2.17}$$

When the switch is turned on, the current does not flow through it. Therefore, the drain current can be expressed as follows:

$$i_s = \begin{cases} 0, & 0 \le \omega t < \pi \\ \frac{V_{cc} + I_{cc}R_L}{R_L + r}, & \pi \le \omega t < 2\pi \end{cases} \tag{2.18}$$

From (2.18) it follows that the drain current in the time domain will have square shape, as shown in Fig. 2.5(a), and therefore it has an infinite number of harmonics. The first two terms of the Fourier expansion can be expressed as [19]:

$$I_0 = I_{cc} = \frac{1}{2\pi} \int_0^\pi i(\omega t)d(\omega t) = \frac{V_{cc}}{R_L + 2r_s} \tag{2.19}$$

$$I_1 = \frac{1}{\pi} \int_0^\pi i_s(\omega t) \sin \omega t d\omega t = \frac{4I_0}{\pi} \tag{2.20}$$

The power delivered to the load at the fundamental frequency will be:

$$P_1 = \frac{1}{2} I_1^2 R_L = \frac{8}{\pi^2} \frac{R_L V_{cc}^2}{(R_L + 2r_s)^2} \tag{2.21}$$

The drain efficiency can be found as:

$$\eta = \frac{P_0}{I_0 V_{cc}} = \frac{8R_L}{\pi^2(R_L + 2r_s)} \tag{2.22}$$

In the ideal case, when $r_s = 0$, the drain efficiency of the class-D PA would be $\eta = 81\%$. This means that in the case of square wave drain current 19% of the DC power supply energy is spent for higher harmonics.
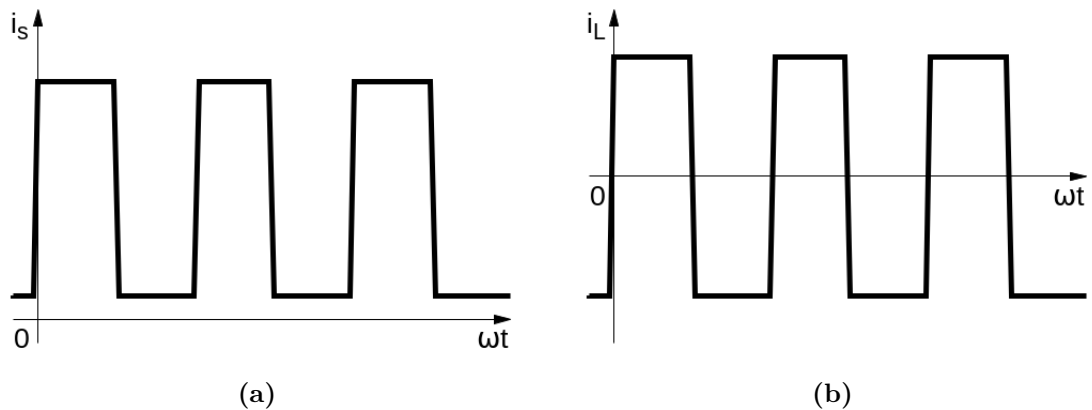
Fig. 2.5 Waveforms of a class-F PA: (a) - drain current; (b) - output current.

Usually class-D PAs consist of two devices operate in push-pull mode. Both devices are driven by the same source with duty cycle of 50% or less in order to prevent overlapping of drain current. The main advantage of the class-D PA is its low voltage across drain-source transition, which makes them an attractive choice for system-on-chip (SoC) applications. However, as it has been shown earlier, this type of PA has efficiency losses due to generation of high harmonics.

2.2.2 Class-F power amplifiers

The general structure of the class-F PA is shown in Fig. 2.6. It consists of an active device (vacuum tube, BJT or FET), drain voltage supply V_{cc} connected via RF choke, and an active load R_L connected to the output of the device via a band-pass filter BPF. As it was shown in [27, 28] if the drain voltage waveform of a class-B PA is flattened it is possible to significantly improve the output power without increasing the DC power consumption, and therefore, improve the efficiency of the PA. If the voltage waveform has a square shape, as shown in Fig. 2.7(a), the drain efficiency will approach 100%. In [28] this operation mode was referred to as *the optimum efficiency case* class-B PA. Drain current in this case will have the shape of a half-sinusoidal waveform (see Fig. 2.7(b)).

Since the square shaped waveform consists of an infinite number of harmonics, the BPF has to filter out the harmonics and provide only the fundamental frequency
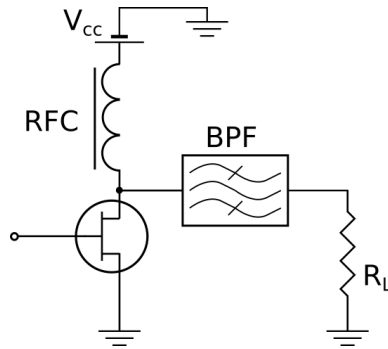
Fig. 2.6 The general structure of the class-F PA.

at the output load. For the ideal operation the BPF must provide short circuit input impedance at the even harmonics, open circuit impedance at the odd harmonics and active impedance R_{L} at the fundamental frequency (see Fig. 2.8(a)). The higher number of harmonics provided, the closer the waveforms will be to the ideal shape, and therefore, the higher efficiency can be achieved. However, it is extremely difficult to provide the ideal harmonics suppression using lumped component resonators or transmission line resonators. The possibility to maximize the flatness of the drain voltage and drain current waveforms using a finite number of resonators was analyzed in [29]. It was demonstrated, that providing the required conditions for the second and third harmonics results in drain efficiency of 75%, which is close to the class-B PA. Providing additional conditions for five voltage harmonic components increases the efficiency to 83.3%.

Further improvement of the drain efficiency can be achieved by minimizing the downward excursion of the waveform [30]. By adjusting harmonic amplitudes in this way it is possible to minimize the DC power consumption of the PA while maintaining the same level of the output power at the fundamental frequency. It should be noted that the maximum output power and the maximum efficiency can be achieved with the same set of coefficients [30].

High efficiency of a PA shown in Fig. 2.6 can also be achieved if the band-pass filter provides open circuit condition for even harmonics and short circuit conditions for odd harmonics. In this case the drain voltage in the time domain will have half-sinusoidal shape, and the drain current will be a square wave. This type of PA
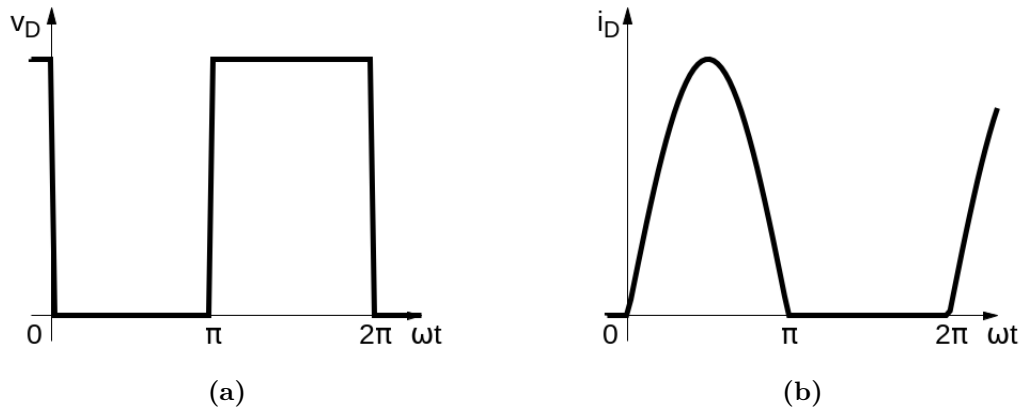
Fig. 2.7 Waveforms of a class-F PA: (a) - drain voltage; (b) - drain current.
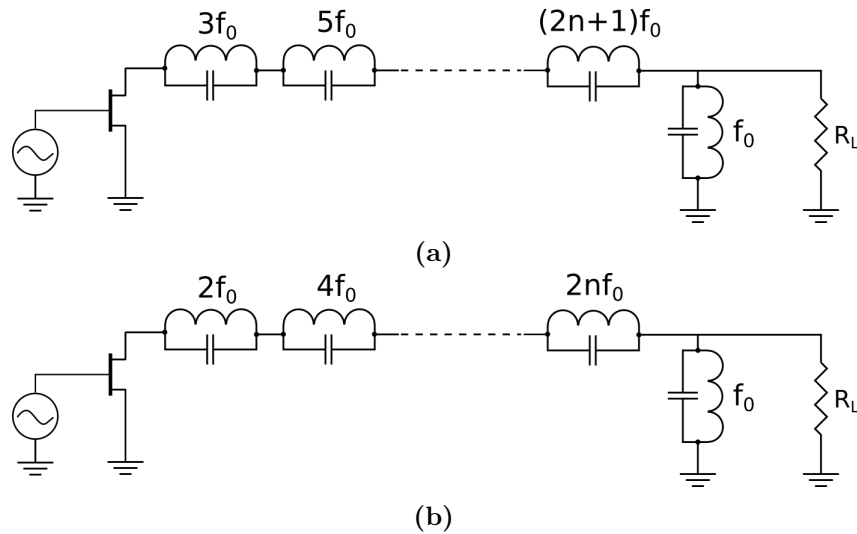
Fig. 2.8 Load circuit of PA: (a) - class-F PA; (b) - inverse class-F PA.

operation is referred to as inverse class-F PA. The load consists of a finite number of series resonators tuned to the even harmonics (see Fig. 2.8(b)).

At high frequencies the implementation of load network and RF choke with lumped components is difficult and therefore transmission line implementation is widely used. The design of a distributed circuit is based on Richard's transformation which establishes the equivalence between lumped circuit elements and transmission line sections [31]. As a result of this transformation, the capacitances can be represents as open-circuited stubs and the inductances as short-circuited stubs with electrical length of 45°. The achieved impedance and electrical length values can

then be optimized in order to provide the required load impedance at the specified frequencies.

Since all resonant circuits (implemented with either lumped components or transmission line) provide ideal load at one frequency only, several techniques have been proposed in order to address limited bandwidth issue. A load network with low loaded Q-factor has been proposed [32]. This load provides a quasi-optimal class-F operation at the fundamental frequency and second harmonic. As a result, relative bandwidth of 45% (575 MHz - 915 MHz) was achieved. Another way of improving the bandwidth of is called continuous class-F [33, 34]. In this type of PA the bandwidth enchancement is provided by means of stabilizing the load impedances for the second and third harmonics across the frequency band. A class-F PA demonstrating over 61% power added efficiency across the fractional bandwidth of over 20% (2.15 - 2.65 GHz) was presented in [34].

2.2.3 Class-E power amplifiers

As it has been shown in the previous sections, the drain efficiency of a PA can be significantly improved by driving a device in a switchmode and eliminating the overlapping of the drain current and drain voltage waveforms. In the class-F mode this is achieved by forming a square drain voltage waveform in the time domain. In the middle of the 20th century it was shown that high efficiency can also be achieved by forming an asymmetric anode waveforms for tube PAs. For example, in [35] anode efficency of 92% was achieved by simply tuning the load resonator to a higher frequency. In this case the anode load circuit had an inductive impedance and, therefore, caused a phase shift between the output voltage and the fundamental voltage at the anode.

In [36] a PA was demonstrated that exceeded the efficiency of a class-C PA by adding a shunt capacitor to the load network along with a series LC-resonator. The achieved class of operation was later called the class-E PA [37]. The ideal class-E PA can be defined as an amplifier with an active device operating as an ideal switch
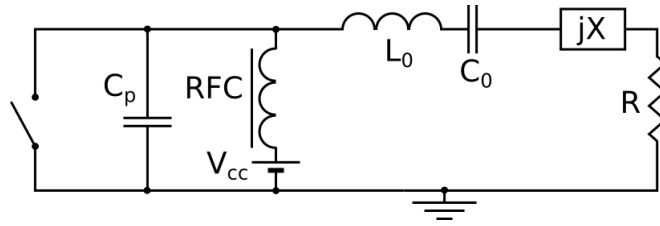
Fig. 2.9 General structure of the class-E PA.

and load network which fulfils three conditions: 1) there is no voltage drop across the switch when the switch is on, 2) the voltage across the switch reaches the zero value at the moment when the switch turns on, 3) the slope of the voltage reaches the zero value at the moment when the switch turns on. The last two conditions are referred as zero voltage switching (ZVS) and zero voltage derivative switching (ZVDS) conditions respectively.

A detailed theoretical analysis of the class-E PA was presented in [38]. The operation can be demonstrated on a simple model shown in Fig. 2.9. The transistor is represented as an ideal switch, the load network consists of a shunt capacitor C_{p}, series filter L_0C_0 and a load $R + jX$. The active device is fed from a DC voltage source via infinitely large inductance RFC. In the model the following assumptions are made:

1. The switch has zero resistance when it is turned on and infinite resistance when it is off.

2. All the lumped components of the circuit are linear.

3. All the components except the active load are lossless.

4. The load resonator is tuned to the fundamental and has infinite Q-factor.

5. The input signal is a squre wave with 50% duty cycle.

Without loss of generality, one can assume that the switch is on at the time $0 \leq \omega t < \pi$ and the switch is off at the time $\pi \leq \omega t < 2\pi$, where $\omega = 2\pi f_{\mathrm{c}}$ is the operating angular frequency. Hence, the ZVS and ZVDS conditions can be
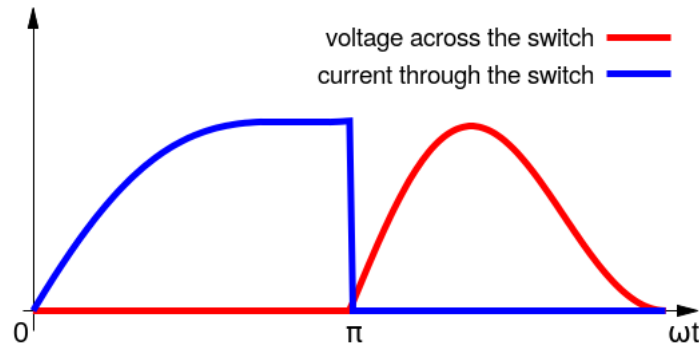
Fig. 2.10   Voltage and current waveforms of an ideal class-E PA.
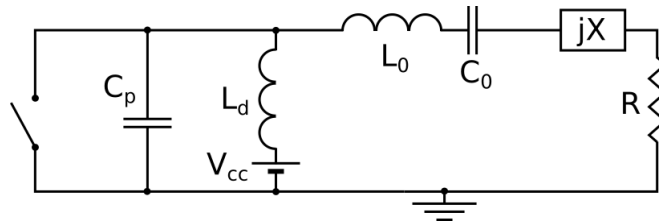
Fig. 2.11   Class-E PA with finite DC-feed inductance.

mathematically expressed as:

$$v(\omega t)\Big|_{\omega t=2\pi} = 0 \tag{2.23}$$

$$\frac{dv(\omega t)}{d\omega t}\bigg|_{\omega=2\pi} = 0 \tag{2.24}$$

where $v(\omega t)$ is instantaneous value of the voltage across the switch. The behaviour of the switch voltage in time domain can be described by a first-order differential equation. The solution of this equation gives the optimum values for C_{p} and X depending upon the required output power and drain supply voltage V_{cc}. Typical voltage and current waveforms are shown in Fig. 2.10. However, the ideal class-E operation can be achieved only for one frequency and for 50% duty cycle input signal, which is called *optimum class-E*. If the central frequency and duty cycle deviate, the PA is referred to as *suboptimal class-E* [38].

Although the load network with RF choke and shunt capacitor can provide the ideal class-E operation, it requires a large inductance connected to the DC power supply, which makes the circuit bulky. However, the class-E operation can also
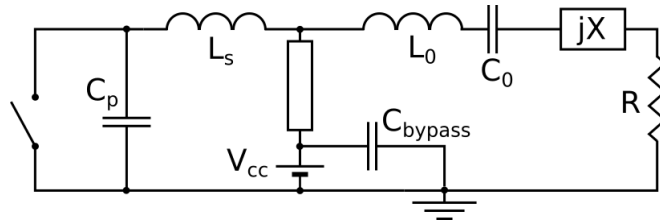
Fig. 2.12 Class-E PA with finite quarterwave transmission line.

be achieved with a load network consisting of one finite inductance and one shunt capacitance [39–41]. The general structure of such a PA is shown in Fig. 2.11. Unlike the class-E PA with an RF choke, the load network contains an inductance L_d connected in parallel with the shunt capacitance C_p. The load is connected to the device through a resonator $L_0 C_0$ which has sufficiently high loaded Q-factor. In this case, the voltage across the switch in the time domain is described by a second-order differential equation which has an infinite number of solutions. Consequently, for the given values of output power, drain supply voltage and carrier frequency there is an infinite number of combinations of L_d, C_p and complex load $Z = R + jX$ that provide the ideal class-E operation. In order to separate a particular solution, an additional parameter can be defined as:

$$q = \frac{1}{\omega \sqrt{L_d C_p}} \tag{2.25}$$

where $\omega = 2\pi f_c$ is angular carrier frequency. As it was demonstrated in [42], the arbitrary chosen parameter q along with input design parameters uniquely defines the circuit components C_p, and L_d and complex load Z. The possibility to choose an arbitrary value of q gives an additional flexibility to a designer when it is necessary to take into account parasitic reactance of a transistor. It also enables the manipulation of load modulation properties of a PA, which can be used in high efficiency PA structures, such as outphasing or Doherty PA [43, 44].

At RF frequencies the infinite inductance in Fig. 2.9 can be replaced with a quarterwave transmission line. In this case the device parasitics can be taken into account by including an additional inductance L_s, as shown in Fig. 2.12. The switch
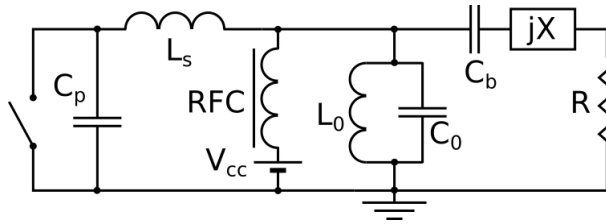
Fig. 2.13 Class-E PA with shunt capacitance and shunt filter.

voltage and current waveforms can be found from solving a second-order differential equation in the time domain. The parameter $q = (\omega\sqrt{L_s C_p})^{-1}$ defines a particular solution from an infinite number of solutions and allows one to take into account device parasitic capacitance and bondwire induction. The load network parameters L_s, C_p and $Z = R + jX$ can be derived from the procedure outlined in [19]. The optimal load Z can be matched with the required output impedance using either a single section of a transmission line or an L-shaped section. In the latter case an additional suppression of the third harmonic can be provided which improves the overall efficiency of the PA.

The possibility to achieve high efficiency when the zero switching conditions are provided for switch current and current slope was demonstrated in [45]. This type of operation was later referred to as inverse class-E PA. The switch voltage and current waveforms are provided by an L-shaped circuit implemented as a high-pass filter (a series capacitance and a parallel inductance), and the harmonics are filtered with a series band-pass filter. In [46] the same PA operation was achieved using a low-pass filter shaping circuit (a series inductance and a parallel capacitance) with a parallel filter, which provides short circuit conditions for all harmonics.

The load network of a class-E PA with shunt capacitance and shunt filter was presented in [15]. In this case the voltage waveforms fulfilling the ZVS and ZVDS conditions are provided by a load network containing a parallel capacitance C_p and a series inductance L_s, as shown in Fig. 2.13, and the harmonics are suppressed by a shunt resonator $L_0 C_0$. The detailed analysis of this type of PA was presented in [47]. As it was shown, the ideal class-E operation can be provided for any value of the shunt capacitance C_p which allows a designer to incorporate device capacitance into the

23

load network. The more detailed analysis of the class-E PA with shunt capacitance and shunt filter along with its properties will be presented in the following chapters.

Due to their high efficiency, compact output load network size and ability to operate at wide range of output power levels, class-E amplifiers are widely used in modern transmitters. Besides, due to the load network configuration, the parasitic reactances of an active device can be incorporated into the output circuit. Typically, at RF frequencies the output capacitance of a transistor acts as the shunt capacitance C_p forming the class-E voltage and current waveforms. More information about history of the class-E PA, modern trends and design techniques can be found in [19, 48, 49].

2.3 Outphasing power amplifiers

Although all the single-ended PAs can amplify RF signals, they can provide either high linearity or high efficiency. For example, class-A PAs are capable of providing a very high linearity but the efficiency of this type of PA is less than 50%, since there is power dissipation at the active device at all times. Switchmode PAs, such as class-F and class-E provide very high efficiency, however, the ideal operation can be achieved at a certain level of output power and therefore, these types of PA introduce a significant nonlinear distortion into the transmitted signal.

In order to overcome this issue a technique called outphasing modulation was proposed in [10]. In this work the overall efficiency of an RF transmitter was improved by splitting a transmitted amplitude modulated signal into two phase modulated signals using a signal component separator (SCS), as shown in Fig. 2.14. The phase modulated signals have constant magnitude and can be amplified with high efficiency without any nonlinear distortion. After amplification these two signals can be added together with the output combiner in order to achieve an amplified replica of the input amplitude and phase modulated signal $S_\mathrm{in}(t)$, as shown in Fig. 2.14. The same technique was later reintroduced by Cox in [50] where it was called linear amplification with nonlinear components (LINC).
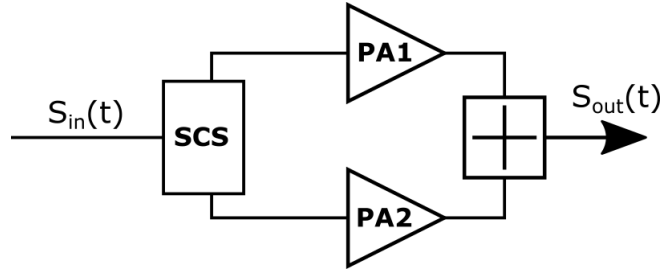
Fig. 2.14 A block-diagram of the outphasing transmitter.
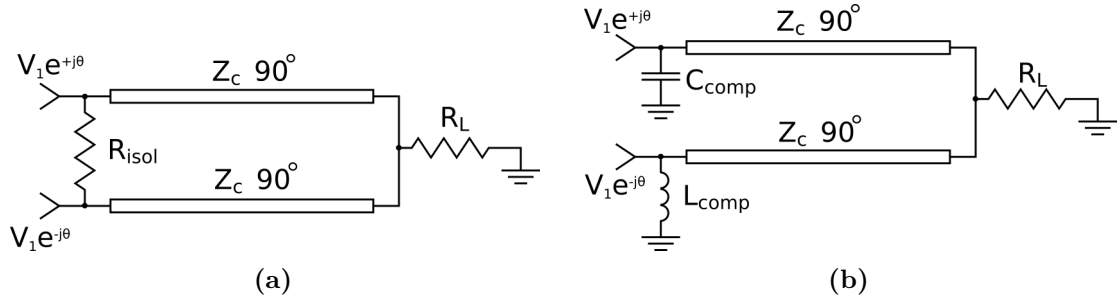
Fig. 2.15 Outphasing combiners (a) - Wilkinson isolated combiner; (b) - Chireix non-isolated combiner.

Different types of output combiners have been used in outphasing transmitters. All off these types can be categorized into three general classes: isolated combiners [51, 52], non-isolated combiners [43, 44, 53–57], and partially isolated combiners [58]. Isolated combiners contain resistive elements that isolate branch PA outputs from each other, as shown in Fig 2.15(a). Therefore, each branch PA sees a constant load impedance and very high linearity can be provided. However, as it was shown in [59], the instantaneous efficiency of isolated combiners depends on the outphasing angle value as:

$$\eta_{\text{inst}} = \cos^2 \theta \tag{2.26}$$

The average efficiency defined by expression

$$\eta_{\text{avg}} = \int_0^{\pi/2} \eta_{\text{inst}} p(\theta) d\theta \tag{2.27}$$

where $\mathbf{p}(\theta)$ is the probability density function of the transmitted signal. The higher the peak-to-average power ration (PAPR) of a signal, the more often the outphasing

angle takes on values close to 90° and, therefore, the lower the average efficiency of the isolated combiner.

Nonisolated combiners do not contain lossy elements and, therefore, provide higher efficiency. The general structure of a Chireix combiner is shown in Fig. 2.15(b). Two inputs are connected to an output load R_{L} through quarterwave transmission lines with characteristic impedance Z_{c}. The input impedance of nonisolated combiners depends on the outphasing angle and therefore on the level of input signal. For two signals with the same magnitude and opposite phases the input impedance will be two complex conjugate values. The reactive components L_{comp} and C_{comp} are chosen in order to provide purely active load impedance for peak and back-off output power. This load modulation can significantly improve the average efficiency of the transmitter. However, since these combiners introduce significant nonlinear distortion, digital predistortion (DPD) techniques should be used for these transmitters [60–62]. Partially isolated combiners provide trade-off between nonlinear distortion and linearity and are capable of improving the bandwidth performance of an outphasing transmitter [58].

Generally, any type of amplifiers can be used as branch amplifiers in outphasing transmitters. Up to the present time, outphasing transmitters based on class-A,B [10, 54], class-AB [58], class-D [61, 63], class-F [62, 64, 65], class-E [43, 44, 53, 55, 56]. However, since the branch PAs amplify signals with constant magnitude, the switchmode amplifiers provide better efficiency improvement. Besides, the branch PA load impedance provided by nonisolated Chireix combiners depends on outphasing angle, and therefore, on the level of the input signal. Consequently, in order to amplify amplitude modulated signals with high efficiency, the branch PAs have to maintain high efficiency across a wide range of load impedance values.

Due to their potential to provide very high drain efficiency across wide range of output power, the outphasing PA has drawn attention of researchers and engineers. However, there are some significant design challenges concerned with this type of load modulation technique. Firstly, the separation of an amplitude and phase modulated signal into two constant magnitude phase modulated signals causes

significant spectrum regrowth. Therefore, each phase modulated signal has bandwidth 8-10 times wider than the bandwidth of the original signal before the SCS, which causes additional nonlinear distortion. For this reason, the instantaneous bandwidth of outphasing PAs is limited. Secondly, since the amplitude of the input signals is constant and does not depend on the amplitude of the transmitted signal, outphasing PAs demonstrate low gain for low output power. Therefore, outphasing PAs provide relatively low instantaneous power added efficiency PAE for low output power levels, and low average PAE for signals with high PAPR. However, this drawback can be overcome by introducing amplitude modulation into the input signals and drain voltage supply modulation [66, 67].

2.4 Doherty power amplifiers

Doherty PA was proposed by William Doherty in 1936 as an alternative approach to improve the overall efficiency of radio transmitters operating with amplitude modulated signals [11]. The proposed technique was initially demonstrated on a 50 kW transmitter for a transatlantic radiotelephony station. By means of the described novel load modulation technique, the overall efficiency of 60% was achieved along with a very low level of nonlinear distortion - a few per cent depending upon the frequency range. This efficiency improvement enabled a reduction of the overall power consumption of the transmitter two times compared with a traditional single-tube amplifier that would provide the same level of linearity.

The operation principle of the Doherty PA can be described using a simple model shown in Fig. 2.16(a). The two transistors are modelled as ideal voltage-controlled current sources with different bias and output currents I_1 and I_2. If these two current sources are connected directly to an active load, the load impedance that each source
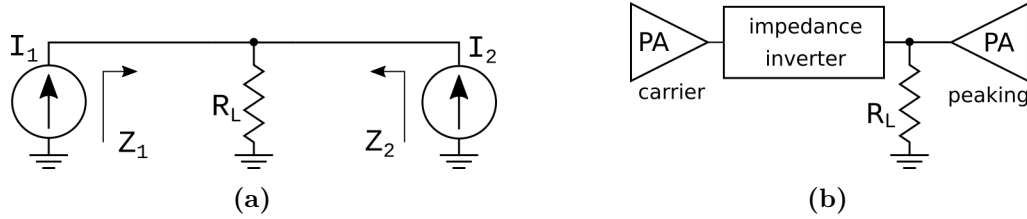
Fig. 2.16 Doherty PA model (a) - model at the active load; (b) - current sources with impedance transformer.

sees will depend on the output current of the other source:

$$Z_1 = R_L\left(1 + \frac{I_2}{I_1}\right) \tag{2.28}$$

$$Z_2 = R_L\left(1 + \frac{I_1}{I_2}\right) \tag{2.29}$$

Therefore, the output current of each current source depends only on the input voltage, whereas the power generated by each of the sources into the load depends on the current of the other source.

When the level of the input signal is low, the peaking amplifier does not generate any output current, and the carrier amplifier sees the impedance R_L. Since the carrier PA operates as an ideal current source, the output current rises linearly up to the transition point where the carrier PA reaches the saturation. Once the transition point is passed, the peaking PA starts generating output current I_2 and, according to (2.28), increases the impedance seen from the carrier PA. In order to reduce the power generated by the carrier PA to the load, an impedance inverter is added, as shown in Fig. 2.16(b). Because of the impedance variation in the time domain, the carrier amplifier remains in the more efficient saturation mode, whereas the power generated by the peaking PA increases. If the current of the peaking PA increases twice as fast as the current of the carrier PA, at the peak value of the input signal they both generate the same peak power.

A Doherty PA at microwave frequencies was presented in [68]. A typical structure of a microwave Doherty PA implemented with transmission lines is shown in Fig. 2.17. The load Z_0 is transformed to an intermediate imoedance $0.5Z_0$ using a quarterwave
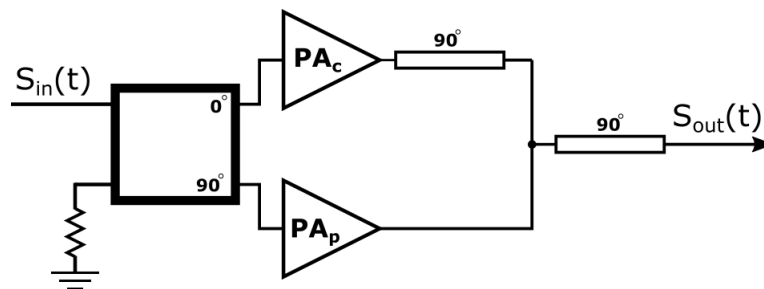
Fig. 2.17 Block-diagram of the Doherty PA implemented using transmission lines.

line with characteristic impedance $0.71Z_0$. At the peak output power the load impedance for both peaking and carrier PAs is Z_0. At the back-off power level -6 dB, when the peaking PA is off, the carrier sees the load impedance $2Z_0$, which is provided by the load $0.5Z_0$ along with the impedance transformer implemented with a quarterwave transmission line with characteristic impedance Z_0. Since the impedance transformer line in the load circuit of the carrier amplifier causes a phase delay of 90°, the input signal is split into two parts with 90° compensation offset. This signal separation is usually done using either a Wilkinson combiner with delay transmission line, or with a 90° hyprid power divider. Since the carrier PA operates in the saturation mode, the Doherty PA maintains the high efficiency for output power levels between the peak power and -6 dB back-off power.

Due to the ability to amplify signals with high PAPR with high efficiency, Doherty PAs have been drawing the attention of researchers. Some modifications of Doherty PA have been proposed targeting an extended back-off power level [69–71], improved bandwidth [72–75]. Some works are targeting the overall efficiency improvement by using class-F amplifiers [76–78] and class-E amplifiers [73, 79].

In the digital Doherty PA configuration the input signal is split digitally and fed to the carrier and peaking amplifiers separetly [80–83]. This approach enables some performance improvement by means of adaptive phase alignment in the digital domain, which compensates the phase impairment between the two paths when the peaking amplifier is turned on. Besides, since the signal separation is performed digitally, digital Doherty PA does not suffer from phase delay caused by impedance mismatch. Usually, the digital block also performs DPD in order to achieve the

required level of the output signal linearity. However, linearization of the PA can be also implemented on the circuit level implementing overdrive voltage control and multiphase RF-clocking [83].

2.5 Envelope elimination and restoration

The envelope elimination and restoration technique (EER) was initially proposed in [84] as a way of improving the efficiency of RF transmitters operating with single sideband modulated signals. Since this type of signal conveyed the information in both amplitde and phase variation, it required more advanced techniques to achieve high efficiency compared to AM transmitters. In an EER transmitter the original amplitude and phase modulated signal

$$v(t) = V(t) \cos\left(\omega t + \varphi(t)\right) \tag{2.30}$$

is split into two parts and supplied to an envelope detector and an RF limiter (see Fig. 2.18). The RF limiter eliminates the amplitude variation $V(t)$ from the transmitted signal and produces a phase modulated signal with constant amplitude, which is fed to the input of a switchmode PA:

$$v_{\mathrm{pm}}(t) = V_{\mathrm{c}} \cos\left(\omega t + \varphi(t)\right). \tag{2.31}$$

The envelope detector extracts the amplitude variation of the transmitted signal, which is then amplified with a low frequency amplifier and used to modulate the drain supply voltage of the transmitter PA. Since for switchmode PAs the output power is proportional to the drain voltage, the PA with a modulated drain supply restores the original amplitude and phase modulated signal.

As well as in the outphasing transmitters, in the EER systems the PA amplifies a signal with a constant envelope which allows the use of high-efficient switchmode PAs, such as class-E [85] or class-F [86]. Compared to the load-modulation techniques
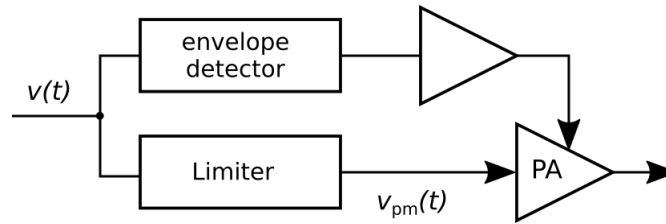
Fig. 2.18 The structure of an envelope elimination and restoration transmitter.

presented in the previous sections, the EER provides higher efficiency across a wide range of output power levels and higher linearity of the output signal [87]. However, the implementation of this transmitter is challenging. Firstly, there is a potential phase mismatch between the phase-modulated signal and the low frequency envelope signal, which causes an intermodulation distortion of the output signal. Secondly, the RF limiter introduces some phase distortion to a phase-modulated signal, which can significant at high frequencies. Thirdly, since the signals supplied to the device input is constant envelope, the low level of the output signal is provided by a low level of the drain supply voltage. This pushes the active device to operate outside of the active region, and may cause severe distortion for signals with high PAPR.

2.6 Envelope Tracking

A similar approach to improving the efficiency of transmitters is called envelope tracking (ET). This technique is based in the fact that the efficiency of a single-ended PA, such as class-AB, class-B or class-C, depends on both output power and drain supply voltage. For example, drain efficiency of a class-B PA increases with the rise of drain-source current, and it reaches 78.5% when the output current reaches the saturation. The difference between the drain supply voltage V_{cc} and the envelope voltage is called voltage overhead. If V_{cc} remains constant, at back-off power levels voltage overhead is big, which decreases the efficiency of the PA. In the ET transmitter the drain supply voltage is varied in the time domain so that the voltage overhead is minimized. Therefore, the active device constantly operates close to its saturation, which improves the transmitter efficiency.
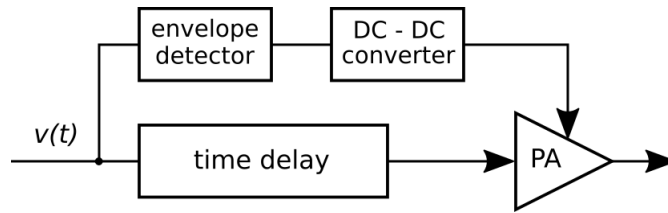
Fig. 2.19   The structure of an envelope tracking transmitter.

The general structure of the ET PA is shown in Fig. 2.19. It consists of a supply modulator and an RF PA. The envelope signal fed to the supply modulator can be generated from the input RF signal itself using an envelope detector. However, in most modern transmitters it is easier to generate an envelope signal in the digital domain using a separate DAC. This signals usually occupy the low frequency spectrum from DC to 3-4 times RF signal bandwidth depending upon the modulation and PAPR of the transmitted signal. The peak power of the envelope signal should be approximately 1.5 times higher than the peak power of the RF signal. For example, if an LTE signal with 10 dB PAPR is transmitted with output power 20 W, then the peak power for the envelope signal will be approximately 300 W.

Time delay block is necessary in the main RF part, since the dynamic supply voltage and the input RF signal should arrive at the RF PA at the same time. The acceptable time error can be estimated as [88]:

$$\Delta t \approx \frac{0.02}{BW_{\mathrm{RF}}} \tag{2.32}$$

where BW_{RF} is the bandwidth of the transmitted signal. In modern transmitters time alignment can be implemented using closed-loop monitoring systems. These systems also perform DPD in order to maintain required level of linearity of the output signals.

The idea was initially proposed by Loy Barton [89] and was addressing the issue of high power consumption of transmitters operating with amplitude modulated signals. The ET transmission in the modern form was described in [90, 91] as a way of transmitting single-sideband modulated signals. This technique has recently
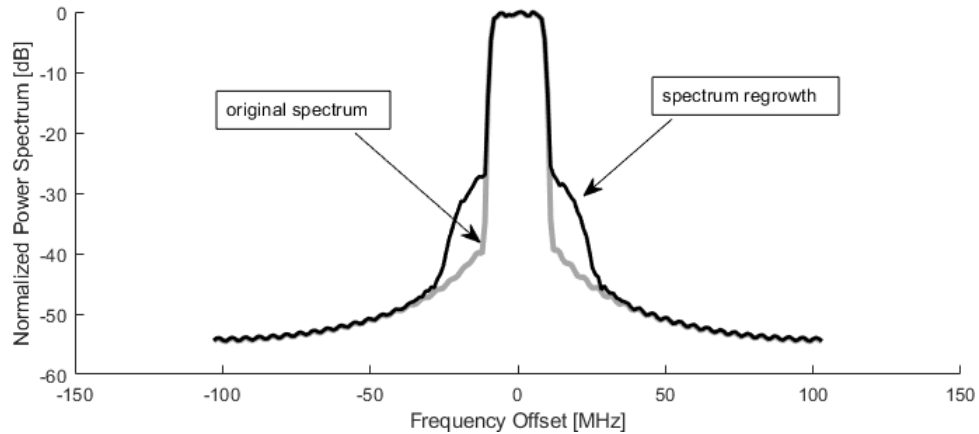
Fig. 2.20 Spectrum regrowth as a result of PA distortion.

drawn the attention of researchers as a way to reduce energy consumption of wireless systems operating with WCDMA and LTE signals. Compared to other efficiency enhancement techniques ET transmitters are capable of providing wider bandwidth and wide range of back-off power levels.

2.7   Linearization Techniques

According to the Shannon-Hartley theorem, the channel capacity of any wireless system is proportional to the occupied bandwidth [92]. However, since the frequency spectrum is a natural resource, transmitted signals should provide as high spectrum efficiency as possible. For this reason, OFDM modulation has been used in LTE transmitters. Most PAs introduce some nonlinear distortion into transmitted signal if amplitude and phase modulation is used, which in turn causes spectrum regrowth, as shown in Fig. 2.20, and reduces the spectrum efficiency. One way to avoid nonlinear distortion is to drive PAs at back-off output power level [93]. As it has been shown previously in this chapter, this approach significantly reduces the overall efficiency of a transmitter.

Another approach to improve the PA linearity is to introduce some nonlinearity into a transmitted signal, which would compensate the nonlinearity of the PA. This approach is called predistortion, and it can be performed either in the analog domain

or in the digital domain. In the latter case it is called digital predistortion (DPD), which is widely used in modern communication systems.

In order to be precompensated, the PA nonlinearity should be accurately modelled. Various behavior models have been proposed based on the trade-off between accuracy and computational efficiency [14]. If both transmitted and received signals are represented in the digital domain as a finite number of samples, the nonlinear output of the PA can be represented as follows:

$$y(n) = \sum_{p=1}^{P} \alpha_p x^p(n) \tag{2.33}$$

where $x(n)$ is the sampled input signal, $y(n)$ is the sampled output signal, and P is the nonlinearity order. Increasing the order of the polynomial improves the precision of the model at the cost of computational complexity. It should be pointed out, that in the model (2.33) it is assumed that the level of the output signal depends on the level of the input signal only. However, in real PAs it also depends on the level of the input signal at the preceding samples, which is called memory effect. In order to account for memory effects, a Volterra series representation of the baseband signal can be used, which was outlined in [94] as follows:

$$y(n) = \sum_{p=1}^{P} \sum_{m_1=0}^{M} \ldots \sum_{m_k=0}^{M} h_p(m_1, \ldots, m_k) \prod_{j=1}^{(p+1)} x(n - m_j) \prod_{l=p+2}^{(2p+1)} x^*(n - m_l) \tag{2.34}$$

The advantage of this representation is that the model basis contains all possible combinations of the memory depth. However, the full Volterra representation of a signal requires significant computational resources.

Memory polynomial (MP) model is a simplified version of Volterra series representation, in which the cross-terms of signal values and its lagging terms of different values are omitted:

$$y(n) = \sum_{p=1}^{P} \sum_{m=0}^{M} \alpha_{mp} x(n - m) |x(n - m)|^{2p} \tag{2.35}$$

where $|\cdot|$ denotes the absolute value, α_{mp} are the model coeffcients and M is the memory depth, which defines the amount of previous time samples taken into consideration. The MP model defined by equation (2.35) provides a sufficient accuracy for many practical applications [95]. An extension of this model called generalized memory polynomial (GMP) was proposed in [96], wich takes into account cross-term time shifts. Since all the coefficients in the MP and GMP models appear in a linear form, they can be easily calculated using any least-squares (LS) algorithm [96]. Due to the high accuracy and relative simplicity the GMP model remains one of the most popular techniques for behavioral modelling of different types of amplifiers, such as outphasing PA [97] and Doherty PA [98].

Once a behavioral model has been built and the coefficients have been identified, the accuracy of the model needs to be estimated. The precision can be evaluated either in the time domain or in the frequency domain. In the former case the common metrics called mean square error (MSE) and normalized mean square error (NMSE) can be used:

$$\text{MSE} = \frac{1}{n} \sum_{i=1}^{N} \mid y(n) - \tilde{y}(n) \mid^2, \tag{2.36}$$

$$\text{NMSE} = \frac{\sum_{i=1}^{N} \mid y(n) - \tilde{y}(n) \mid^2}{\sum_{i=1}^{N} \mid y(n) \mid^2}, \tag{2.37}$$

where $y(n)$ is the measured signal and $\tilde{y}(n)$ is the modelled signal. In the frequency domain the precision of the model can be estimated using a metric called adjacent channel error power ratio (ACEPR), which was defined in [99]:

$$\text{ACEPR} = \max_{m=\text{L,U}} \left\{ \frac{\sum_{f(\text{adj})_m} |Y(f) - \tilde{Y}(f)|^2}{\sum_{f\text{ch}} |Y(f)|^2} \right\} \tag{2.38}$$

where $Y(f)$ is the discrete spectrum of the output signal $y(n)$, f_{ch} denotes discrete inband frequencies and f_{adj} denotes frequencies in the lower (L) and upper (U) adjacent channels. Since the ACEPR metric estimates the accuracy of the model
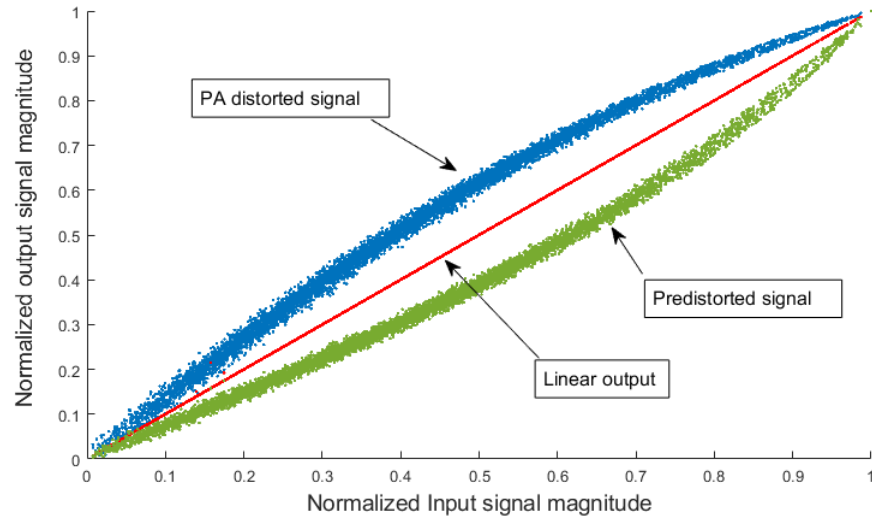
Fig. 2.21 AMAM plots of signals before and after applying DPD.
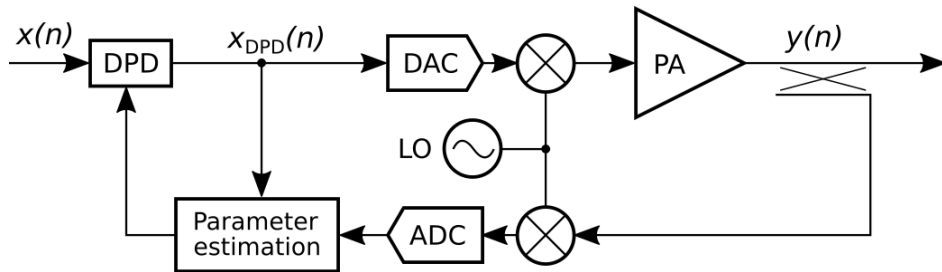
Fig. 2.22 Block-diagram of an indirect learning predistorter.

in the frequency domain it allows to separate the distortion in different adjacent channels and the inband distortion.

The linearization of the PA is implemented by a linearizer which mimics the inverse nonlinear behavior of the PA. Combined with the nonlinearity of the PA, the predistortion provides a linear signal at the output of the PA. This process is illustrated in Fig. 2.21, where initial signal coming from an IQ modulator is distorted after a PA (blue dots). Based on a behavioural model of the PA, a linearizer generates a predistorted signal (green dots), which produces a linear output (red dots) after the PA stage.

The two main approaches to DPD implementation are direct learning and indirect learning algorithms. The principle of the indirect learning DPD can be demonstrated using Fig. 2.22. The predistorter analyzes the difference between a transmitted signal before the PA $x(n)$ and a transmitted signal after the PA $y(n)$. Therefore, the
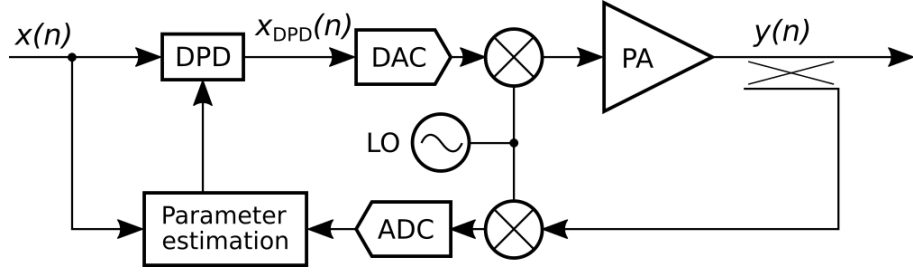
Fig. 2.23 Block-diagram of a direct learning predistorter.

goal of the algorithm is to build a signal x_{DPD} in order to minimize the error, and the cost function can be expressed as follows:

$$J_{\text{ILA}}(n) = \| \, x_{\text{DPD}}(n) - y(n) \, \|_F^2 \tag{2.39}$$

where $\| \cdot \|_F$ denotes the Frobenius norm. The cost function $J_{\text{ILA}}(n)$ can be minimized using different techniques, such as least squares (LS) or least mean squares (LMS) algorithms. Despite its simplicity, the indirect learning technique is sensitive to noise, because the error estimation depends on the noisy output signal measurement [100]. In order to reduce this dependency, a modified technique called model-based indirect learning algorithm was proposed in [101]. In this technique, a model of the real PA is constructed, which replaces the PA in the linearization process.

In the direct learning technique the predistorter iteratively minimizes the difference between the original signal $x(n)$ and the transmitted signal $y(n)$ that comes from the PA output (see Fig. 2.23). In this case the error vector will be written as $e(n) = y(n) - x(n)$, and the cost function can be expressed as follows:

$$J_{\text{DLA}} = \| \, \mathbf{e} - \Phi(\mathbf{x})^T \, \triangle \theta \, \|_F^2 \tag{2.40}$$

where $\Delta\theta$ is the vector of model parameters and $\Phi(\mathbf{x}) = [\mathbf{x}(n), \mathbf{x}(n-1), \ldots, \mathbf{x}(n-M)|\mathbf{x}(n-M)|^{2P}]$ is the matrix constructed of input signal values. Since this matrix is base on undistorted signal, the direct learning algorithm is less sensitive to the noise compared to the direct learning.

Chapter 3

Class-E power amplifier with shunt capacitance and shunt filter

As it has been pointed out in Section 2.2, the class-E PA is capable of providing high drain efficiency and has a compact output load circuit. Besides, class-E amplifiers demonstrate the ability to maintain high drain efficiency across a wide range of output power levels when load modulation is used [44, 102] and wide frequency bands [103–105]. There are several ways of achieving class-E PA operation [19], and a particular choice of the PA structure depends on the operating frequency, used technology, output power level and other factors.

The class-E PA with shunt capacitance and shunt filter has several advantages compared to other structures, such as ability to incorporate the device parasitics into the output load network and potential of broadband operation. Initially, it was proposed in [106], and in [15] a modified version of this PA with pure active load was introduced, which made it easier to match the output to the standard 50 ohms load. The general analysis of this type of class-E PA was presented in [47]. As it was demonstrated, a particular complex load can be found in order to take into account device parasitics. Therefore, it is possible to find an output load configuration that provides very high drain efficiency for a particular device.
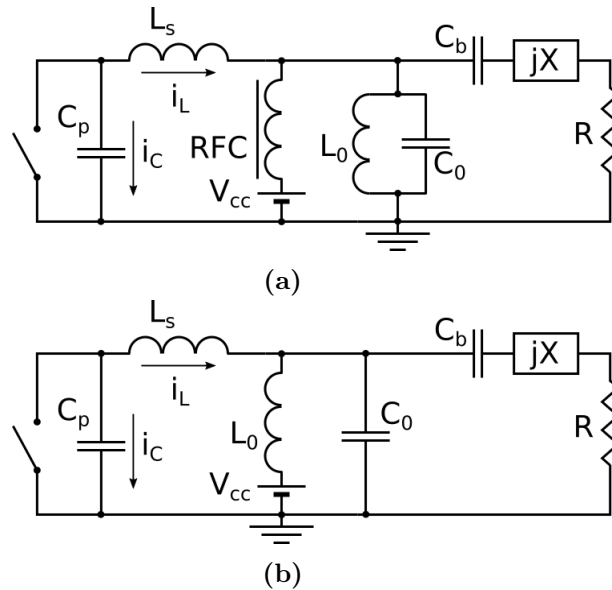
Fig. 3.1 Load network of a class-E power amplifier with shunt capacitance and shunt filter: (a) - drain voltage supply through RF choke; (b) - drain voltage supply through resonator inductance.

In this chapter the general analysis of the class-E PA with shunt capacitance and shunt filter for an arbitrary output power is presented. Firstly, the solution for the ideal class-E operation is presented. Secondly, the operation of the PA at back-off power is analyzed. The derived results are proven using a harmonic balance circuit simulator from Keysight ADS simulation tool. Based on the derived results single-ended amplifiers have been manufactured based on GaN HEMT packaged transistors. The operation of the fabricated amplifiers at the peak power has been tested experimentally.

3.1 Ideal operation

As mentioned in 2.2, the necessary and sufficient conditions for the ideal class-E operation reffered to as ZVS and ZVDS and defined by (2.23) and (2.24) respectively. In [15, 47] it was shown, that class-E operation can be achieved using the load network configuration shown in Fig. 3.1(a) and Fig. 3.1(b). This load network consists of a shunt capacitance C_p, a series inductance L_s, a shunt resonator $L_0 C_0$,

a DC-block capacitance C_b, an active load R and load reactance jX which can be inductive or capacitive depending on the values of L_s and C_p as it will be shown later. A DC voltage V_{cc} is supplied to the drain of the transistor either through an RF choke RFC (see Fig. 3.1(a)) or through the inductance of the shunt resonator L_0 (see Fig. 3.1(b)). The latter case is preferable since it avoids the need for bulky inductive elements. The operation of the PA can be considered separately in two states: when the switch is on ($0 \leq \omega t < \pi$) and when the switch is off ($\pi \leq \omega t < 2\pi$). In this section an ideal model of the output circuit is considered, which means that:

1. The transistor operates as an ideal switch with zero on-resistance and infinite off-resistance.

2. All the lumped components in the circuit are linear.

3. All the components except the load resistance R are lossless.

Throughout this section we denote:

- $v(\omega t)$ is voltage across switch in time domain;

- $v_R(\omega t)$ is voltage across active load in the time domain;

- $v_X(\omega t)$ is voltage across reactive load in the time domain;

- $i_C(\omega t)$ is current through the parallel capacitance C_p in the time domain;

- $i_L(\omega t)$ is current through the series inductance L_s in the time domain;

- V_R is amplitude of the voltage across the active load at the fundamental frequency;

- V_X is amplitude of the voltage across the reactive load at the fundamental frequency;

- $\omega \equiv 2\pi f$ is the fundamental angular frequency.

In order to simplify the equations, the following parameters are used:

$$q \equiv \frac{1}{\omega\sqrt{L_{\mathrm{s}}C_{\mathrm{p}}}} \tag{3.1}$$

$$x \equiv \omega t \tag{3.2}$$

$$r_{\mathrm{R}} \equiv \frac{V_{\mathrm{R}}}{V_{\mathrm{cc}}} \tag{3.3}$$

$$r_{\mathrm{X}} \equiv \frac{V_{\mathrm{X}}}{V_{\mathrm{cc}}} \tag{3.4}$$

$$u(x) \equiv \frac{v(\omega t)}{V_{\mathrm{cc}}} \tag{3.5}$$

In the normalized form, the conditions for ideal class-E operation ZVS and ZVDS can be written as:

$$u(x)\Big|_{x=2\pi} = 0 \tag{3.6}$$

$$\frac{du(x)}{dx}\Big|_{x=2\pi} = 0 \tag{3.7}$$

When the switch is on $(0 \leq \omega t < \pi)$, there is no voltage drop across the switch, and Kirchoff's law for voltages can be written as:

$$V_{\mathrm{cc}} - v_{\mathrm{X}}(\omega t) - v_{\mathrm{L}}(\omega t) - v_{\mathrm{R}}(\omega t) = 0 \tag{3.8}$$

where the voltages in the time domain can be expressed as:

$$v_{\mathrm{L}}(\omega t) = \omega L_{\mathrm{s}}\frac{di_{\mathrm{L}}(\omega t)}{d\omega t} \tag{3.9}$$

$$v_{\mathrm{R}}(\omega t) = V_{\mathrm{R}}\sin(\omega t + \varphi) \tag{3.10}$$

$$v_{\mathrm{X}}(\omega t) = V_{\mathrm{X}}\cos(\omega t + \varphi) \tag{3.11}$$

In (3.10) and (3.11) it is assumed that the shunt filter L_0C_0 has very high loaded Q-factor and provides ideal short circuit for all harmonics. Therefore, only the fundumental current flows through the active load R with phase shift φ. Since the

switch is on, the current does not flow through the capacitor:

$$i_C(\omega t) = \omega C_p \frac{dv(\omega t)}{d\omega t} = 0 \tag{3.12}$$

When the switch is off ($\pi \leq \omega t < 2\pi$), the current does not flow through the switch and flows through the parallel capacitance instead:

$$
\begin{aligned}
i_C(\omega t) = \omega C_p \frac{dv(\omega t)}{d\omega t} &= \frac{1}{\omega L_s} \int_\pi^{\omega t} v_L(\omega t) d(\omega t) + i_L(\pi) \\
&= \frac{1}{\omega L_s} \int_\pi^{\omega t} [V_{cc} - v(\omega t) - v_R(\omega t) - v_X(\omega t)] d(\omega t) + i_L(\pi)
\end{aligned}
\tag{3.13}
$$

Differentiating the equation (3.13) and using definitions (3.1) - (3.5) one can derive an equation for the voltage across the switch in the normalized form:

$$\frac{d^2 u}{dx^2} + q^2 u = q^2 \Big(1 - r_R \sin(x + \varphi) - r_X \cos(x + \varphi)\Big) \tag{3.14}$$

Equation (3.14) is a linear ordinary differential equation with four unknown parameters: q, r_R, r_X and φ. Here we assume that parameter q is a variable and the rest of the parameters can be found from the solution of the equation and application of initial conditions. The solution of the equation (3.14) can be found using the method of constant variation. The solution is:

$$
\begin{aligned}
u(x) = 1 + \frac{q^2}{1 - q^2}\Big(r_R \sin(x + \varphi) + r_X \cos(x + \varphi)\Big) + \\
+ C_1 \cos qx + C_2 \sin qx
\end{aligned}
\tag{3.15}
$$

Here C_1 and C_2 are constants that do not depend on x. These constants can be defined from the initial conditions for the moment when $x = \pi$.

The first condition follows from the assumption that when the switch is on ($0 \leq x < \pi$), there is no voltage drop across the switch:

$$u(x = \pi) = 0 \tag{3.16}$$

At the same time the current through the inductance L_s can be expressed as:

$$i_\mathrm{L}(x) = \frac{1}{\omega L_\mathrm{s}} \int_0^x \Big(V_\mathrm{cc} - V_\mathrm{X}\cos(x+\varphi) - V_\mathrm{R}\sin(x+\varphi)\Big)dx =$$
$$= \frac{V_\mathrm{cc}}{\omega L_\mathrm{s}}x - \frac{V_\mathrm{X}}{\omega L_\mathrm{s}}\Big(\sin(x+\varphi) - \sin\varphi\Big) + \frac{V_\mathrm{R}}{\omega L_\mathrm{s}}\Big(\cos(x+\varphi) - \cos\varphi\Big)+ \quad (3.17)$$
$$+ i_\mathrm{L}(0)$$

At the moment when the switch turns off, this current flows through the parallel capacitance C_p and therefore

$$i_\mathrm{C}(x=\pi) = i_\mathrm{L}(x=\pi) = \omega C_\mathrm{p}\frac{dv(x)}{dx} \quad (3.18)$$

On the other hand, the current through the inductance L_S at the moment $x=0$ is defined as

$$i_\mathrm{L}(0) = \omega C_\mathrm{p}\frac{dv(x)}{dx}\bigg|_{x=2\pi} \quad (3.19)$$

and therefore, from the ZVDS condition (3.7) it follows that $i_\mathrm{L}(0) = 0$. However, as it will be shown later, in the case of back-off power operation the ZVDS conditions is violated and, therefore, $i_\mathrm{L}(0) \neq 0$. From equations (3.17) and (3.18) and using (3.1) - (3.5) one can derive an equation for the slope of the voltage across the switch at the moment when the switch turns off:

$$\frac{du(x)}{dx}\bigg|_{x=\pi} = q^2\Big(\pi + 2(r_\mathrm{X}\sin\varphi - r_\mathrm{R}\cos\varphi)\Big) \quad (3.20)$$

Applying the conditions (3.16) and (3.20) to the equation (3.15) one can obtain the system of two linear equations for the variables C_1 and C_2. The solution of this system will be:

$$C_1 = -p_2\Big(\frac{q}{1-q^2} - 2q\Big)\sin q\pi - q\pi\sin q\pi + \frac{q^2 p_1}{1-q^2}\cos q\pi - \cos q\pi \quad (3.21)$$
$$C_2 = \frac{q^2 p_2}{1-q^2}\sin q\pi - \sin q\pi + q\pi\cos q\pi + p_2\Big(\frac{q}{1-q^2} - 2q\Big)\cos q\pi \quad (3.22)$$
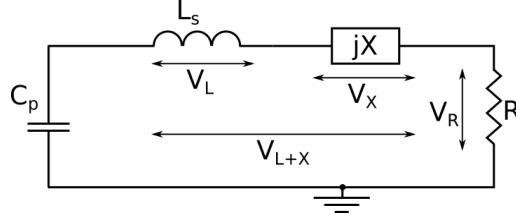
Fig. 3.2 Equivalent circuit of class-E PA at the fundamental frequency.

where

$$p_1 \equiv r_R \sin \varphi + r_X \cos \varphi \tag{3.23}$$

$$p_2 \equiv r_R \cos \varphi - r_X \sin \varphi. \tag{3.24}$$

In order to find the circuit parameters it is necessary to use conditions for ideal class-E operation (3.6) and (3.7). Substituting expression (3.15) along with the expressions for constants (3.21) and (3.22), one can achieve a system of two independent linear equations with two unknown parameters p_1 and p_2. The solution for the system would be:

$$p_1 = \frac{(q^2 - 1)\Big(q\pi \sin q\pi - 2(q^2 - 1)(1 - \cos q\pi)\Big)}{2q^4(1 + \cos q\pi)} \tag{3.25}$$

$$p_2 = \frac{(q^2 - 1)\Big(q^2\pi \cos q\pi + 2q \sin q\pi + q^2\pi\Big)}{2q^4(1 + \cos q\pi)}. \tag{3.26}$$

The circuit parameters can be found by considering the load PA network in the frequency domain. The DC component of the drain current can be found from applying the Fourier transform to the current waveform:

$$I_0 = \frac{1}{2\pi} \int_0^{2\pi} i_L(x)dx = \frac{V_{cc}}{2\pi\omega L_s}\left(\frac{\pi^2}{2} - 2p_1 - \pi p_2\right). \tag{3.27}$$

Since all the components except the active load are lossless, one can assume that the drain efficiency is 100%. Therefore, all the energy of the DC power supply is transformed into the energy dissipated into the active load R. Consequently, $P_{out} = I_0 V_{cc}$, and, taking into accout (3.1), the values L_s and C_p can be derived from

the following expressions:

$$L_\mathrm{s} = \frac{V_\mathrm{cc}^2}{2\pi\omega P_\mathrm{out}}\left(\frac{\pi^2}{2} - 2p_1 - \pi p_2\right) \tag{3.28}$$

$$C_\mathrm{p} = \frac{1}{L_\mathrm{s}(q\omega)^2} \tag{3.29}$$

The values r_R, r_X and φ can be found from considering the operation of the PA in the frequency domain at the fundamental frequency as shown in Fig. 3.2. The normalized voltage magnitude across L_s and X can be found as:

$$U_\mathrm{L+X} \equiv \frac{V_\mathrm{L+X}}{V_\mathrm{cc}} = -\frac{1}{\pi}\int_0^\pi u(x)\cos(x+\varphi)dx \tag{3.30}$$

The voltage across the active load R has 90° phase shift relative to $V_\mathrm{L+X}$ and consequently can be found from the Fourier transform:

$$U_\mathrm{R} \equiv \frac{V_\mathrm{R}}{V_\mathrm{cc}} = -\frac{1}{\pi}\int_0^\pi u(x)\sin(x+\varphi)dx \tag{3.31}$$

It should be noted that in (3.30) and (3.31) the normalized voltage $u(x)$ is defined by (3.15) and the integration can be performed analytically. From the first Kirchoff's law for the circuit it follows that

$$\frac{U_\mathrm{L+X}}{r_\mathrm{R}} = \frac{\omega L_\mathrm{s} + X}{R} \tag{3.32}$$

However, from the output power definition

$$R = \frac{V_\mathrm{R}^2}{2P_\mathrm{out}} = \frac{(r_\mathrm{R}V_\mathrm{cc})^2}{2P_\mathrm{out}} \tag{3.33}$$

From (3.32) and (3.33) it follows that

$$U_\mathrm{L+X} = \frac{r_\mathrm{X}}{r_\mathrm{R}} + \frac{2P_\mathrm{out}}{V_\mathrm{cc}^2}\cdot\frac{\omega L_\mathrm{s}}{r_\mathrm{R}} \tag{3.34}$$

By performing integration on expression (3.31) and substituting it into the equation (3.34) one can derive an equation that, along with the equations (3.25) and (3.26), form a system of three independent equations with three unknown variables. The solution of this system can be written as:

$$\varphi = \frac{A}{2|A|}\left[\arccos\left(\frac{B}{\sqrt{A^2 + B^2}} \right) \pm \right.$$
$$\left. \pm \arccos\left(\frac{T}{\sqrt{A^2 + B^2}} \right) \right] \tag{3.35}$$

where

$$A = M_1 p_1 + M_2 p_2 - M_3 p_1^2 + M_3 p_2^2 \tag{3.36}$$

$$B = M_1 p_2 - M_2 p_1 - 2M_3 p_1 p_2 \tag{3.37}$$

$$T = 2M_4 - M_1 p_2 - M_2 p_1 \tag{3.38}$$

$$M_1 = \frac{q}{\pi(q^2 - 1)}\left(C_2(\cos 2q\pi + \cos q\pi) - C_1(\sin 2q\pi + \sin q\pi) \right) \tag{3.39}$$

$$M_2 = -\frac{2q}{\pi} + C_2 q \frac{\sin 2q\pi + \sin q\pi}{\pi(q^2 - 1)} + C_1 q \frac{\cos 2q\pi + \cos q\pi}{\pi(q^2 - 1)} \tag{3.40}$$

$$M_3 = 1 + \frac{q^2}{2(1 - q^2)} \tag{3.41}$$

$$M_4 = \frac{2P_{\text{out}}}{V_{\text{cc}}^2}\omega L_{\text{s}} \tag{3.42}$$

The constants C_1 and C_2 are uniquely defined by the parameter q and can be found from expressions (3.21) and (3.22) respectively. Once the phase shift value has been found, the voltage ratio parameters can be derived:

$$r_{\text{X}} = p_1 \cos\varphi - p_2 \sin\varphi \tag{3.43}$$

$$r_{\text{R}} = p_1 \sin\varphi + p_2 \cos\varphi \tag{3.44}$$

The values r_R and r_X in turn define the load impedance:

$$R = \frac{(r_R V_{cc})^2}{2 P_{out}} \tag{3.45}$$

$$X = \frac{r_X}{r_R} R \tag{3.46}$$

The presented solution shows that it is always possible to provide an ideal class-E operation for the given values of output power, drain supply voltage, operating frequency and the parameter q. Any deviations of the input parameters will violate the ideal class-E operation.

3.2 Back-off operation

Although the ideal load network parameters can be found for the specified output power, in real transmitters output power changes with time which causes non-ideal class-E operation. This is the case when a class-E PA is used in transmitters implementing load modulation techniques, such as Doherty PA or outphasing PA. In these systems the load presented to the PA changes with time, whereas the values of C_p and L_s do not alter.

As it was shown in [102], a class-E PA can have very high drain efficiency even when the condition (2.24) for drain voltage is not satisfied. This means that at the moment when the switch turns on, the initial drain current $i_L(0)$ (the last term in (3.17)) is non-zero:

$$i_L(x = 0) = V_{cc} \omega C_p \frac{du}{dx}\bigg|_{x=2\pi} \tag{3.47}$$

Therefore, the initial condition for normalized drain voltage u at the moment $x = \pi$ will be

$$\frac{du}{dx}\bigg|_{x=\pi} = q^2 \Big(\pi + 2(r_X \sin \varphi - r_R \cos \varphi) \Big) + \frac{du}{dx}\bigg|_{x=2\pi} \tag{3.48}$$

Applying the condition (3.48) along with the condition for zero voltage condition at the moment when the switch turns on, expressions for the constants C_1 and C_2 can

be expressed as follows:

$$C_1 = c_{10} + c_{11}p_1 + c_{12}p_2 \tag{3.49}$$

$$C_2 = c_{20} + c_{21}p_1 + c_{22}p_2 \tag{3.50}$$

where the coefficients c_{ij} can be calculated as follows, using the given value of q:

$$
\begin{aligned}
c_{11} &= \frac{q^2}{1-q^2} \cdot \frac{\cos 2q\pi - \cos q\pi}{\cos q\pi - 1} \\
c_{12} &= \frac{q^2}{1-q^2} \cdot \frac{2q\sin q\pi}{\cos q\pi - 1} \\
c_{10} &= \frac{q\pi \sin q\pi + \cos q\pi - \cos 2q\pi}{\cos q\pi - 1} \\
c_{21} &= \frac{q^2}{1-q^2} \cdot \frac{\sin 2q\pi - \sin q\pi}{\cos q\pi - 1} \\
c_{22} &= -\frac{q^2}{1-q^2} \cdot \frac{2q\cos q\pi}{\cos q\pi - 1} \\
c_{20} &= \frac{\sin q\pi - \sin 2q\pi - q\pi \cos q\pi}{\cos q\pi - 1}
\end{aligned}
\tag{3.51}
$$

The DC component of the drain current will be:

$$
\begin{aligned}
I_0 &= \frac{1}{2\pi} \int_0^{2\pi} i_{\mathrm{L}}(x)dx = \\
&= \frac{V_{\mathrm{cc}}}{2\pi\omega L_{\mathrm{s}}} \left(\pi^2 - 2p_1 - \pi p_2 \right) + \frac{V_{\mathrm{cc}}}{2}\omega C_{\mathrm{p}} \cdot \frac{du}{dx}\Big|_{x=2\pi}
\end{aligned}
\tag{3.52}
$$

The first derivative of the normalized voltage $\frac{du}{dx}\Big|_{x=2\pi}$ in (3.52) can be found by differentiating the expression (3.15) with constants defined by (3.49) and (3.50). By assuming that the drain efficiency is 100%, P_{out} becomes

$$P_{\mathrm{out}} = V_{\mathrm{cc}} \cdot I_0 \tag{3.53}$$

Therefore, one can derive the first equation for variables p_1 and p_2:

$$K_{11}p_1 + K_{12}p_2 = K_{10} \tag{3.54}$$

where

$$K_{11} = \frac{\omega C_{\mathrm{p}}}{2} \cdot \frac{q^3}{q^2 - 1} \cdot \frac{\sin q\pi}{1 - \cos q\pi} \tag{3.55}$$

$$K_{12} = -\frac{\omega C_{\mathrm{p}}}{2} \cdot \frac{q^2}{q^2 - 1}\left(1 + \frac{2q^2 \cos q\pi}{1 - \cos q\pi}\right) - \frac{1}{2\omega L_{\mathrm{s}}} \tag{3.56}$$

$$K_{10} = \frac{P_{\mathrm{out}}}{V_{\mathrm{cc}}^2} - \frac{\omega C_{\mathrm{p}}}{2} \cdot \frac{q(\sin q\pi + q\pi \cos q\pi)}{1 - \cos q\pi} - \frac{\pi}{4\omega L_{\mathrm{s}}} \tag{3.57}$$

The second equation can be derived from the condition (3.6). Therefore the parameters p_1 and p_2 can be calculated from these two equations as:

$$p_1 = \frac{K_{10} - K_{12}p_2}{K_{11}} \tag{3.58}$$

$$p_2 = \frac{q^2 - 1}{q^2}\left(\frac{1 - \cos q\pi}{q \sin q\pi} + \frac{\pi}{2}\right) \tag{3.59}$$

Once the values p_1 and p_2 have been found, one can define the parameters φ, r_{R} and r_{X} from the expressions (3.35), (3.44) and (3.43) respectively. These parameters define the optimal load impedance according to the expressions (3.45) and (3.46).

The class-E PA design procedure operating under a given back-off power can be outlined in the following steps:

1. From the chosen value q calculate the values p_1 and p_2 for ideal class-E operation using the expressions (3.25) and (3.26).

2. Using the calculated values p_1 and p_2 obtain values for constants C_1 and C_2 using (3.21) and (3.22).

3. From the calculated values C_1, C_2, p_1, p_2 along with the given drain supply voltage V_{cc}, output power P_{out} and operating frequency f_{c} calculate circuit parameters using (3.28), (3.29), (3.45), (3.46).

4. For the given back-off power level calculate p_1 and p_2 using (3.58) and (3.59).

5. Once the values p_1 and p_2 have been found for the back-off power, the optimum load can be calculated using the same expressions (3.45) and (3.46).
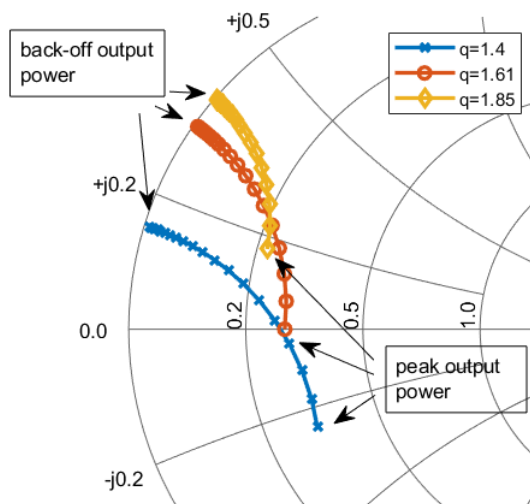
Fig. 3.3   Load contours for different values q

It should be pointed out, that the derived solution provides the ideal class-E operation only for the model described in Section 3.1. In real PAs, however, drain efficiency is degraded by a finite saturation resistance, finite cutoff resistance, non-ideal harmonic suppression, etc. Hence, the circuit parameters derived from the outlined procedure cannot be used as a final design, however, they provide a good initial approximation for optimization with a circuit simulator.

3.3   Waveform analysis

In order to demonstrate the proposed technique 3 different class-E PA load networks are analyzed: $q = 1.4$, $q = 1.61$ [15] and $q = 1.85$ [47]. The load networks are designed for the following parameters: $f_c = 2.14$ GHz, $V_{cc} = 20$ V, $P_{out} = 12$ W. The load contours are shown in Fig. 3.3. From the presented curves it can be seen that the active part of the load decreases with decreasing output power, which makes the class-E PA with shunt capacitance and shunt filter similar to a current source. The reactive part of the load becomes more inductive for lower output power levels for all values q.

The drain current and voltage waveforms for ideal class-E operation along with waveforms for different back-off power levels are shown in Fig. 3.4 - 3.6. From these
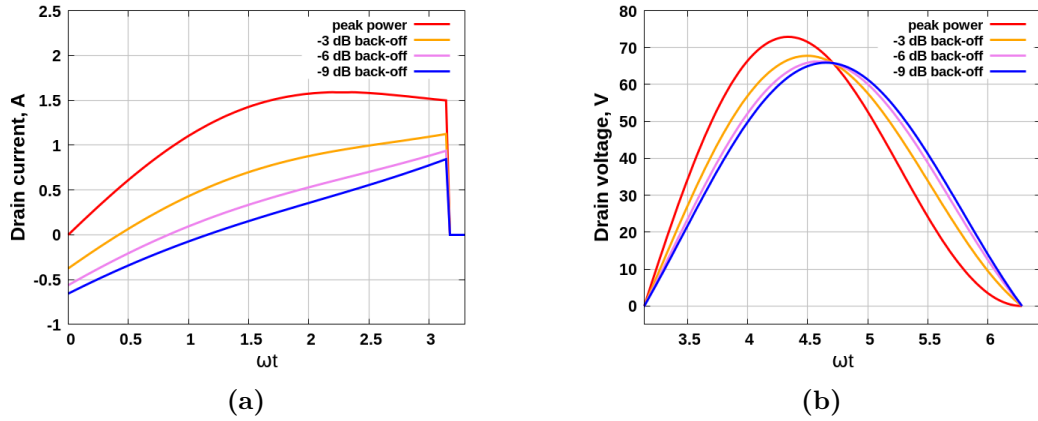
Fig. 3.4 Waveforms for different output power levels ($q = 1.4$): (a) - current waveforms; (b) - voltage waveforms.
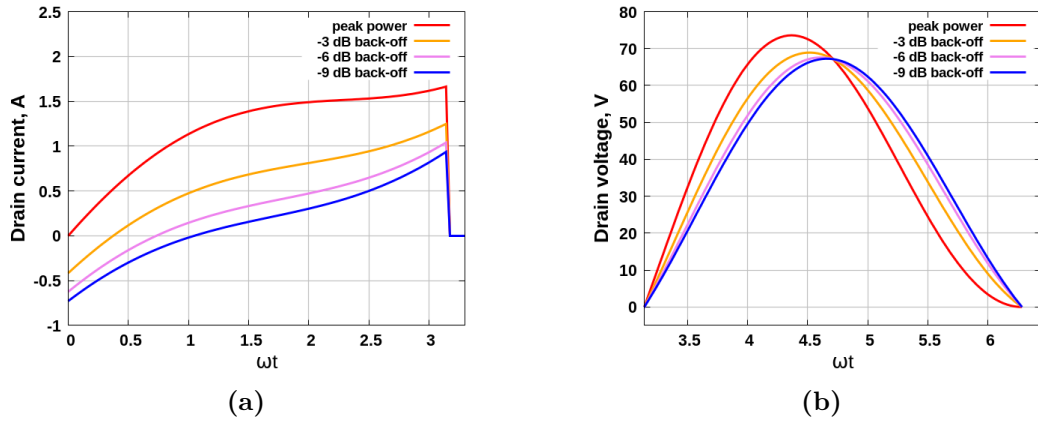
Fig. 3.5 Waveforms for different output power levels ($q = 1.61$): (a) - current waveforms; (b) - voltage waveforms.

waveforms it can be observed that for lower output power level the voltage at the end of the period has negative slope. This, in turn, causes non-zero drain current at the moment the switch is turned on (see Fig. 3.4(a), 3.5(a), 3.8(a)).

It should be pointed out, that a particular choice of a value of q depends on many factors, such as used active device, required bandwidth, etc. From Fig. 3.3 it can be seen that the PA with $q = 1.61$ has a pure active load ($X = 0$ ohm), which makes it easier to match the output to the standart 50 ohm impedance. When $q < 1.61$, the optimum load at a peak power has capacitive reactance, however, reducing the output power increases the reactance. Therefore, the optimum load impedance becomes
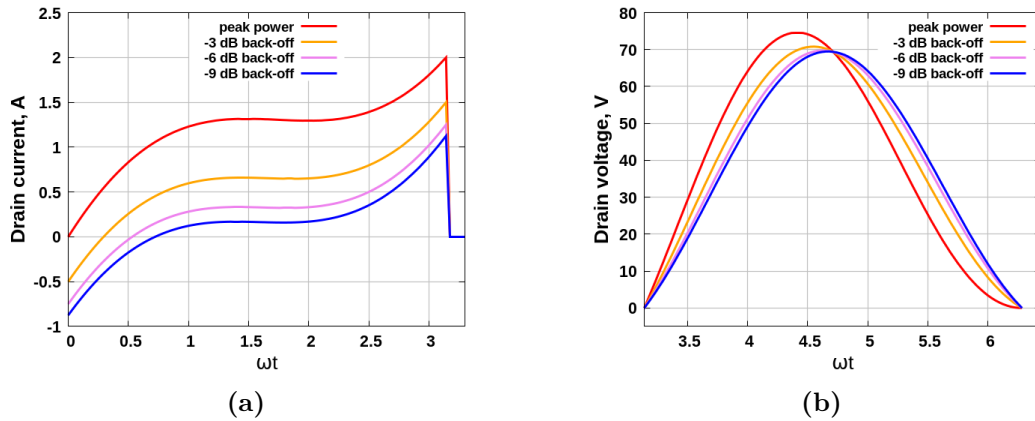
Fig. 3.6 Waveforms for different output power levels ($q = 1.85$): (a) - current waveforms; (b) - voltage waveforms.

purely active at a certain value of back-off power. If $q > 1.61$, the optimum load reactance is always inductive (see Fig. 3.3).

3.4 Idealized simulation

The circuit simulator Keysight ADS was used to analyze the operation of class-E PA load network at peak and back-off power levels. There are two ways to simulate the operation of the PA - in the time domain and in the frequency domain. The first approach provides better accuracy, however it is relatively time consuming. The second approach is provided by the harmonic balance simulator from ADS. It is much faster compared to the time domain simulator and can provide a sufficient accuracy if the number of harmonics taken into account is large enough.

The simulated circuit topology is shown in Fig. 3.7. It is analyzed with the harmonic balance simulator, and the number of harmonics is set to 50. The active device is modeled as a voltage controlled switch with 10^{-3} ohm on-resistance and 10^6 ohm off-resistance. The bigger difference between the values of the on- and off-resistance provides better accuracy, however, it might cause convergence problems for the simulator. The single-tone signal is fed to the input of the amplifier from a P_1Tone power source. If the amplitude of the input signal is much higher than the voltage threshold of the voltage-controlled switch, the effect of the single tone signal
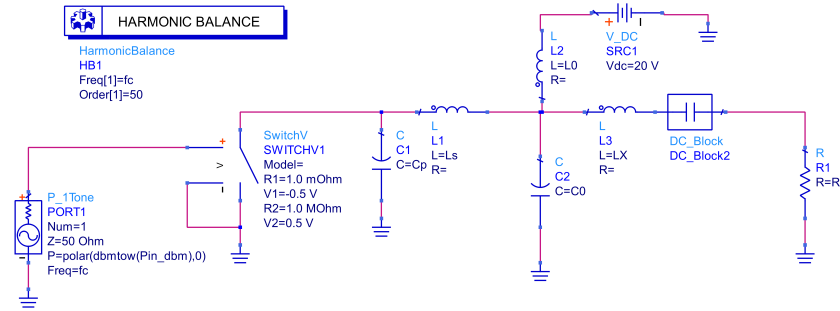
Fig. 3.7 Ideal class-E PA with shunt capacitance and shunt filter simulated in Keysight ADS.
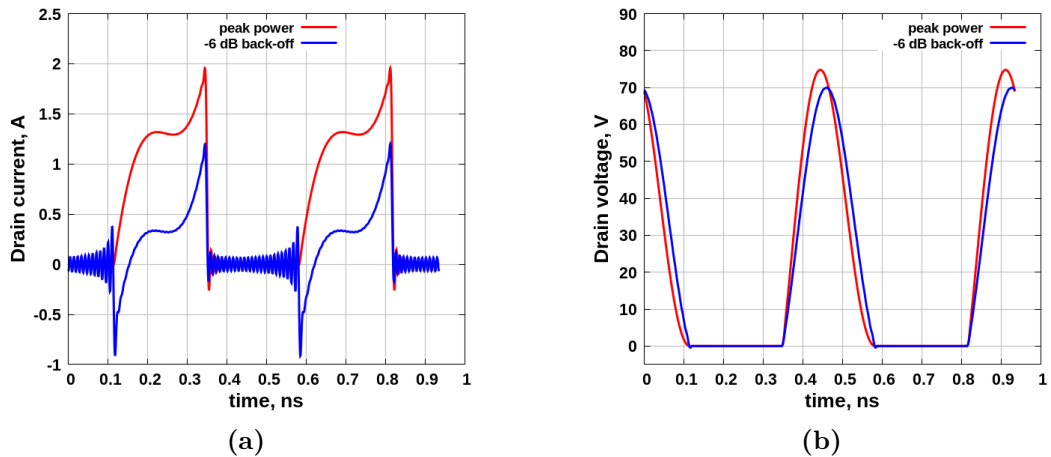
Fig. 3.8 Simulated waveforms for the peak and back-off power levels ($q = 1.85$): (a) - current waveforms; (b) - voltage waveforms.

will be the same as the effect of an square wave with 50% duty cycle. The parallel resonator consisting of a lumped capacitance $C0$ and a lumped inductance $L0$ has a loaded Q-factor $Q_L = 100$, which is sufficently high to provide harmonics supression.

The load network was optimized for the values of output power $P_{out} = 12$ W, operating frequency $f_c = 2.14$ GHz, drain supply voltage $V_{cc} = 20$ V. As well as in the previous section, three cases are considered: $q = 1.4$, $q = 1.61$, $q = 1.85$. All the circuit components are simulated as ideal components without losses. The simulated voltage and current switch waveforms for the PA with $q = 1.85$ are shown in Fig. 3.8. From these plots it can be seen, that the waveforms calculated analytically are in very good agreement with the simulated plots. The impedance is calculated for the peak power and for back-off power levels -3 dB, -6 dB, -9 dB, -12 dB. The

Table 3.1 Simulated output power and drain efficiency for different output load impedance values.

$\mathbf{P}_{\text{BO}}$, dB	$\mathbf{Z}_{\text{L}}$, ohm	$\mathbf{P}_{\text{out}}$, W	η_{drain}, %
q = 1.4, $L_{\mathbf{s}}$ = 2.5 nH, $C_{\mathbf{p}}$ = 1.1 pF			
0	16.0 - j12.5	12.0	100
-3	14.8 - j1.74	6.0	100
-6	9.4 + j4.6	3.00	99.9
-9	5.0 + j6.76	1.50	99.7
-12	2.56 + j7.34	0.75	99.3
q = 1.61, $L_{\mathbf{s}}$ = 1.56 nH, $C_{\mathbf{p}}$ = 1.36 pF			
0	14.2 + j0.14	12.0	100
-3	12.2 + j9.3	6.0	100
-6	7.5 + j14.0	3.00	99.9
-9	3.95 + j15.6	1.50	99.7
-12	2.0 + j16.0	0.75	99.3
q = 1.85, $L_{\mathbf{s}}$ = 0.82 nH, $C_{\mathbf{p}}$ = 1.97 pF			
0	11.1 + j8.7	12.0	100
-3	8.4 + j14.9	6.0	100
-6	4.8 + j17.6	3.00	99.9
-9	2.5 + j18.4	1.50	99.6
-12	1.26 + j18.7	0.75	99.1

output power and drain efficiency simulated in ADS are presented in Table 3.1. From the presented results one can see that even for the ideal case, the efficiency of the PA decreases for back-off power level. The reason for that is harmonics, that are generated due to a quick change of the drain current at the moment $x = 0$.

3.5 Output load matching

As it has been shown in Section 3.1, for the ideal class-E operation it is necessary to provide a specific load impedance, which is complex in the general case. However, for most practical applications it is necessary to match the output load to a standard
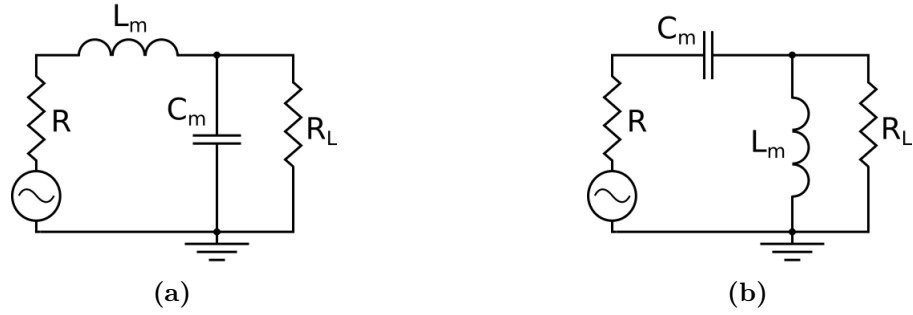
Fig. 3.9 L-shaped matching circuits: (a) - low-pass circuit; (b) - high-pass circuit.

50 ohm transmission line. The easiest way to implement the matching using lumped components is using an *LC*-matching circuit [107]. For example, if the value of a source active impedance R and the value of a load active impedance R_L and $R_L > R$, the impedance matching can be performed using two *LC*-circuit configurations, as shown in Fig. 3.9. The matching network consists of two reactive elements - a capacitance C_m and an inductance L_m, and can be implemented either in the form of a low-pass circuit 3.9(a) or a high-pass circuit 3.9(b). In the former case the circuit elements can be found from the following expressions:

$$L_m = \frac{RQ_L}{\omega} \tag{3.60}$$

$$C_m = \frac{Q_L}{R_L\omega} \tag{3.61}$$

where Q_L is the loaded Q-factor of the matching circuit, which is defined by the following expression:

$$Q_L = \sqrt{\frac{R_L}{R} - 1} \tag{3.62}$$

If the matching circuit is implemented in the form of a high-pass circuit, the series capacitance and the parallel inductance can be found from the following expressions:

$$L_m = \frac{R_L}{\omega Q_L} \tag{3.63}$$

$$C_m = \frac{1}{\omega R Q_L} \tag{3.64}$$

The impedance matching can also be implemented using T-shaped and π-shaped matching circuits which consist of three reactive elements [107]. This approach may be useful if the reactive part of an output load impedance cannot be incorporated into an LC-circuit. Besides, the loaded Q-factor of a 3-element matching circuit can be chosen by adjusted by a designer, however it will always be higher than the loaded Q-factor defined by (3.62), which in turn reduces the bandwidth of a PA.

3.6 Implementation with transmission lines

The load network considered in the previous chapters consists of lumped components. However, microwave power amplifiers are often implemented using transmission lines, such as microstrip lines, coplanar waveguides (CPW) etc. A transition from a lumped components prototype to a transmission line circuit can be performed by applying Richard's transformation and Kuroda identities.

A diagram of a class-E PA load network implemented using transmission lines is shown in Fig. 3.10. The shunt capacitance C_p can be implemented with an open-circuited section of a transmission line, however, it is often represented by a device output capacitance. The series inductance L_s can be replaced with a short line section, whose electrical length can be approximately estimated using the following expression [19]:

$$\theta_\mathrm{s} \approx \arctan\left(\frac{\omega L_\mathrm{s}}{Z_\mathrm{s}}\right) \tag{3.65}$$

where Z_s is the characteristic impedance of the line, ω is the operating angular frequency. In practical amplifiers inductance L_s is partially formed by device bondwire inductance, which makes the electrical length θ_s smaller.

The resonator $L_0 C_0$ can be implemented using two sections of transmission line with electrical length 45° and characteristic impedance:

$$Z_0 = \omega L_0 = \frac{1}{\omega C_0} = QR \tag{3.66}$$
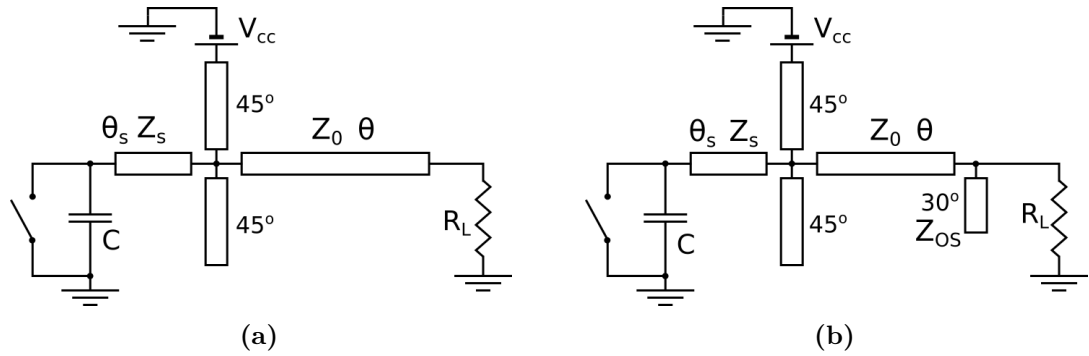
Fig. 3.10 Output circuit of the class-E PA with shunt capacitance and shunt filter
designed with transmission lines: (a) - a single line output matching; (b) - an
L-shaped line output matching.

From (3.66) it follows, that the higher the characteristic impedance of the lines, the
higher the loaded Q-factor of the resonator.

The matching of the output load to the optimum load impedance can be realized
in several ways. In the simplest case the matching can be performed either by a single
transmission line section or an L-shaped transmission line section. If the optimum
load impedance is $Z = R + jX$, then the parameters of a single transformer line can
be derived by solving a system of two equations:

$$R = \frac{Z_0^2 R_{\mathrm{L}}(1 + \tan^2 \theta)}{Z_0^2 + R_{\mathrm{L}}^2 \tan^2 \theta} \tag{3.67}$$

$$X = \frac{(Z_0^2 - R_L^2) Z_0 \tan \theta}{Z_0^2 + R_{\mathrm{L}}^2 \tan^2 \theta} \tag{3.68}$$

where R_{L} is the load of an output transmission line (usually 50 ohm), Z_0 and θ are
the characteristic impedance and the electrical length of the transformer respectively.
It should be noted that if the optimum load reactance $X = 0$ ($q = 1.61$), the
single matching line becomes a well-known quarterwave impedance transformer with
characteristic impedance $Z_0 = \sqrt{RR_{\mathrm{L}}}$. If $q > 1.61$, the optimum impedance becomes
inductive ($X > 0$), and therefore, if $R < R_{\mathrm{L}}$, the impedance matching line becomes
longer than 90°. If $q < 1.61$, the optimum load is capacitive and the electrical length
of the transformer should be less than 90°.

An impedance matching can also be implemented using an L-shaped transmission line, as shown in Fig. 3.9. In this case the open stub usually has 30° electrical length and provides additional third harmonic suppression. At the fundamental frequency this stub can be considered as a capacitance connected in paralled with the active load:

$$C_{\mathrm{OS}} = \frac{\tan 30°}{\omega Z_{\mathrm{OS}}} \tag{3.69}$$

where Z_{OS} is the characteristic impedance of the open stub. The length of the series segment of the line and its characteristic impedance can be found by solving the system of equations (3.67) and (3.68), where the active load R_{L} needs to be replaced with a parallel connection of R_{L} and the capacitance defined by (3.69).

It should be noted that the derivation of the transmission lines parameters outlined in this section is based on the assumption, only transverse electromagnetic (TEM) waves exist in the line. This assumption is valid for coaxial lines and for striplines. Most PAs are implemented with microstrip line technology, where quasi-TEM waves propagate. However, the approximate result given by expressions (3.67) and (3.68) provide sufficient accuracy in most cases and can be improved using more accurate microstrip line models or by electromagnetic simulation.

3.7 Implementation with GaN HEMT transistor

Until now all the calculations have been performed assuming that the active device operates as an ideal switch. In order to implement a PA, a model of a real device must be used. Compared to other semiconductors, gallium nitride (GaN) has wide bandgap (3.4 eV), and consequently is able to withstand higher power density. Therefore, for the same output power a GaN HEMT device will have a smaller size, which in turn provides smaller output capacitance and low saturation resistance. Besides, due to relatively small output parasitic reactance, it is easier to provide wideband operation of a PA.

Fig. 3.11   ADS schematic of a GaN HEMT class-E PA operating at 2.14 GHz.
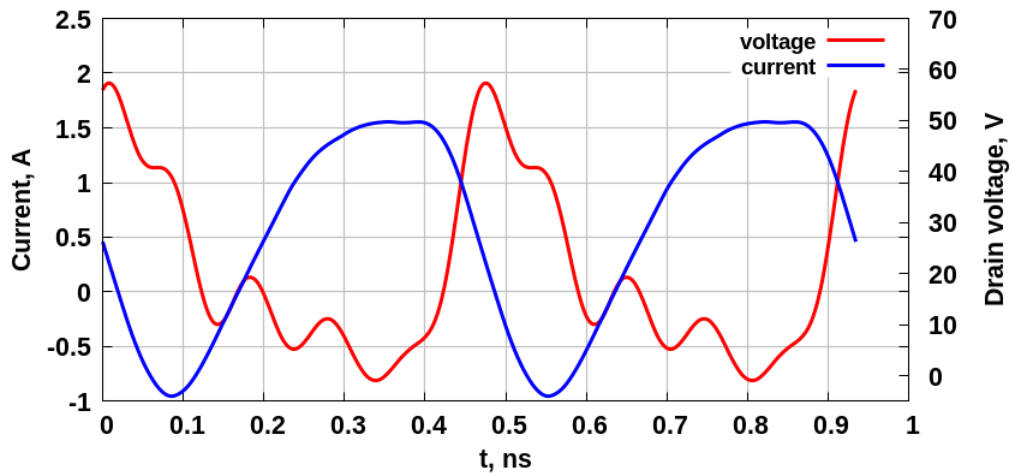
Fig. 3.12   Simulated voltage and current waveforms of Class-E GaN HEMT power amplifier.

In order to experimentally demonstrate the class-E operation, a GaN HEMT device Cree CGH40010F was used [108]. The schematic of a single-ended class-E PA operating at its peak power is shown in Fig. 3.11. The PA is optimized for operation at the frequency 2.14 GHz and at the peak power level of 10W. The input and output circuits are modelled using microstrip line models with the substrate RO4350B with 0.762 mm thickness. The input signal is a single-tone power source with 30 dBm output power. The behaviour of the PA was analyzed using the harmonic balance simulator, and the number of harmonics was set to 50.

The shunt capacitance of the PA is represented by the drain-source capacitance of the packaged device, and according to the datasheet $C_{\mathrm{p}} \approx 1.3$ pF. The drain supply voltage for the transistor is 28 V, however, since there is some voltage drop across the drain-source transition in the on-state, the voltage in the model is assumed to be 20 V. Following the procedure outlined in Section 3.1 one can calculate the following output circuit parameters:

- $q = 1.71$

- $L_{\mathrm{s}} = 1.46$ nH

- $C_{\mathrm{p}} = 1.3$ pF

- $Z_{\mathrm{peak}} = 15.7 + j5.3$ ohm

The series inductance L_{s} is partially represented by a short section of a microstrip line connected to the drain of the transistor, and partially by the drain bondwire. The L-shaped transmission line provides a matching of the standard output line impedance 50 ohm to the optimum peak power impedance Z_{peak}. The open microstrip stub is adjusted to minimize the third harmonic of the output signal. The input circuit provides the matching of a device input impedance $Z_{\mathrm{in}} \approx 2.7 + j0.5$ ohm to the standard 50 ohm transmission line. In order to provide stability, a bias voltage is connected through a 10 ohm resistor. The simulated input matching is presented in Fig. 3.13(a).

The simulated PA demonstrates drain efficiency of 85% with output power 10 W. The drain current and voltage waveforms simulated at the frequency 2.14 GHz are shown in Fig. 3.12. From these plots one can see, that the high efficiency is achieved by minimizing the overlap between drain voltage and current in the time domain. However, due to the finite saturation resistance and non-ideal harmonic supression, the maximum drain efficiency is below 90% [19]. The gain and drain efficiency dependence on the input power is presented in Fig. 3.13(b).

The optimized PA was fabricated on RO4350B substrate as shown in Fig. 3.15(a). In order to prevent overheating, the PA was installed on a brass heatsink. The input
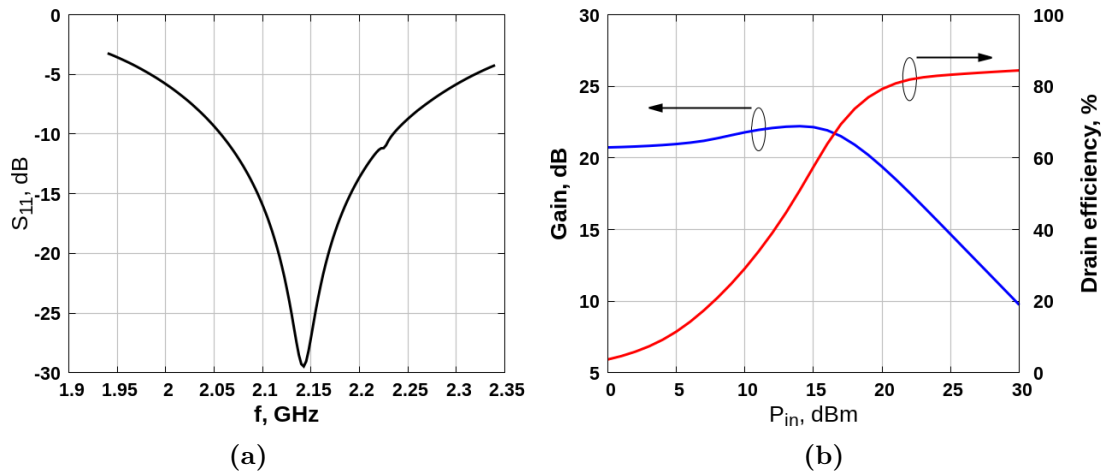
Fig. 3.13 Simulated results for a GaN HEMT Class-E PA with shunt capacitance and shunt filter: (a) - a single line output matching; (b) - an L-shaped line output matching.
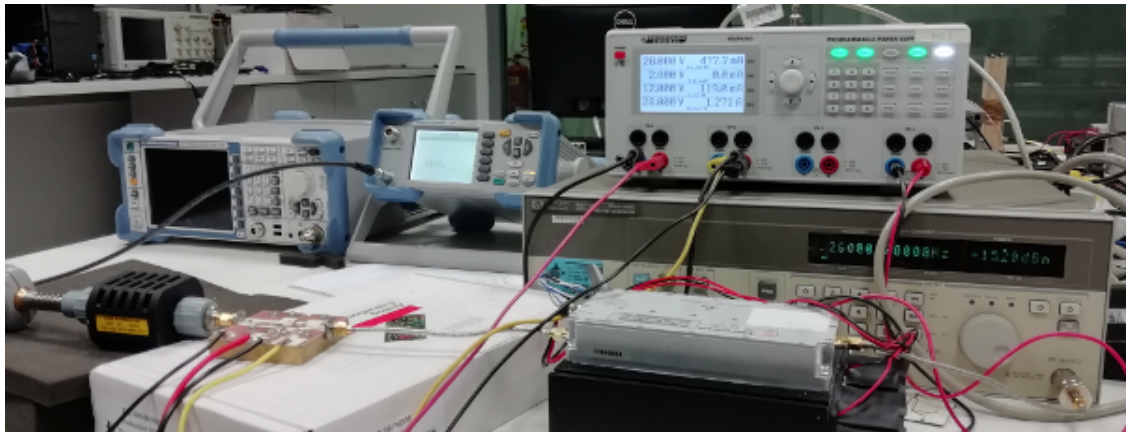
Fig. 3.14 A class-E PA test setup.

and output microstrip lines are connected to coaxial cables through subminiature version A (SMA) connectors. The gate bias line and the inductance of the output resonator are connected DC voltage supplies using decoupling capacitors. The performance of the fabricated PA was tested with a single tone excitation using a test setup shown in Fig. 3.14. The single tone signal was generated from an HP83712 signal generator and preamplified with a linear EMPOWER driver PA to the level +40 dBm. The output power of the PA was measured using a Rohde&Schwarz NRP power meter. The measured output power and drain efficiency are presented in Fig. 3.15(b).
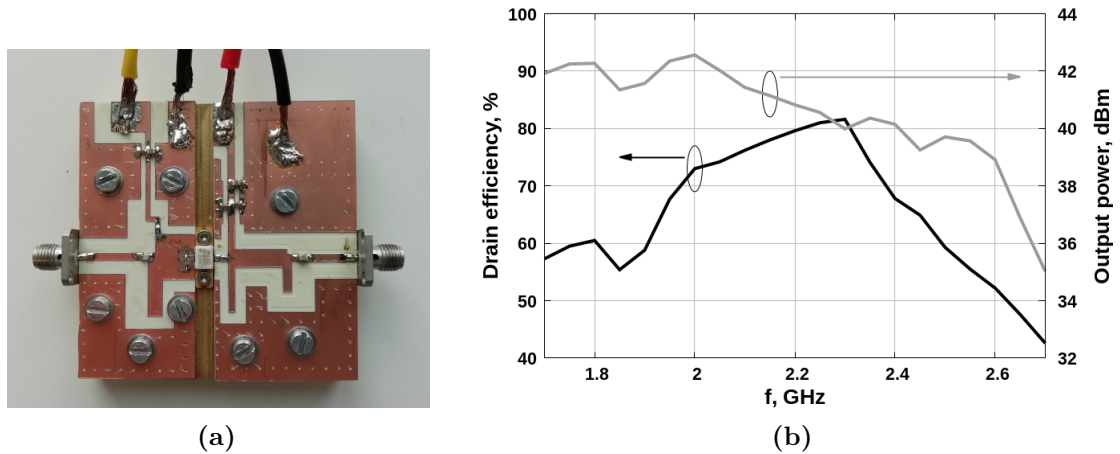
Fig. 3.15 Fabricated class-E PA: (a) - PA board; (b) - measured drain efficiency and output power.

3.8 Conclusions

In this chapter a novel analysis of the class-E power amplifier with shunt capacitance and shunt filter was presented in order to analyze the behaviour of a PA under back-off power conditions. The values of a series inductance and parallel capacitance are found from the peak power operation conditions, assuming that the ZVS and ZVDS conditions are fulfilled. As it has been shown, each value of back-off output power can be achieved adjusting the value of the output load only, assuming the only the the ZVDS condition is violated. The results achieved using the proposed analytical model have been proven using the ideal simulations in Keysight ADS circuit simulator. The operation of the class-E PA at the peak power level was demonstrated by implementing a single-ended class-E PA using a GaN HEMT transistor. The PA was optimized for the central frequency 2.14 GHz and the output power of 10W and fabricated on RO4350B substratre. The experimental results are demonstrated.

Chapter 4

Wideband operation of the class-E power amplifier with shunt capacitance and shunt filter

In Chapter 1 it has been mentioned that the channel capacity of a wireless channel is proportional to the bandwith. Consequently, one of the main trends in wireless communication systems development is extending the bandwidth occupied by RF signals. Indeed, according to the 3GPP standard, the bandwidth for the LTE signals is up to 100 MHz, and for 5G systems the maximum bandwidth is 100 MHz for the FR1 range and 400 MHz for the FR2 range. Along with providing sufficient bandwidth for a particular signal, many RF systems should provide reconfigurable or multiband operation. Each of these operation conditions impose additional requirements on the operational bandwidth of the RF transmitters.

In this chapter a wideband class-E PA with shunt capacitance and shunt filter is demonstrated. Firstly, the reactance compensation technique and double reactance compensation technique as a way of extending the bandwidth of resonant circuits is discussed. Secondly, the application of this technique to extend the bandwidth of a class-E PA is presented. Lastly, a novel wideband class-E PA based on a GaN HEMT transistor is demonstrated. The simulated and measured results are presented.
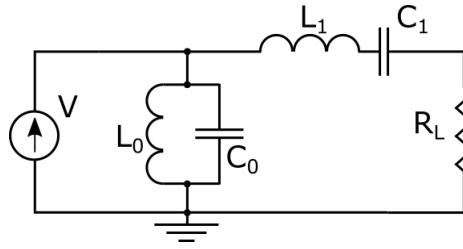
Fig. 4.1 Reactance compensation of a shunt filter resonator.
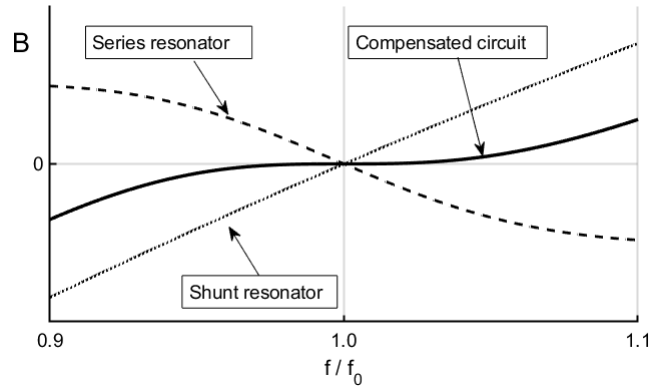
Fig. 4.2 Input susceptance of a shunt resonator, series resonator and combined compensated circuit.

4.1 Reactance compensation technique

The reactance compensation technique was initially proposed in [109] as a way of improving gain-frequency response of diode parametric amplifiers. If an amplifier has an output shunt resonator for harmonic supression, the operating frequency range can be extended by adding a series resonator, as shown in Fig. 4.1. It was shown that the bandwidth of a shunt resonator can be maximized if the first derivative of input susceptance becomes zero at the resonant frequency [110]:

$$\left.\frac{dB}{d\omega}\right|_{\omega=\omega_0} = 0 \tag{4.1}$$

In a similar manner, the bandwidth of a series resonator is maximized by connecting a shunt resonator to the output. In this case, the first derivative of input reactance becomes zero:

$$\left.\frac{dX}{d\omega}\right|_{\omega=\omega_0} = 0 \tag{4.2}$$
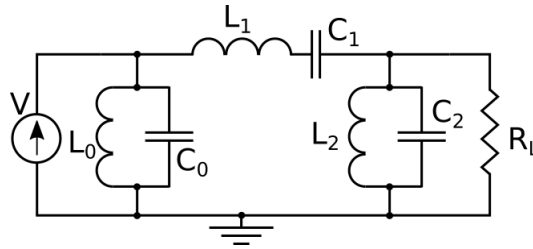
Fig. 4.3 Double reactance compensation of a shunt filter resonator.
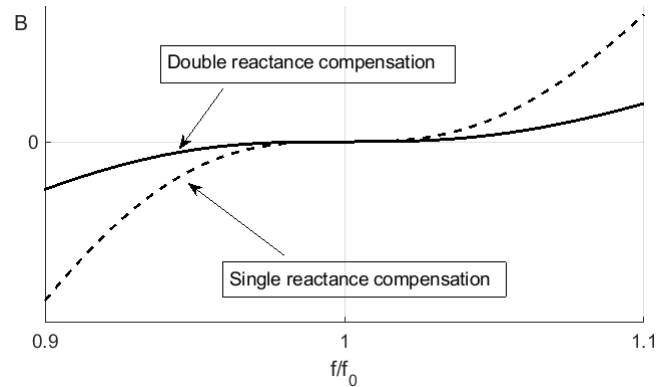
Fig. 4.4 Input susceptance of a shunt resonator, series resonator and combined compensated circuit.

The principle of the reactance compensation technique can be demonstrated if the frequency response of a series and the parallel resonators are considered separately, as shown in Fig. 4.2. From these plots one can see, that the input susceptance of a shunt resonator increases with frequency, while the input susceptance of a series resonator decreases. If the two resonators are combined together and the loaded Q-factors are adjusted so that the condition (4.1) is fulfilled, the overall susceptance has zero slope, as shown in Fig. 4.2, and the overall bandwidth is increased.

In [110] it was shown that the bandwidth of a resonant circuit can be further increased by adding two or more resonant circuits, as shown in Fig. 4.3. If two compensating resonators are connected to the output of the first resonator, the technique is called double reactance compensation technique. In Fig. 4.3 the first resonator is a shunt resonator, and therefore, the second LC-circuit is connected in series, and the third LC-circuit is connected in parallel. However, in a case of series resonator bandwidth extension, the second circuit would be connected in parallel, whereas the third resonator would be connected in series.

In a case of double reactance compensation technique of a shunt resonator (see Fig. 4.4), the circuit parameters are chosen in order to satisfy the following conditions for the input susceptance:

$$B\Big|_{\omega=\omega_0} = 0 \tag{4.3}$$

$$\frac{dB}{d\omega}\bigg|_{\omega=\omega_0} = 0 \tag{4.4}$$

$$\frac{d^3B}{d\omega^3}\bigg|_{\omega=\omega_0} = 0 \tag{4.5}$$

It should be pointed out, that if all three conditions (4.3) - (4.5) are fulfilled, the second derivative of the input susceptance is set to zero automatically [110]. It also should be noted, that in most cases an analytical solution of the equations (4.3) - (4.5) lead to very complex mathematical expressions, which makes the direct application of this technique impractical. However, various numerical optimization techniques can be used in order to minimize the input susceptance or reactance derivatives.

4.2 Extension of the bandwidth of a class-E PA

In order to increase operational bandwidth several structures of the class-E PA have been proposed [111–113]. However, the maximum frequency range of such a PA is limited by the parasitic drain capacitance of the transistor. Another approach to achieve high efficiency across wide frequency range is called continuous class-F PA [34, 114]. Using this technique broadband operation is achieved by drain impedance adjustment at fundamental, 2nd and 3rd harmonics across the required frequency range. However, this approach requires a load circuit containing several resonators.

Since its introduction in [109, 110] the reactance compensation technique has been used to extend the bandwidth of power amplifiers. In [115] a GaAs MESFET amplifier demonstrating gain ripple of ±0.1 dB across the frequency range 3.7 - 4.2 GHz was demonstrated. In [116] an analytical design approach to calculating load network parameters of class-E PA was presented. A parallel circuit class-E PA based
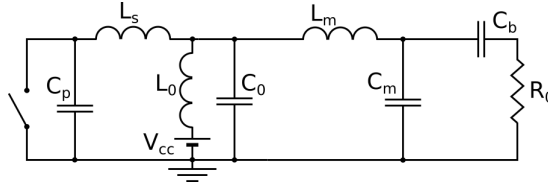
Fig. 4.5 Equivalent circuit of a class-E PA with matching circuit.
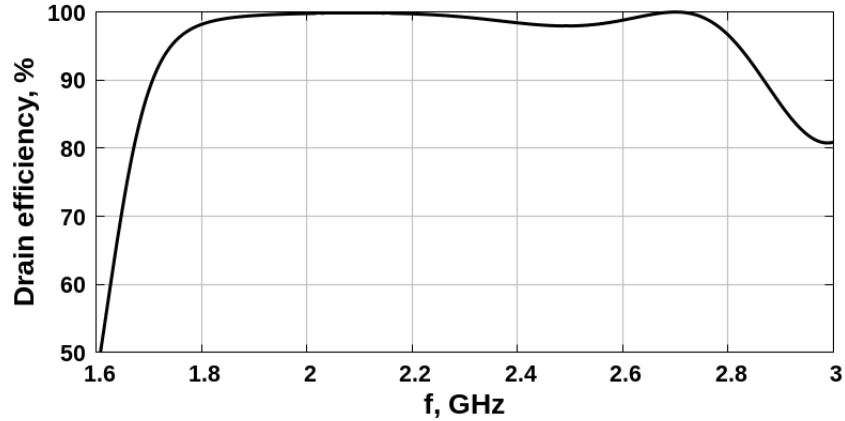
Fig. 4.6 Drain efficiency of the simulated ideal class-E PA (active device is simulated as an ideal switch).

on a laterally-diffused metal-oxide semiconductor (LDMOS) transistor was presented in [117]. The proposed PA provided drain efficiency over 74% across the frequency band 136 - 174 MHz, maintaining output power of 8W with 0.7 dB variation.

As it was mentioned previously in Chapter 3, a class-E PA with shunt capacitance and shunt filter is able to incorporate the device parasitics into the PA load structure, has relatively high output load impedance and finite DC-feed inductance. All of these factors make possible switchmode operation across a wide frequency range. The main objective of the presented design is a class-E PA providing high drain efficiency across the frequency range 1.7 - 2.7 GHz, and output power 40 dBm. The presented power amplifier is build on a GaN HEMT transistor CGH40010F. The equivalent circuit of a class-E PA with matching circuit is shown in Fig. 4.5. The PA is optimized for the output power of 10W and carrier frequency 2.14 GHz. The values the parallel capacitance C_{p} and the series inductance L_{s} were found in Chapter 3: $C_{\mathrm{p}} = 1.3$ pF, $L_{\mathrm{s}} = 1.46$ nH. The resonator $L_0 C_0$ is tuned to the carrier frequency. The matching circuit $L_{\mathrm{m}} C_{\mathrm{m}}$ provides impedance transformation from the standard
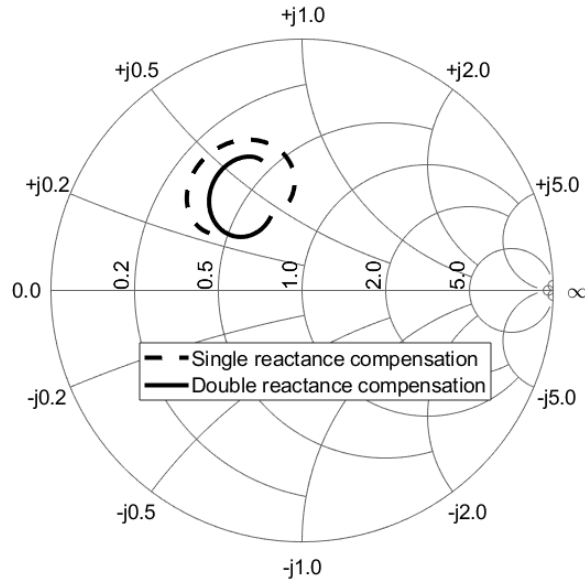
Fig. 4.7 Simulated load impedance for single reactance compensation and double reactance compensation.

load 50 ohm to the required impedance $Z_1 = 15.7 + j5.3$ ohm. The calculated values of the matching circuit are: $C_m = 2.196$ pF, $L_m = 1.727$ nH. By adjusting the loaded Q-factor of the shunt resonator and the matching circuit components, drain efficiency of higher than 90% was achieved across the frequency range 1.7 - 2.8 GHz, as shown in Fig 4.6.

At microwave frequencies the input and output circuits of an amplifier are often implemented with transmisson lines. The load network of a wideband class-E PA with shunt capacitance and shunt filter can be implemented with microstrip transmission lines as was shown in Fig. 3.10. The shunt capacitance can be fully replaced by the output drain-source capacitance of a transistor, and the series inductance L_s is replaced with a section of a microstrip line. The output load matching can be realized with either a straight section of transmission line (see Fig. 3.10(a)), or an L-shaped section (see Fig. 3.10(b)). In the latter case, the open stub provides the third harmonic suppression, while at the fundamental it can be described as a shunt capacitance. Consequently, the L-shaped line is an equivalent of the $L_m C_m$ circuit in Fig. 4.5, and the load network in Fig. 3.10(b) implements the double reactance compensation technique. The simulated drain impedance

for the single reactance compensation and the double reactance compensation are shown in Fig. 4.7. From these plots it can be seen, that the double reactance compensation technique implemented with microstrip transmission line can provide better impedance stabilization, and therefore, provides better efficiency across the required frequency range.

4.3 Design of wideband class-E PA

The design procedure for the wideband PA consists of two parts: input circuit design and output circuit design. The input network should transform the device input impedance to the standard 50 ohm line across the required frequency range, and the output circuit should provide the class-E operation across the frequency band. Both the input and output networks are implemented using microstrip transmission lines on the substrate RO4350B with dielectric constant 3.48.

4.3.1 Input circuit design

In Chapter 3 a class-E PA was demonstrated with a simple input circuit that transforms the input device impedance ($Z_{\text{in}} \approx 2.7 + j0.5$) to the standard 50 ohm line at one 2.14 GHz. However, for wideband operation broadband matching is required, which would provide the necessary impedance transformation across the fractional bandwidth:

$$BW = \frac{2.7\ GHz - 1.7\ GHz}{2.14\ GHz} \approx 0.47$$

Consequently, the loaded Q-factor of the matching circuit should be:

$$Q_{\text{L}} = \frac{f_{\text{c}}}{\Delta f} = 2.14$$

where f_{c} is the central frequency, and Δf is operational bandwidth. It is well-known, that the bandwidth of a matching network transforming a resistance R_1 to a resistance R_2 can be extended if the impedance R_1 is transformed to a certain
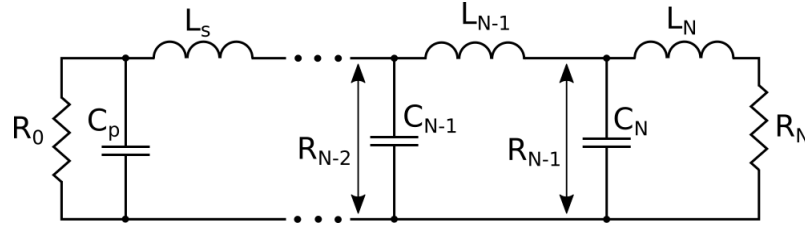
Fig. 4.8 Wideband matching circuit with lumped components.

intermediate impedance R_i and then to the required impedance R_2. In order to extend the bandwidth, the following inequalities must be fulfilled:

$$R_1 < R_i < R_2$$

The more intermediate stages are added, the wider operational bandwidth can be achieved. Each impedance can be transformed to the next one using an LC matching circuit, as shown in Fig. 4.8. At RF the impedance transformation from R_N to intermediate stages R_i and then to R_0 is performed by microstrip transmission lines. The optimized topology of the input circuit is shown in Fig. 4.9. The gate bias voltage is supplied through a section of a transmission line and a resistor. This bias structure provides isolation of voltage supply and stability at the same time. The simulated S_{11} versus frequency is presented in Fig. 4.10.

4.3.2 Load network design

The microstrip load network optimized for wideband class-E operation is presented in Fig. 4.9. As well as for the narrowband case, the shunt capacitance is implemented with the device output capacitance, the shunt filter consists of two microstrip lines 45° each. The standard 50 ohm load is transformed to the required impedance using an L-shaped microstrip line. The output transmission line topology is optimized using the presented technique in order to minimize the first and third derivatives of the susceptance that the device drain sees. The whole structure is then optimized in order to maximize the drain efficiency across the given bandwidth.
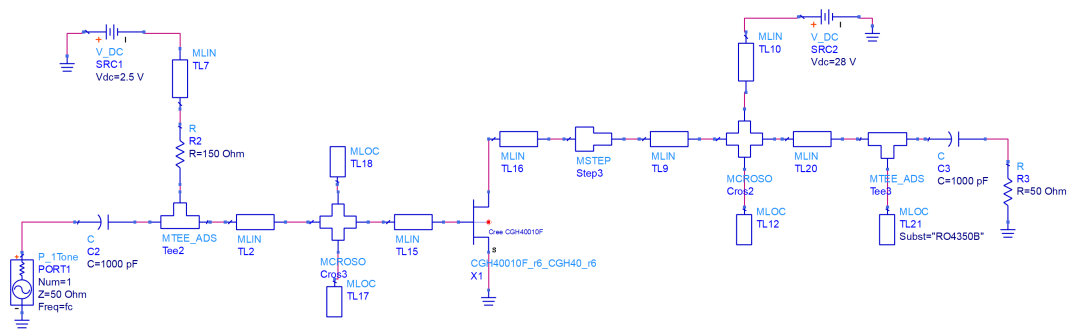
Fig. 4.9 Optimized schematic of the broadband class-E PA.
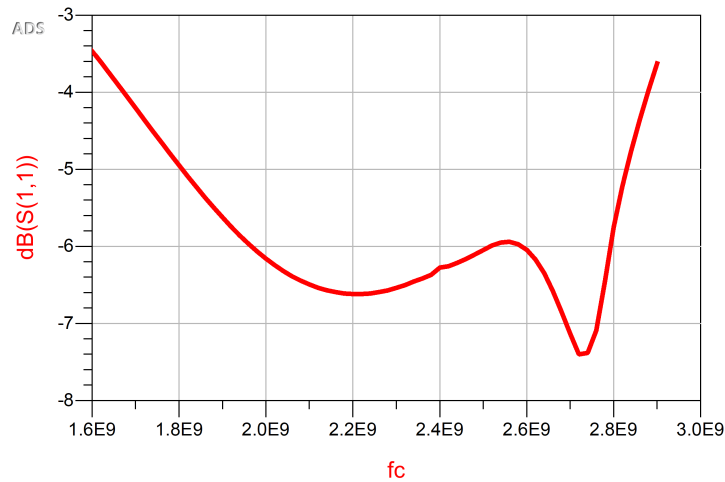
Fig. 4.10 Input matching of the optimized wideband PA.

4.4 Implementation and Measured Results

The optimized PA structure was simulated using the harmonic balance solver from Keysight ADS simulation tool. In the simulation a model of GaN HEMT device CGH40010F was used which enabled the optimization of the input and output circuits of the PA taking into account device parasitic reactance. The simulated results for output power and drain efficiency are shown in Fig. 4.11. The voltage and current waveforms at the 1.8 GHz and 2.7 GHz are presented in Fig 4.12 and Fig 4.14. From these plots one can see, that high drain efficiency is provided by minimizing current and voltage waveforms intersection across the frequency range. However, it should be pointed out, that the CGH40010F device model does not provide access to the

71
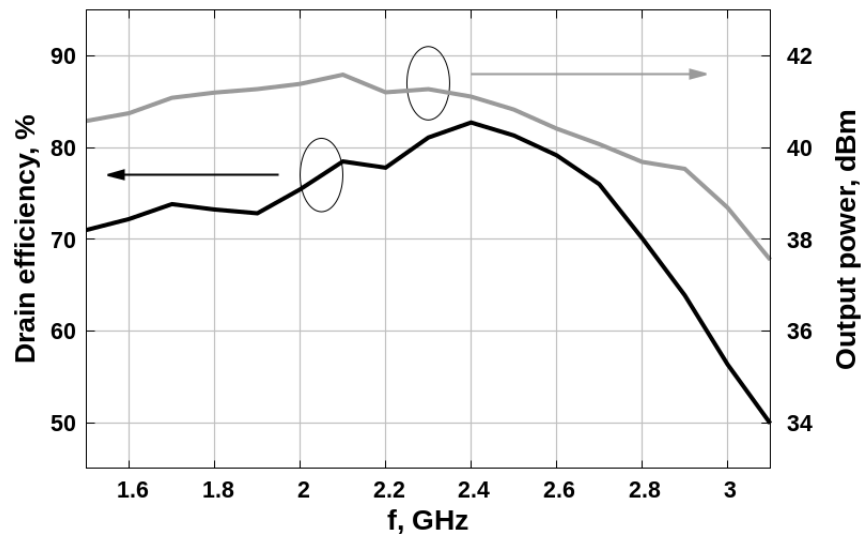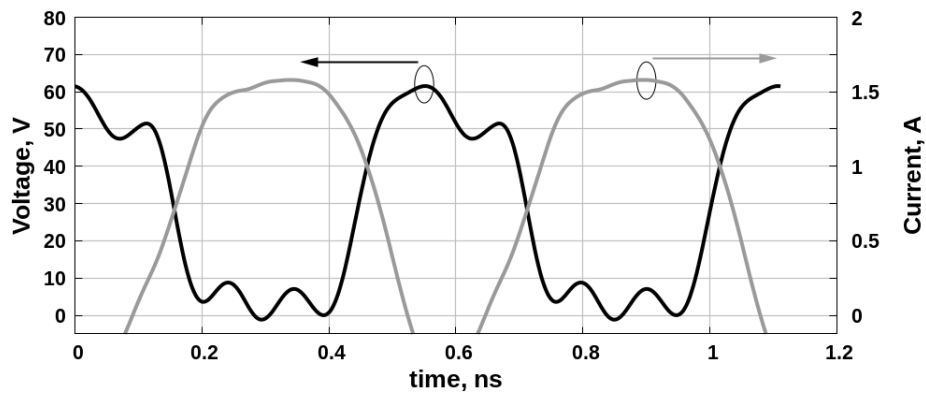
Fig. 4.11 .

Fig. 4.12 Simulated drain and current waveforms at 1800 MHz.

intrinsic device drain, and the waveforms shown in Fig. 4.12 - 4.14 are taken at the packaged device bondwire.

The optimized PA was manufactured using CGH40010F GaN HEMT packaged transistor as shown in Fig. 4.15. The input and output circuits were implemented on Rogers RO4350B substrate with dielectric constant 3.66 and thickness 0.762 mm. The transistor and both the input and output microstrip boards are installed on a brass heatsink, which provides sufficient heat dissipation. The fabricated PA has a very compact output circuit ($0.164\lambda \times 0.164\lambda$ mm), which makes it suitable for highly integrated transmitters.
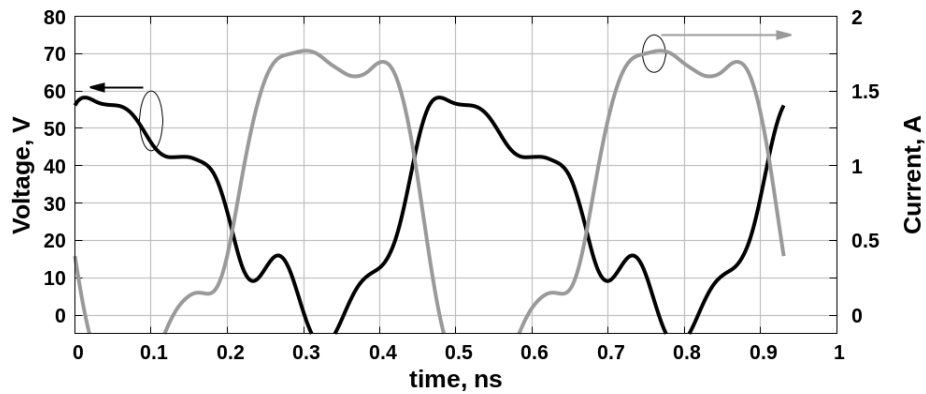
Fig. 4.13   Simulated drain and current waveforms at 2150 MHz.
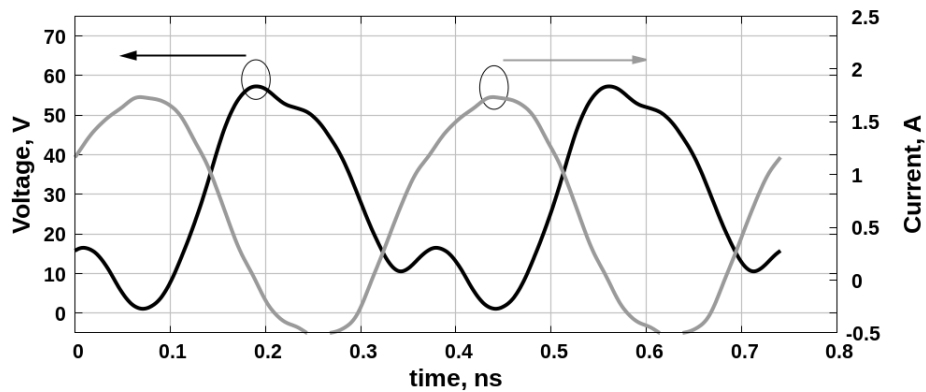
Fig. 4.14   Simulated drain and current waveforms at 2700 MHz.

The efficiency of the PA was tested using single-tone signal. The signal was generated from HP83712B generator and preamplified to the level of 30 dBm using a linear PA EMPOWER CA90301. The frequency of the input signal was swept from 1.4 to 3.1 GHz. Since the gain of driver preamplifier depends on frequency, a look-up table was created in order to keep the input power of the tested PA around 1W. The output power was measured using Rohde&Schwarz NRP-Z23 power meter. It should be pointed out, that for the ideal class-E operation the input signal must have a rectangular form in the time domain. However, when a sinusoidal input signal is applied that overdrives the active device between saturation and cut-off, the performance of the PA can be tested with this signal without significant loss of efficiency [19].
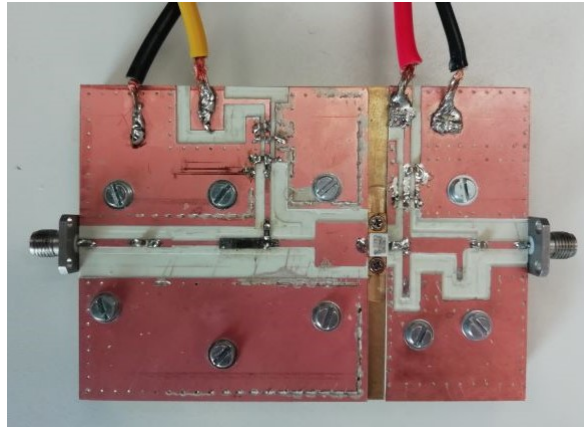
Fig. 4.15 Fabricated wideband class-E PA.
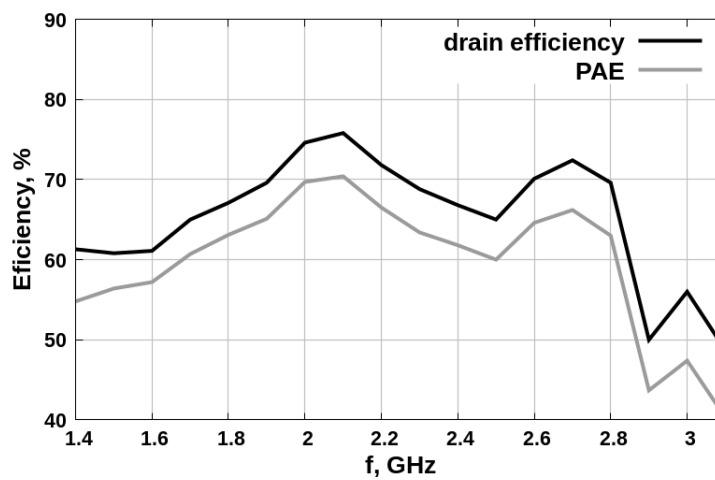
Fig. 4.16 Measured efficiency of the fabricated PA

Table 4.1 Switchmode PA comparison.

PA	Class of operation	Frequency, GHz	P_{out}, dBm	Drain efficiency
[111]	Class-E	1.9-2.4	35-38.7	> 54%
[112]	Class-E	2.1-2.7	39.7-41	> 56%
[112]	Class-E	2.0-2.5	38.5-41.1	> 75%
[34]	Class-F	2.15-2.65	40.6-41.8	> 65%
[15]	Class-E	1.4-2.7	39.7-41.5	> 63%
This work	**Class-E**	**1.7-2.8**	**40.3-42.3**	> 65%
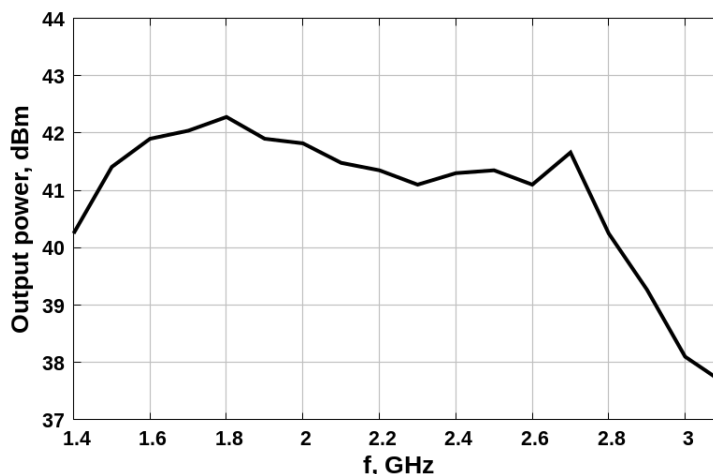
Fig. 4.17   Measured output power of the fabricated PA

The measured output power and drain efficiency are shown in Fig. 4.16 and Fig. 4.17. From these plots one can see that the proposed PA provides over 65% drain efficiency across frequency band 1.7 - 2.8 GHz and over 60% drain efficiency across frequency band 1.4 - 2.8 GHz. The variation of output power is 2 dB across frequency range 1.4 - 2.8 GHz. The comparison if the demonstrated PA with other amplifiers is presented in Table 4.1.

It should be noted that when a PA is operating in a switchmode, the output power is almost independent of the input power level. Therefore, when operating in class-E mode, the PA introduces strong nonlinearity in the transmitted signal. For this reason, this type of PA can be used in transmitters realizing load modulation concept, such as Doherty or outphasing PA.

4.5   Conclusion

A broadband class-E PA with shunt capacitance and shunt filter has been described. In the proposed design, an L-shaped output matching section and shunt resonator are used to compensate for the reactance variation in the *LC*-circuit. The proposed technique has been demonstrated on a PA built using a GaN HEMT transistor. The fabricated PA shows over 65% drain efficiency across frequency range 1.7-2.8 GHz, 60% drain efficiency across frequency range 1.4-2.8 GHz, and 2 dB variation of

output power. The fabricated PA has a very compact output circuit which makes it suitable for highly integrated 5G transmitters.

Chapter 5

Load modulation transmitters based on class-E PA

In the previous chapters it has been mentioned, that when a PA is driven in a switch-mode, the output signal level weakly depends on the input signal level. Therefore, if such a PA is used on its own for transmission of an amplitude modulated signal, the signal will suffer from strong nonlinear distortion. Therefore, in most cases switch-mode amplifiers are used in complex transmitter blocks, such as Doherty, outphasing transmitters and envelope tracking transmitters. These types of transmitters provide improved efficiency for the signals with amplitude modulation. When used with appropriate linearization technique, they can maintain low level of distortion along with high efficiency.

In this chapter we demonstrate the usage of class-E PA with shunt capacitance and shunt filter in outphasing and Doherty PAs. Firstly, an analytical description of load modulation in outphasing PAs is presented. It is demonstrated how linearity can be achieved by adding an isolated resistor to a combiner. Secondly, an outphasing PA based on a class-E PA with shunt capacitance and shunt filter is proposed. It is shown, that by proper design of a nonisolated combiner, which provides the required impedance values for the peak and back-off power level, it is possible to maintain high drain efficiency across wide dynamic range of a signal. The possibility of building an
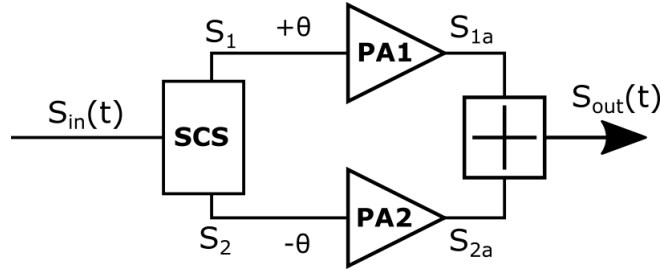
Fig. 5.1 A block-diagram of the outphasing transmitter.

outphasing PA with improved bandwidth is discussed. Lastly, a wideband Doherty PA, where both peaking and carrier amplifiers are implemented as class-E PAs with shunt capacitance and shunt filter is demonstrated.

5.1 Outphasing power amplifier principles

As it was discussed in Chapter 2, the outphasing PA transforms an amplitude and phase modulated signal into two phase modulated signals, as shown in Fig. 5.1. In modern transmitters this transform can be performed in the digital domain using the following expressions:

$$S_1(t) = \frac{S_{\text{in,max}}}{2} \cdot e^{+j\theta(t)} \tag{5.1}$$

$$S_2(t) = \frac{S_{\text{in,max}}}{2} \cdot e^{-j\theta(t)} \tag{5.2}$$

$$\theta(t) = \arccos\left(\frac{S_{\text{in}}(t)}{S_{\text{in,max}}}\right) \tag{5.3}$$

It should be pointed out, that the signal separation defined by expressions (5.1) - (5.3) is nonlinear and therefore causes significant bandwidth expansion, as shown in Fig. 5.2. After amplification, the signals S_{1a} and S_{2a} can be recombined together with one of the types of power combiners. The two main types of the combiners are: isolated combiners and non-isolated combiners. The properties of each type of combiner will be discussed in the following subsections.
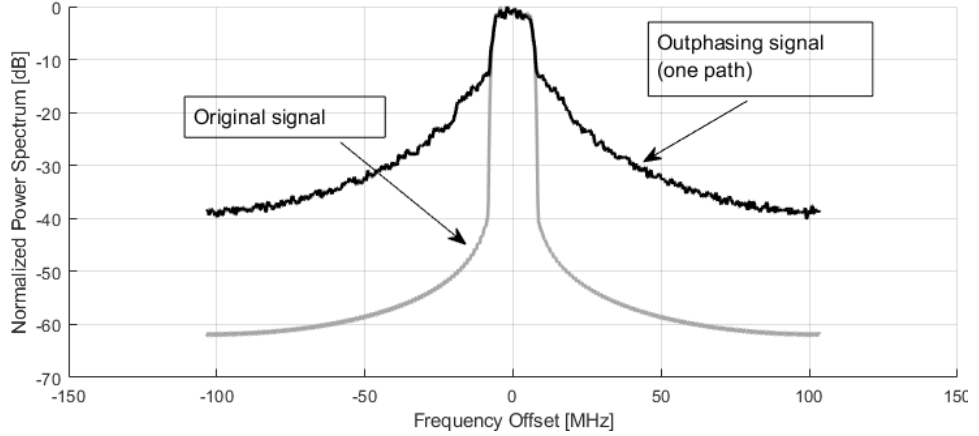
Fig. 5.2 Bandwidth expansion after outphasing signal separation.

5.1.1 Nonisolated outphasing combiners

In order to analyse the properties of the power combining structures, we consider a structure shown in the Fig. 5.3(a). It consists of two transmission lines connected to a load resistor R_{L}, which is usually active and represents input impedance of a transmitting antenna. The characteristic impedance of the lines is Z_{c}, their electrical length is 90° at the operating frequency and they are fed with two voltage sources with the same voltage magnitude V_0 and opposite phases. The phases of the input signals correspond to value of outphasing angle $\pm\theta$ defined by expression (5.3). The behaviour of the combiner at the junction is demonstrated in Fig. 5.3(b). This model consists of two current sources with currents: $\dot{I}_1 = I_0 e^{+j\theta}$ and $\dot{I}_2 = I_0 e^{-j\theta}$. Therefore, the current through the load R_{L} can be expressed as:

$$\dot{I}_{\mathrm{L}} = \dot{I}_1 + \dot{I}_2 = I_0(e^{+j\theta} + e^{-j\theta}) = 2I_0 \cos\theta \tag{5.4}$$

Hence, if the current magnitude I_0 is constant, the current through the load can be manipulated by variation of θ. The voltage that drops across the load will be:

$$\dot{V}_{\mathrm{L}} = I_0 R_{\mathrm{L}}(e^{+j\theta} + e^{-j\theta}) = 2I_0 R_{\mathrm{L}} \cos\theta \tag{5.5}$$
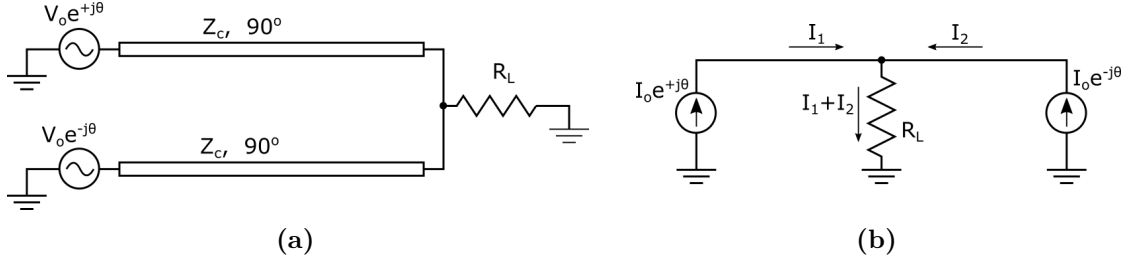
Fig. 5.3 Basic power combining structure: (a) - model with voltage sources; (b) - model with current sources.

From (5.5) it follows that the current sources will see the following impedance values:

$$Z_{\text{cs1}}(\theta) = \frac{\dot{V}_{\text{L}}}{\dot{I}_1} = \frac{2I_0 R_{\text{L}} \cos\theta}{I_0 e^{+j\theta}} = 2R_{\text{L}} \cos^2\theta - jR_{\text{L}} \sin 2\theta \tag{5.6}$$

$$Z_{\text{cs2}}(\theta) = \frac{\dot{V}_{\text{L}}}{\dot{I}_2} = \frac{2I_0 R_{\text{L}} \cos\theta}{I_0 e^{-j\theta}} = 2R_{\text{L}} \cos^2\theta + jR_{\text{L}} \sin 2\theta \tag{5.7}$$

Since the resistive load is connected to the voltage sources through two quarter-wave transmission lines, as shown in Fig. 5.3(a), the input impedance that the voltage sources see can be expressed as:

$$Z_{\text{in1}}(\theta) = \frac{Z_c^2}{Z_{\text{cs1}}} = \frac{Z_c^2}{2R_L}\left(1 + j\tan\theta\right) \tag{5.8}$$

$$Z_{\text{in2}}(\theta) = \frac{Z_c^2}{Z_{\text{cs2}}} = \frac{Z_c^2}{2R_L}\left(1 - j\tan\theta\right) \tag{5.9}$$

From the expressions (5.8) and (5.9) one can see that real part of input impedance remains constant when outphasing angle changes. However, the imaginary parts of the impedance do depend on the outphasing angle. Graphically it can be shown in a Smith chart as shown in the Fig. 5.4(a). Input reactance values for the combiner branches for a particular value of outphasing angle have the same absolute values and opposite signs.

From the circuit theory it is well-known, that when a complex load is connected to a voltage source, the power is dissipated in the resistive part of the impedance, whereas the energy stored in the reactive part is then reflected back to the generator.
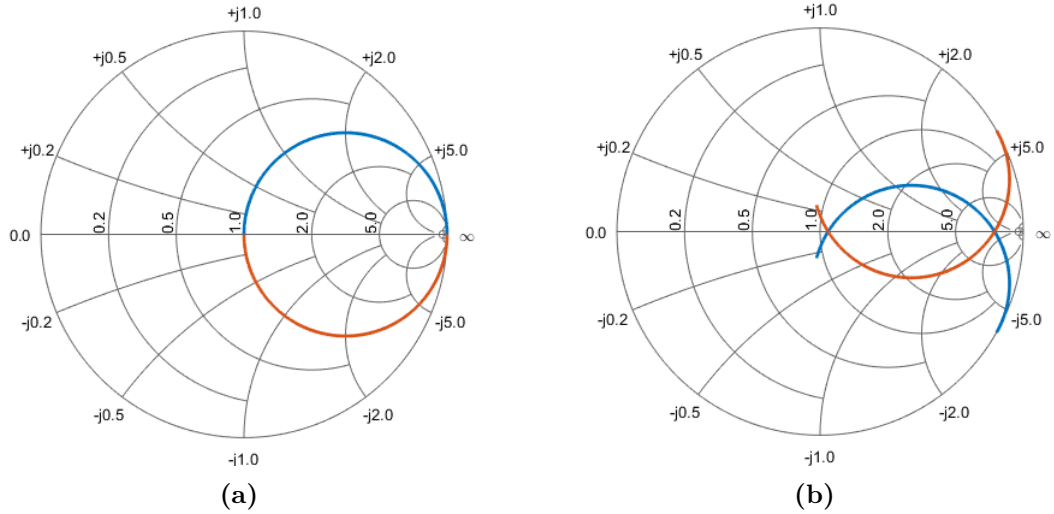
Fig. 5.4 Input impedance of a non-isolated combiner: (a) - without compensating elements; (b) - with compensating elements.
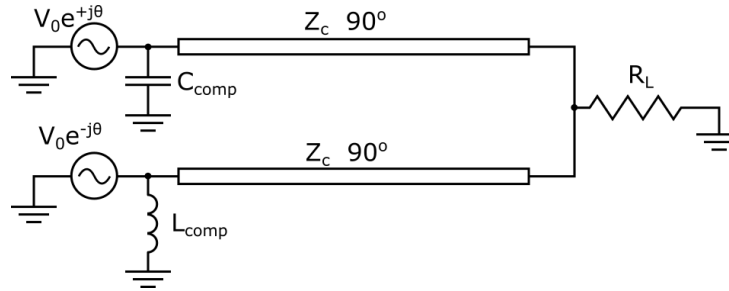
Fig. 5.5 A block-diagram of the outphasing transmitter.

Therefore, the instantaneous efficiency of the combiner can be defined as a ratio of the real part of the input impedance to the magnitude of the impedance [118]:

$$\eta_{\text{comb}} = \frac{\text{real}(Z_{\text{in}})}{|Z_{\text{in}}|} \tag{5.10}$$

From the definition (5.10) it follows, that the combiner shown in Fig. 5.3(a) provides the maximum efficiency only for the value of outphasing angle $\theta = 0°$. However, for most practical applications it is required to have high efficiency for a range of back-off power level values. In [10] it was demonstrated, that if two reactive components are added to the inputs of the combiner, as shown in Fig. 5.5, and the reactive components provide additional susceptance with the same magnitude B_{comp} and opposite signs, the input impedance will be purely resistive for two values of

outphasing angle (see Fig. 5.4(b)):

$$\theta_{\text{peak}} = \frac{1}{2} \arcsin\left(\frac{Z_{\text{c}}^2 B_{\text{comp}}}{R_{\text{L}}}\right) \tag{5.11}$$

$$\theta_{\text{BO}} = \frac{\pi}{2} - \frac{1}{2} \arcsin\left(\frac{Z_{\text{c}}^2 B_{\text{comp}}}{R_{\text{L}}}\right) \tag{5.12}$$

Here the outphasing angle θ_{peak} corresponds to the peak power level, and θ_{BO} corresponds to the back-off power level. Since back-off power level is usually given as an input parameter for PA design procedure, it is convenient to express the angles θ_{peak} and θ_{BO} with back-off power, which follows from (5.3):

$$\theta_{\text{BO}} = \arccos 10^{\frac{\Delta P_{BO}}{20}} \tag{5.13}$$

$$\theta_{\text{peak}} = \frac{\pi}{2} - \arccos 10^{\frac{\Delta P_{BO}}{20}} \tag{5.14}$$

where ΔP_{BO} is the back-off power level expressed in dB. Therefore, the shunt susceptance that provides 100% combiner efficiency at the required back-off level ΔP_{BO} can be determined from (5.12):

$$B_{\text{comp}} = \frac{R_{\text{L}}}{Z_{\text{c}}^2} \sin 2\theta_{\text{BO}} \tag{5.15}$$

Since the compensating susceptance for two branches must have opposite sign, the shunt reactance for the $+\theta$ branch is realized as a capacitance and for the $-\theta$ branch as an inductance:

$$C_{\text{comp}} = \frac{B_{\text{comp}}}{2\pi f_c} \tag{5.16}$$

$$L_{\text{comp}} = \frac{1}{2\pi f_c B_{\text{comp}}} \tag{5.17}$$

where f_{c} is the carrier frequency of the transmitted signal. The input impedance of the branches of Chireix combiner with compensating components can be found from
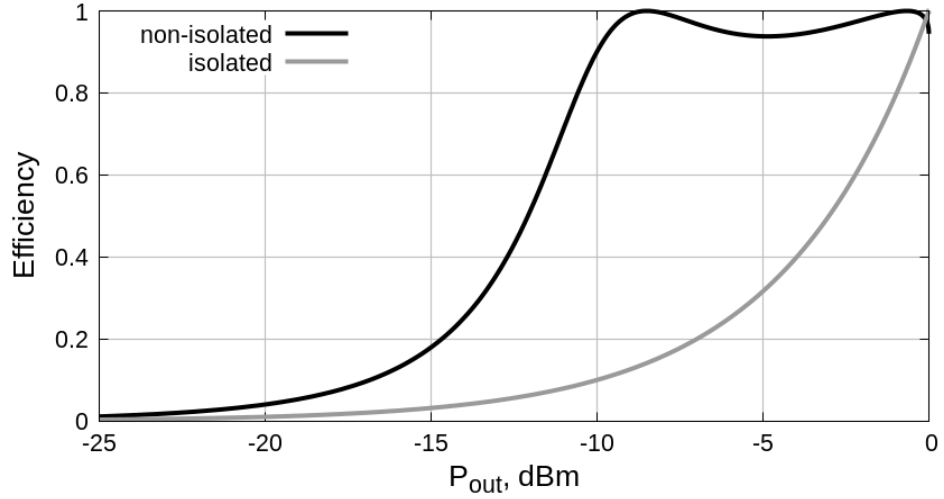
Fig. 5.6 Instantaneous efficiency of combiners used in outphasing transmitters: an outphasing Chireix combiner, optimized for -8.5 dB back-off power level (black line); isolated Wilkinson combiner (grey line).

the expressions:

$$\frac{1}{Z_{\text{in1}}(\theta)} = \frac{2R_{\text{L}}}{Z_{\text{c}}^2} \cos^2\theta - j\left(\frac{R_{\text{L}}}{Z_{\text{c}}^2} \sin 2\theta - 2\pi f_{\text{c}} C_{\text{comp}}\right) \tag{5.18}$$

$$\frac{1}{Z_{\text{in2}}(\theta)} = \frac{2R_{\text{L}}}{Z_{\text{c}}^2} \cos^2\theta + j\left(\frac{R_{\text{L}}}{Z_{\text{c}}^2} \sin 2\theta - \frac{1}{2\pi f_{\text{c}} L_{\text{comp}}}\right) \tag{5.19}$$

The dependence of instantaneous efficiency on the back-off power level with compensating reactive elements optimized for -8.5 dB back-off power is shown in Fig. 5.6. From this plot one can see, that although the 100% efficiency is provided for two back-off power values, the combiner maintains high efficiency between these two ideal power levels. Due to this property, it Chireix combiners can be used for transmitters when signals with high PAPR are used.

From (5.18) and (5.19) it follows, that the power coming to the Chireix combiner branches can be found as:

$$P_{\text{in1,2}} = \frac{V_0^2}{Z_{\text{in1,2}}(\theta)} = \frac{2V_0^2 R_{\text{L}}}{Z_c^2} \cos^2\theta \mp jV_0^2\left(\frac{R_{\text{L}}}{Z_c^2} \sin 2\theta - |B_{\text{comp}}|\right) \tag{5.20}$$

From the energy conservation law it follows, that the real part in the expression (5.20) is equal to the power dissipated in the output load:

$$P_{\text{out}} = \frac{2V_0^2 R_{\text{L}}}{Z_c^2} \cos^2 \theta \tag{5.21}$$

Consequently, taking into account (5.3), when a Chireix combiner is excited with voltage sources with equal magnitudes, the combiner does not introduce any nonlinear distortion into the transmitted signal.

It should be noted that the described combiner provides high efficiency assuming that the two outphasing signals are generated from ideal voltage sources. However, the behaviour of the most of the amplifiers resemble current sources rather than voltage sources. Therefore, as it will be shown in the following chapters, some additional circuit elements need to be added in order to provide high efficiency for real PAs.

5.1.2 Isolated outphasing combiners

In this subsection the properties of isolated Wilkinson combiners are analyzed. The simplest Wilkinson combiner is formed by adding a resistor in parallel to the quarterwave combiner, as shown in Fig. 5.7(a). In order to derive analytical expressions for the input impedance, it is convenient to rewrite the expressions (5.8) and (5.9) for input admittance values:

$$Y_{\text{in1}}(\theta) = \frac{R_{\text{L}}}{Z_c^2}(2\cos^2\theta - j\sin 2\theta) \tag{5.22}$$

$$Y_{\text{in2}}(\theta) = \frac{R_{\text{L}}}{Z_c^2}(2\cos^2\theta + j\sin 2\theta) \tag{5.23}$$

An isolating resistance excited by two voltage sources is shown in Fig. 5.7(b). If the magnitudes of the two exciting voltages are equal to V_0, then the voltage drop across the resistance will be $\dot{V}_{\text{IR}} = V_0(e^{+j\theta} - e^{-j\theta})$. Consequently, this voltage drop
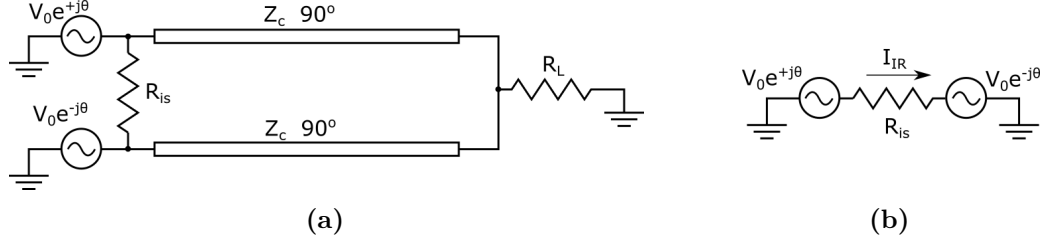
Fig. 5.7 Isolated Wilkinson combiner: (a) - the general structure of a Wilkinson combiner; (b) - isolating combiner.

will cause current flowing through the isolating resistor:

$$\dot{I}_{\text{IR}}(\theta) = \frac{V_0(e^{+j\theta} - e^{-j\theta})}{R_{\text{is}}} = \frac{2jV_0 \sin \theta}{R_{\text{is}}} \tag{5.24}$$

Therefore, the voltage sources in Fig 5.7(b) will see the following admittance:

$$Y_{\text{IR1}}(\theta) = \frac{\dot{I}_{\text{IR}}}{V_0 e^{+j\theta}} = \frac{1}{R_{\text{IR}}}\left(2\sin^2\theta + j\sin 2\theta\right) \tag{5.25}$$

$$Y_{\text{IR2}}(\theta) = \frac{\dot{I}_{\text{IR}}}{V_0 e^{+j\theta}} = \frac{1}{R_{\text{IR}}}\left(2\sin^2\theta - j\sin 2\theta\right) \tag{5.26}$$

The input admittance of a Wilkinson combiner's inputs in Fig. 5.7(a) can be therefore expressed as:

$$Y_{\text{wc1}}(\theta) = \frac{R_{\text{L}}}{Z_{\text{c}}^2}\left(2\cos^2\theta - j\sin 2\theta\right) + \frac{1}{R_{\text{is}}}\left(2\sin^2\theta + j\sin 2\theta\right) \tag{5.27}$$

$$Y_{\text{wc2}}(\theta) = \frac{R_{\text{L}}}{Z_{\text{c}}^2}\left(2\cos^2\theta + j\sin 2\theta\right) + \frac{1}{R_{\text{is}}}\left(2\sin^2\theta - j\sin 2\theta\right) \tag{5.28}$$

From the expressions (5.27) and (5.28) it follows, that if the isolation resistance is equal to $R_{\text{is}} = \frac{Z_{\text{c}}^2}{R_{\text{L}}}$, the input impedance of both branches is $Z_{\text{wc1}} = Z_{\text{wc2}} = \frac{Z_{\text{c}}^2}{2R_{\text{L}}}$ and does not depend on the outphasing angle. Therefore, such a combiner presents a constant load impedance for both branch amplifiers, which makes it possible to operate both amplifiers in high efficiency mode. However, since an isolated Wilkinson combiner contains a lossy isolating resistor, its efficiency is defined as a ratio of output power to the input power. If the input of the combiner is assumed to be

perfectly matched, the power coming to the combiner is defined using expression:

$$P_{\text{in}} = 2V_0^2 Y_{\text{wc}} = \frac{2V_0^2 R_{\text{L}}}{Z_{\text{c}}^2} \tag{5.29}$$

This power is partially dissipated in the isolating resistor, and the amount of dissipated power can be defined as follows:

$$P_{\text{IR}} = \frac{2V_0^2 R_{\text{L}} \sin \theta}{Z_{\text{c}}^2} \tag{5.30}$$

Therefore, the output power can be found as difference between the power coming to the combiner's inputs and the power dissipated in the resistor:

$$P_{\text{out}} = P_{\text{in}} - P_{\text{IR}} = \frac{2V_0^2 R_{\text{L}} \cos^2 \theta}{Z_{\text{c}}^2} = P_{\text{in}} \cos^2 \theta \tag{5.31}$$

From the expression (5.31) it follows, that instantaneous efficiency of isolated Wilkinson combiner is $\eta_{\text{inst}} = \cos^2 \theta$, as shown in Fig. 5.6. From these plots one can see, that the bigger the level of the back-off power, the better efficiency a non-isolated combiner can provide compared to an isolated one.

5.2   Design of a class-E outphasing PA

In this section a design procedure for a class-E outphasing PA is demonstrated. Class-E PAs with shunt capacitance and shunt filter are used as branch amplifiers. As it was shown in Chapter 3, this type of class-E PA can provide high drain efficiency across a wide range of output power levels. In order to provide high efficiency for an amplitude modulated signal, a non-isolated Chireix combiner is used for amplified signal recombination. Both class-E PAs and the Chireix combiner are implemented using microstrip transmission lines. A packaged GaN HEMT transistor CHG40010F is used for both PAs. The operating frequency of the PA is 2.14 GHz, the peak power $P_{\text{out}} \approx 30$ W, PAPR ≈ 8.5 dB.

The design procedure can be outlined as follows:

1. Calculation of load network parameters for a class-E PA for the peak and back-off power levels. At this stage the class-E amplifiers are simulated with ideal lumped components and the active device is represented as an ideal switch. The optimum load network impedance for the peak and back-off power are calculated using the procedure outlined in Chapter 3.

2. Simulation of the class-E PA based on the packaged device model. The derived load impedance values are tuned in order to provide high efficiency at the peak and back-off power levels for the actual active device. The optimization is performed in circuit simulation software using a model provided by the device manufacturer.

3. Design of a non-isolated Chireix combiner that provides the required load impedance values for the given outphasing angles. The values of the outphasing angles are defined from the required back-off power level according to expression (5.13).

4. The whole outphasing PA is simulated and optimized in the circuit simulator in order to provide the required efficiency and the output power. Ideally, if the optimization at the previous stages has been done properly, only minor adjustment of circuit parameters is required at this step.

Using the algorithm presented in Chapter 3, the following circuit parameters were derived: $L_{\mathrm{s}} = 1.625$ nH, $C_{\mathrm{p}} = 1.3$ pF. The load impedance for peak output power ($P_{\mathrm{out,peak}} = 15$ W) $Z_{\mathrm{L,peak}} = 15 + j0.5$ ohm, and for -8.5 dB back-off level ($P_{\mathrm{out,BO}} = 2.12$ W) $Z_{\mathrm{L,BO}} = 4.65 + j16.53$ ohm. The ADS schematic for the ideal single-ended class-E PA is shown in Fig. 5.8. It is worth noting, that for the same output power, 100% drain efficiency can be achieved for many values of the parameter q. Hence, the parameter q is chosen in order to achieve $C_{\mathrm{p}} \approx 1.3$ pF, which allows incorporation of the packaged device drain-source capacitance into the load network.

The same single-ended class-E PA optimized for GaN HEMT device CGH40010F is presented in Fig. 5.9. In order to drive the PA in a switchmode, which is necessary
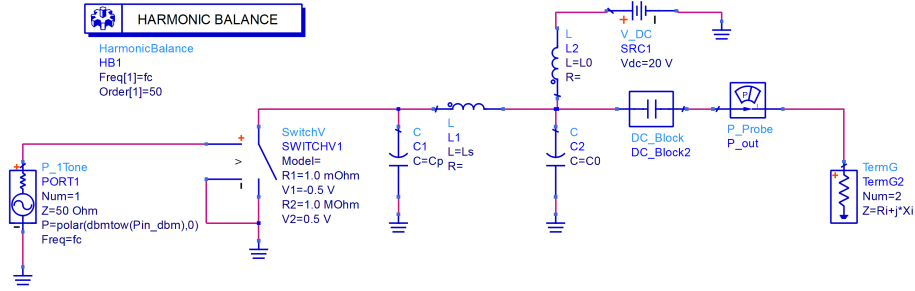
Fig. 5.8 Ideal class-E PA with shunt capacitance and shunt filter simulated in Keysight ADS.
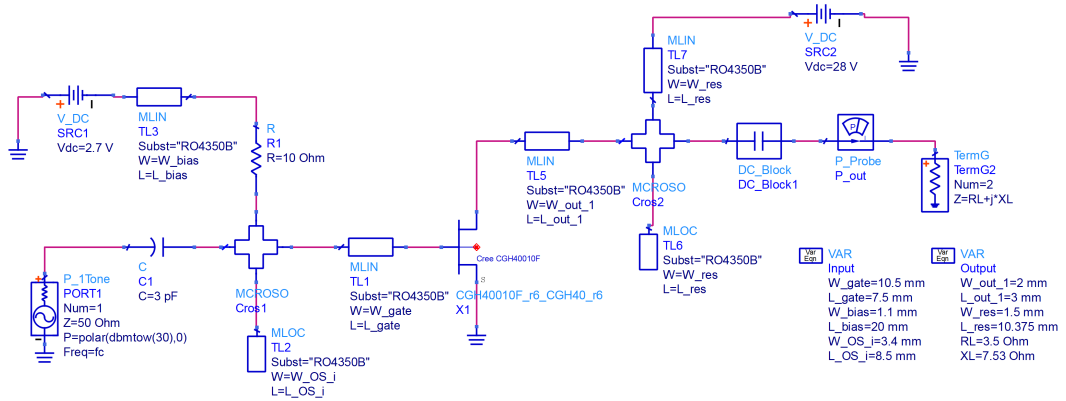
Fig. 5.9 Simulated class-E PA with shunt capacitance and shunt filter based on GaN HEMT transistor.

for the class-E operation, a single-tone power source is used, and the input matching circuit provides the required impedance transformation. As well as in the previous chapters the shunt resonator is realized as two sections of microstrip lines with electrical length 45° degrees. The shunt capacitance C_p is implemented with the drain-source output capacitance of the device. It should be pointed out, that the output capacitance of a GaN HEMT device decreases with the raise of drain-source voltage. If this dependence significantly affects the performance, a transistor model that takes into account output capacitance variation can be used [119, 120]. However, if the tracking of the optimum load impedance is provided, the drain-source voltage variation is not significant for the peak and back-off power levels, as shown in Fig. 3.4 - 3.6. Therefore, in this work the output capacitance is assumed to be constant. The optimized values for the peak and back-off load impedance are: $Z_{L,peak} = 14.1 + j0.2$, $Z_{L,BO} = 2.3 + j8.5$ ohm. According to the simulated results, when these load impedance values are presented to the PA output, the class-E PA demonstrates 86%
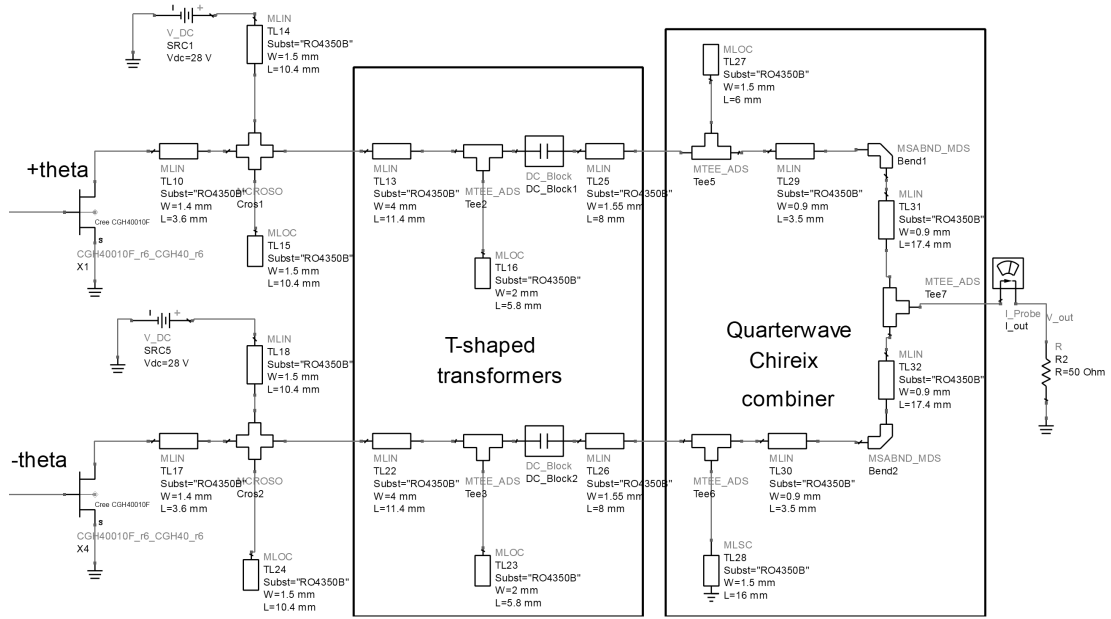
Fig. 5.10 The optimized load network of class-E outphasing PA simulated in Keysight ADS.

(a)

(b)
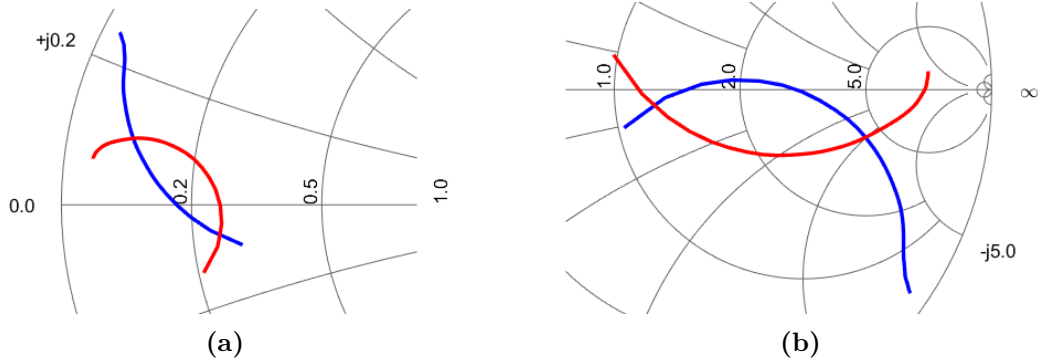
Fig. 5.11 Simulated impedance at two reference planes: (a) - at the output of the class-E PAs; (b) - at the input of the Chierix combiner.

drain efficiency at the peak output power ($P_{\text{out}} = 14$W) and 73% drain efficiency at the back-off power level ($P_{\text{out}} = 2$W).

A non-isolated quarterwave Chireix combiner is used in order to add the amplified signals at the output. Since the required back-off power level is -8.5 dB, the outphasing angle at the back-off calculated from (5.13) is $\theta_{\text{BO}} \approx 68°$. If the load impedance is 50 ohm and the transmission lines of the combiner have characteristic impedance of 70.7 ohm, then according to (5.15), the compensating susceptance must be $B_{\text{comp}} \approx 6.97$ mS. Along with the outphasing angle θ_{BO}, a combiner with this

compensating susceptance will provide a purely resistive impedance at the outphasing angle $\theta_{\text{peak}} = \pi - \theta_{\text{BO}} \approx 22°$. The input impedance of the quarterwave combiner at these outphasing angles will be $Z_{\text{CH,peak}} = 58.2$ ohm and $Z_{\text{CH,BO}} = 354$ ohm.

The compensating susceptance can be implemented using lumped capacitor and inductor for the $+\theta$ branch and $-\theta$ branch respectively. For the frequency $f_{\text{c}} = 2.14$ GHz the values for the components will be $C_{\text{comp}} = 0.518$ pF and $L_{\text{comp}} = 10.68$ nH. At microwave frequencies these components are usually implemented using open and short circuit sections of transmission line. If a line with pure T-wave is used (such as symmetrical stripline) with 50 ohm characteristic impedance, the capacitance can be realized as an open circuit section with 19.2° length, and the inductance can be implemented as a short-circuited section with 70.8° length. The same results can be used for the microstrip transmission lines with quasi-T waves with minor modification.

In order to transform the values $Z_{\text{CH,peak}}$ and $Z_{\text{CH,BO}}$ to the previously found required values $Z_{\text{L,peak}}$ and $Z_{\text{L,BO}}$, two T-shaped transformers have been added, as shown in the left box in Fig. 5.10. The structure of the T-shaped lines was optimized using the 2-goals optimization procedure. The first goal was minimization of the reflection when the load impedance is equal to $Z_{\text{CH,peak}}$ and the source impedance is equal to $Z_{\text{L,peak}}^*$. The second goal is the minimization of the reflection coefficient when the load impedance is equal to $Z_{\text{CH,BO}}$ and the source impedance is equal to $Z_{\text{L,BO}}^*$. During the optimization process, the electrical length of the open stub line should remain approximately 30° at the central frequency, since it has to provide the third harmonic termination, and therefore, overall efficiency improvement. The simulated combiner impedance trajectories at the plane of compensating reactive elements is shown in Fig. 5.11(b). It can be seen, that these trajectories are close to the ideal ones shown in Fig. 5.4(b). The simulated impedance at the class-E amplifiers outputs is shown in Fig. 5.11(a). As one can see, these impedance trajectories are relatively close to the ideal ones shown in Fig. 3.3. However, since the T-shaped lines transform complex conjugated impedance values, the two trajectories intersect in two points only. These two points correspond to the peak and back-off power
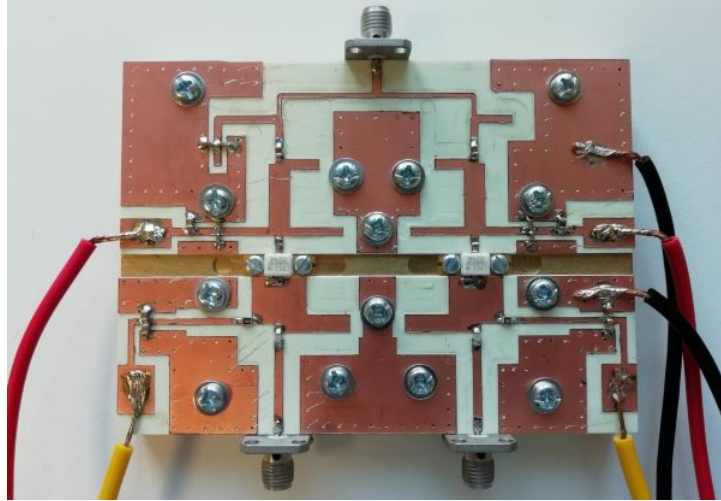
Fig. 5.12   Fabricated outphasing class-E PA prototype.
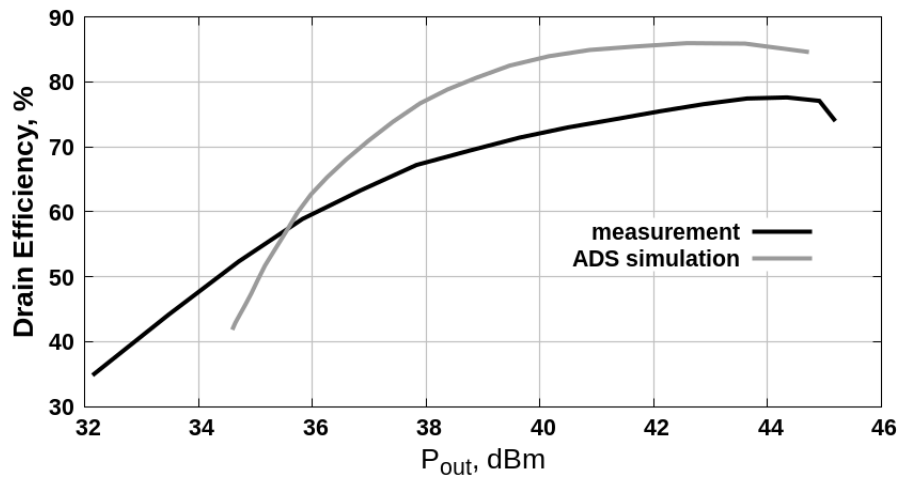
Fig. 5.13   Simulated and measured drain efficiency of the outphasing PA.

levels. It should be pointed out that, based on the required impedance values, other combiner synthesis techniques can be used, such as the ones proposed in [53, 57].

The calculated structure was optimized using Keysight ADS simulation software. The transmission lines were modelled as microstrip lines on Rogers RO4350B substrate with thickness 0.762 mm. The harmonic balance solver was used for PA parameters simulation, which provides a good trade-off between accuracy and computational complexity. The two inputs of the outphasing PA were excited separately with power sources. The power sources generate two single-tone signals at the center frequency $f_c = 2.14$ GHz, and the power $P_1 = 30$ dBm. The phase difference between the

91
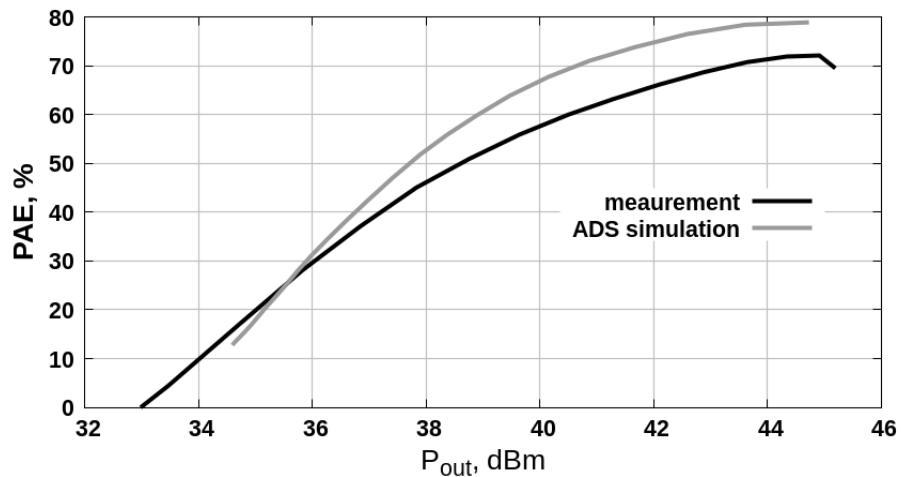
Fig. 5.14 Simulated and measured PAE of the outphasing PA.
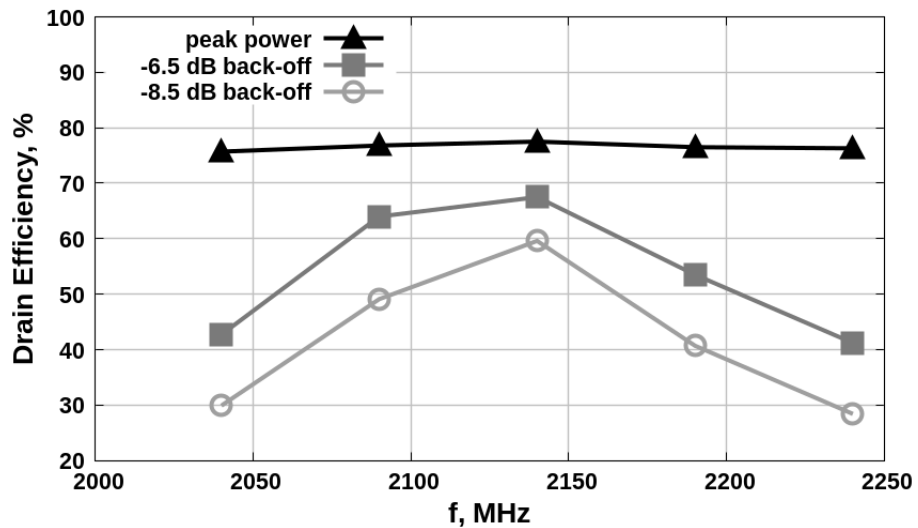
Fig. 5.15 Measured frequency dependence of drain efficiency at peak output power and back-off power levels.

excitation signals is defined as 2θ, where θ is defined by (5.3). The simulated results are presented in Fig. 5.13 and 5.14 along with measured results.

The optimized outphasing PA was implemented using GaN HEMT CGH40010F transistors and Rogers RO4350B substrate. The input and output load circuits were constructed on 0.762 mm thick Rogers RO4350B substrate with dielectric constant 3.48 and dissipation factor 0.0037 (see Fig. 5.12). The setup for output power and efficiency measurement is shown in Fig. 5.16. It consists of a dual-path transmitter board TSW30SH84EVM, linear driver amplifiers and a Rohde&Schwarz NRP output
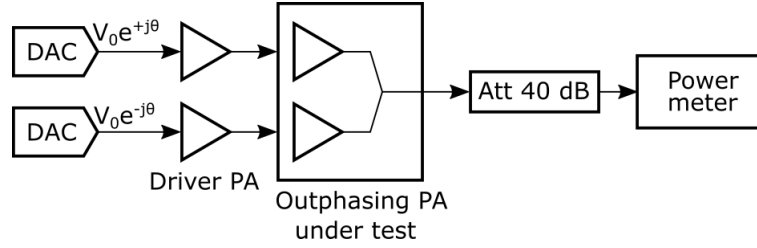
Fig. 5.16 Test bench for the efficiency measurement of outphasing PA.

Table 5.1 Comparison with state-of-the-art outphasing PAs.

Parameters	[53]	[44]	[56]	[121]	[58]	[122]	[123]	[124]	this work
f_0, GHz	0.9	1.8	2.3	2.4	1.85	3.92	2.4	2.6 / 3.5	2.14
$P_{\text{out, peak}}$, W	24	0.1	70.6	0.89	-	5	1.45	31 / 26	28.1
ΔP_{BO}, dB	7.5	12	-	6	-	7	6	6	8.5
DE_{peak}, %	71	65.3	73	46.76	-	77	49.2	74.5 / 62	78
DE_{BO}, %	40	37.2	-	21.16	-	50	33	63.8 / 54.9	60
BW, %	33	5.6	4.4	–	70	-	-	-	4.7

power meter. Two single-tone signals were generated at the frequency 2.14 GHz from the transmitter board. The phase difference between the transmitted signals is defined by the back-off power level according to (5.3). The two signals were preamplified by the linear amplifiers to +30 dBm in order to drive both branch PAs in class-E mode. The power of the output signal was measured at the operating frequency using the power meter.

The dependence of the PA drain efficiency and PAE on the output power level is presented in Fig. 5.13 and Fig. 5.14 respectively. From these plots it can be seen that the fabricated PA provides more than 60% drain efficiency for back-off power levels of -8.5 dB. The frequency dependence of drain efficiency at peak and back-off power levels is presented in Fig. 5.15. It can be seen that the back-off efficiency decreases quickly with frequency offset. The reason for that is the significant difference between the input impedance of the quarterwave combiner and the required back-off load impedance for the class-E PA. The comparison of the demonstrated outphasing PA with some of the state-of-the-art outphasing PAs is presented in Table 5.1.
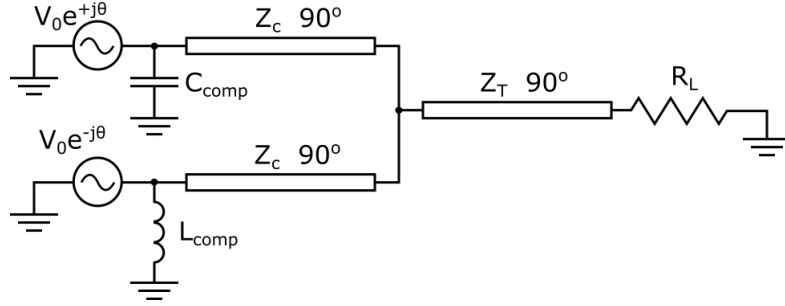
Fig. 5.17 Chireix combiner with improved bandwidth.

5.3 Broadband operation of outphasing PA

As one can see from Fig. 5.15, the outphasing PA provides high efficiency operation across a relatively narrow frequency range. Indeed, the quarterwave combiner with load resistance 50 ohm and characteristic impedance of the transmission lines 70.7 ohm provides input impedance 58.2 ohm for the peak power and 354 ohm for the back-off power level (-8.5 dB). The T-shaped lines transform these impedance values to the impedance required for the peak and back-off class-E operation: $Z_{L,peak} = 14.1 + j0.2$, $Z_{L,BO} = 2.3 + j8.5$ ohm. Therefore, the loaded Q-factor of the T-shaped transformer at the peak power and the back-off power will be:

$$Q_{L,peak} \approx \sqrt{\frac{58.2}{14.1} - 1} \approx 1.77 \tag{5.32}$$

$$Q_{L,BO} \approx \sqrt{\frac{354}{2.3} - 1} \approx 12.4 \tag{5.33}$$

From (5.32) and (5.33) one can see that the impedance matching at the back-off power level is a limiting factor for broadband operation of outphasing PA. In order to reduce the loaded Q-factor and improve the bandwidth, a Chireix combiner shown in Fig. 5.17 can be used. In this case, the output transmission line transforms the standard 50 ohm line impedance to 100 ohm impedance at the output of the combiner. The two quarterwave transmission lines have characteristic impedance 50 ohm. The compensation reactance is defined from the expression (5.15), where $Z_L = 100$ ohm. The dependence of the input impedance upon the outphasing angle for such a combiner is shown in Fig. 5.18. The purely resistive input impedance is
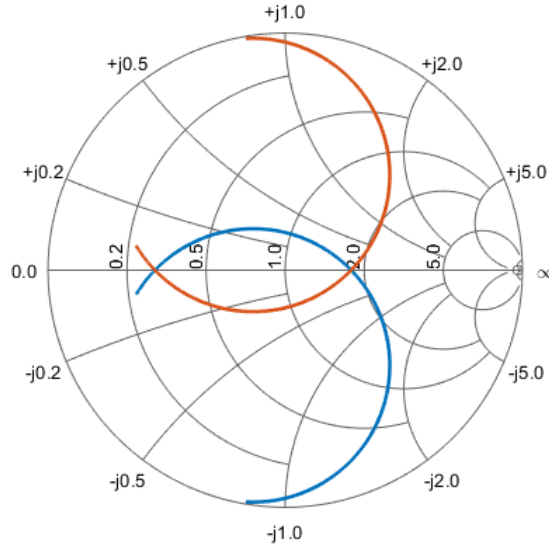
Fig. 5.18 Input impedance of a Chireix combiner with improved bandwidth.

provided for the two outplasing angle values: $\theta_{\text{peak}} = 22°$ and $\theta_{\text{BO}} = 68°$, where the impedance is: $Z_{\text{peak}} = 14.56$ ohm and $Z_{\text{BO}} = 88.5$ ohm respectively.

The operation of a class-E outphasing PA with improved bandwidth performance can be demonstrated using Keysight ADS circuit simulator. As well as in the previous chapters, the class-E PAs with shunt capacitances and shunt filters are used, where the active devices are simulated as ideal switches, the parallel capacitances and the series inductances are represented with lossless lumped components, the shunt filter and the combining network are implemented using ideal transmission lines (see Fig. 5.19). The single-ended class-E amplifiers are optimized for the peak power 12 W, carrier frequency 2.14 GHz and drain supply voltage 20.3 V. The load circuit parameters are: $C_{\text{p}} = 1.31$ pF, $L_{\text{s}} = 1.65$ nH. The required peak power can be achieved if the load presented to a single-ended PA is $Z_{\text{L,peak}} = 14.8 - j0.35$ ohm. The -8.5 dB back-off power level (1.7 W) can be achieved if the load $Z_{\text{L,BO}} = 4.65 + j15.6$ ohm is presented to the PA output.

The output of the single-ended PAs are connected to the inputs of the Chireix combiner through two sections of transmission lines with characteristic impedance $Z_{\text{offset}} = 14.8$ ohm and electrical length 137.5° at the central frequency. These lines transform the input impedance of the Chireix combiner at the back-off power level

95
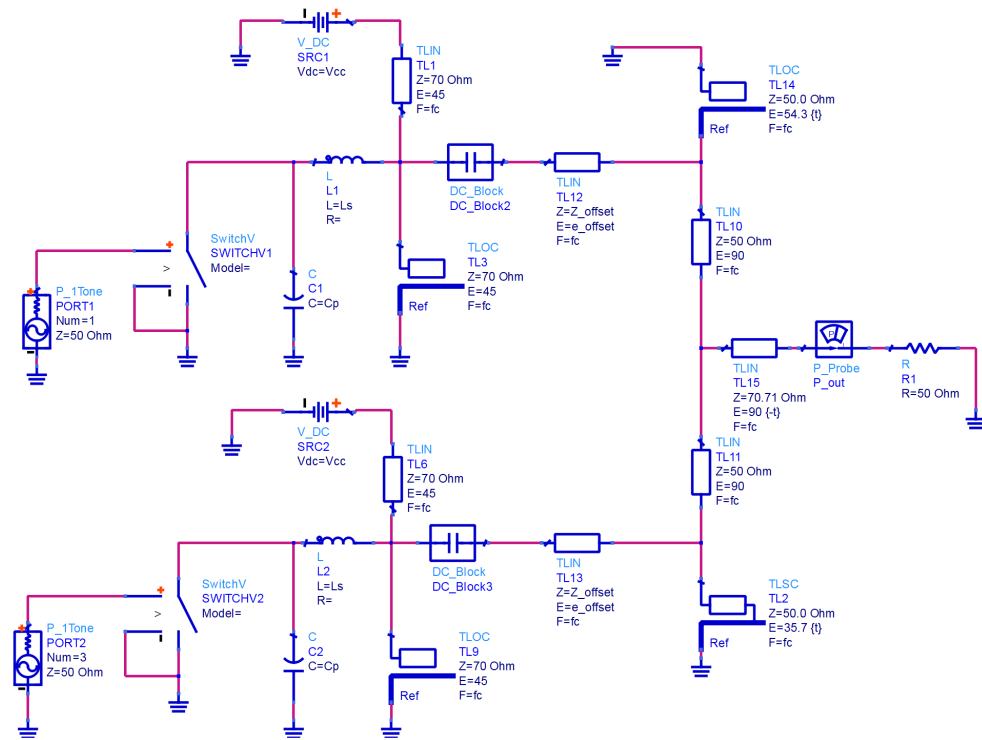
Fig. 5.19 An outphasing PA with improved bandwidth simulated in Keysight ADS.
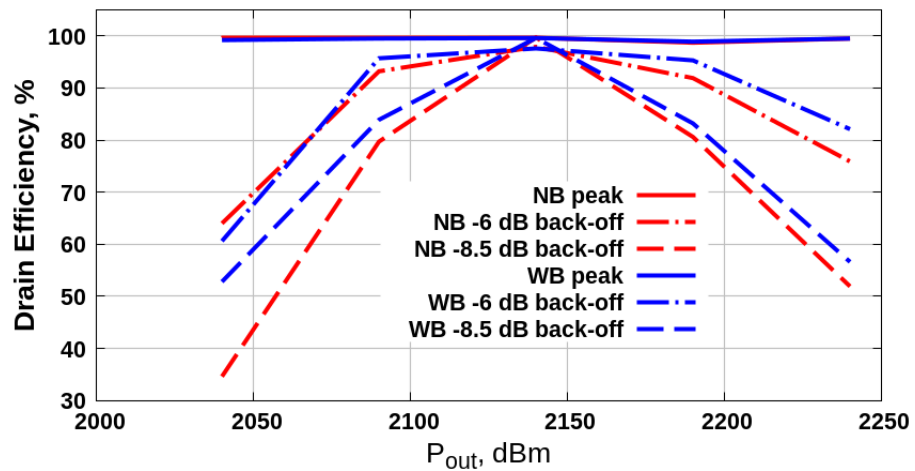
Fig. 5.20 Simulated drain efficiency for the peak and back-off power levels for the narrowband outphasing PA (red line), and the wideband outphasing PA (blue line).
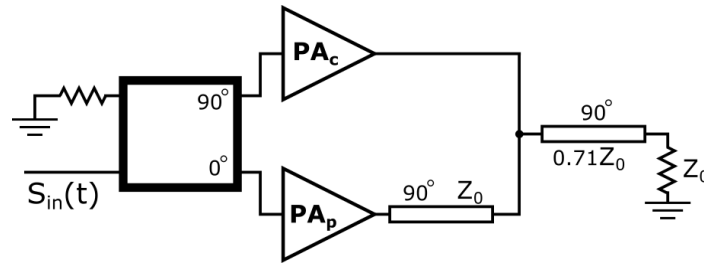
Fig. 5.21 Block-diagram of the inverted Doherty PA.

to the required back-off load impedance without affecting the impedance at the peak power level. The designed PA was simulated using a harmonic balance simulator from ADS. The simulated drain efficiency for the peak and back-off power levels is presented in Fig. 5.20. Since required load impedance for class-E PA almost coincides with the input impedance of the Chireix combiner, the main limiting factor for the peak power efficiency is quarterwave combiner lines. The loaded Q-factor of these lines is relatively low, therefore both simulated outphasing PAs provide almost 100% drain efficiency at the peak output power level. However, at the back-off output power the difference between the Chireix combiner input impedance and the required load impedance grows significantly, and the loaded Q-factor of the transformer becomes a major factor limiting for wideband operation. For this reason, the PA with reduced Q-factor demonstrates better drain efficiency across the frequency range. It should be noted that other approaches for wideband Chireix combiner design can be applied [43, 105].

5.4   Doherty PA design

As it was outlined in Sec. 2.4, a Doherty PA consists of input divider, carrier PA, peaking PA and an output combiner. In a traditional Doherty PA, when the level of the input signal is low, the output of the carrier PA rises linearly, while the open circuit condition is provided at the output of the peaking PA. However, in some cases it is preferable to provide short circuit condition for the peaking PA output. This can be realized using an inverted Doherty PA, whose block-diagram is shown
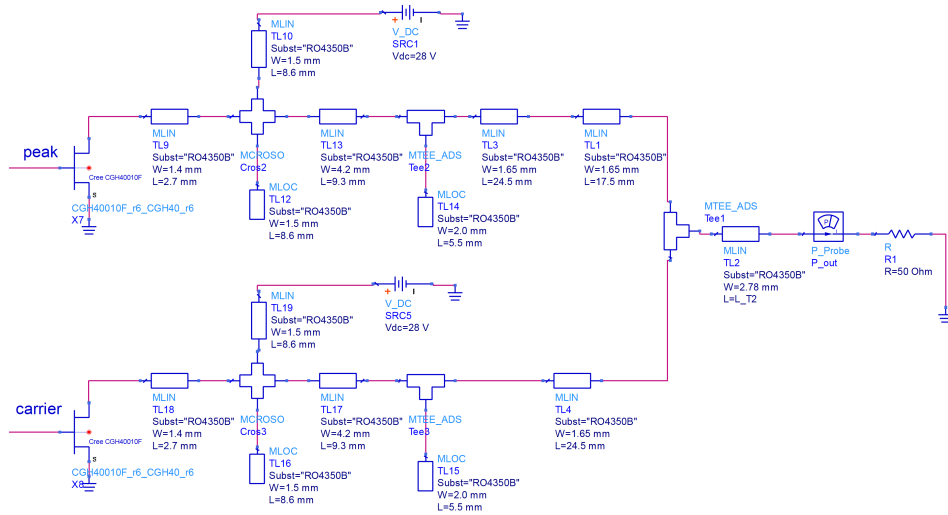
Fig. 5.22   Load network of the inverted Doherty PA simulated in Keysight ADS.

in Fig. 5.21. As one can see, the impedance inverter is connected to the output of the peaking PA, as opposite to conventional Doherty PA where it is connected to the output of the carrier PA. Therefore, if the impedance of the load is 50 ohm, then the output section of the transmission line transforms it to 25 ohm. When the peaking PA is switched off (output power $\Delta P_{\text{out}} < -6$ dB), no power comes from the peaking PA, and consequently, the carrier PA sees impedance of 25 ohm. When the peaking PA is turned on and driven into saturation mode, two equal signals come from the outputs of the PAs. Consequently, if the characteristic impedance of the impedance inverter in the peaking PA circuit is 50 ohm, both PAs will see the impedance 50 ohm at the peak output power. The key difference between the conventional Doherty PA and the inverted Doherty PA is that in the latter case the load impedance provided by the combiner is higher when the output power increases. As it was shown in previous sections, this property is natural for class-E PAs, which makes it easier to build wideband PAs.

A simulated load network of inverted Doherty PA is shown in Fig. 5.22. Both peaking and carrier PA are implemented using Cree CGH40010F devices. The PA is optimized for the carrier frequency 2.6 GHz and 20 W output power. The input signal is split into two equal parts using a 90° hybrid divider. The gate of the peaking PA is biased in a way that it starts generating the output signal only when the
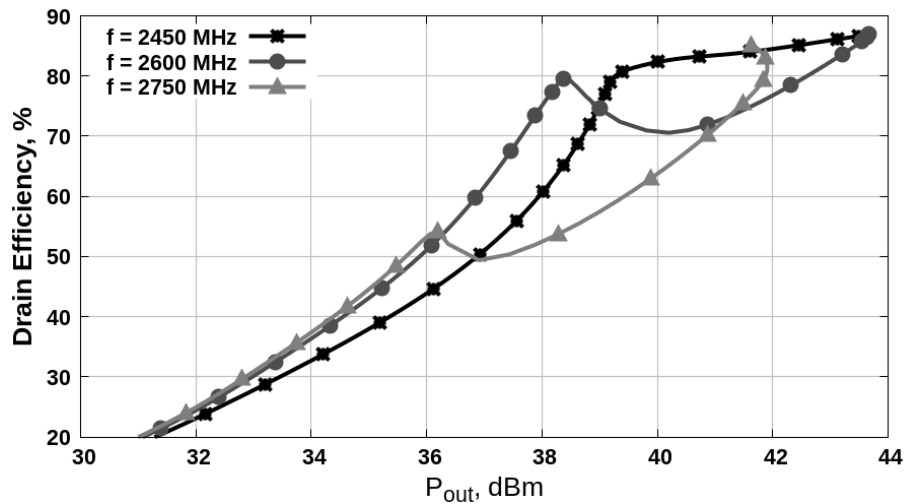
Fig. 5.23 Drain efficiency of the inverted Doherty PA simulated in Keysight ADS.

input power is backed-off approximately -6 dB related to the peak power. The input circuits for both carrier and peaking PAs are designed in order to provide impedance transformation from the gate-source impedance of the GaN transistor to the standard 50 ohm impedance. Both devices for the carrier and peak PAs are depletion mode devices, and therefore they require negative gate-source voltage for operation. In this case the gate-source voltages were set to -2.7 V for the carrier transistor and -7.6 V for the peaking device.

As well as in the case of outphasing PA, the main goal of inverted Doherty PA design is transforming the impedance provided by the combiner to the load impedance required by the class-E PAs. According to the technique described in Chapter 3, the load impedance for the peak power ($P_{\mathrm{L,peak}} = 11$ W) is $Z_{\mathrm{L,peak,ideal}} = 11.8 + j0.5$ ohm and for -6 dB back-off output power ($P_{\mathrm{L,BO}} = 2.75$ W) the load impedance should be $Z_{\mathrm{L,BO,ideal}} = 3.4 + j6.6$ ohm. These impedance values are corrected using the simulation in Keysight ADS with a GaN HEMT transistor model, as shown in Fig. 5.9. The corrected load impedance values are: $Z_{\mathrm{L,peak}} = 12.6 + j0.4$ and $Z_{\mathrm{L,BO}} = 2.9 + j3.7$. The structure of T-shaped microstrip transmission lines is chosen in order to provide the proper impedance transformation at the peak power, at the back-off power, and also to suppress the third harmonic. The entire load network of Doherty PA structure was simulated in Keysight ADS circuit simulator

99

and optimized in order to achieve high efficiency at the peak and back-off power levels. The achieved drain efficiency for three frequencies is shown in Fig. 5.23.

5.5   Conclusion

In this chapter application of the technique proposed in Chapter 3 to high efficiency power amplifiers design has been presented. The concept of outphasing PA with different types of combiners has been described. It has been shown, that non-isolated Chireix combiners with shunt reactive components provide higher efficiency for amplitude modulated signals compared to isolated combiners. An outphasing PA based on class-E PA with shunt capacitance and shunt filter has been designed and manufactured. The proposed PA was tested with two constant envelope input signals. The fabricated PA demonstated over 60% drain efficiency for back-off output power -8.5 dB and over 30% power added eficiency. The concept of an outphasing PA with improved bandwidth performance has been described. Ideal circuit simulations demonstrate some efficiency improvement compared to the outphasing PA demonstrated previously. A Doherty PA based on class-E PA with shunt capacitance and shunt filters has been demonstrated. The simulated PA provides drain efficiency higher than 50% for back-off power levels up to -7.5 dB.

Chapter 6

Linearity of outphasing power amplifiers

The load modulation architectures discussed in Chapter 2 and Chapter 5 provide efficiency improvement for transmitters operating with amplitude modulated signals. It has been shown, that all these techniques force active devices of RF PAs to operate in saturation even at back-off power levels. However, modern wireless systems must also provide very low level of nonlinear distortion. In order to maintain high level of linearity of transmitted signals, various DPD techniques are used in modern transmitters. The type of linearization technique used depends on many factors, such as the architecture of the transmitter, signal bandwidth, acceptable computational complexity, etc.

In this chapter the linear operation of outphasing PA based on class-E power amplifiers with shunt capacitance and shunt filter is discussed. Firstly, the sources of nonlinearity in an outphasing PA are discussed and an analytical technique predicting the nonlinear behaviour of a Chireix outphasing combiner excited with signals with different magnitudes is presented. Secondly, a simple analytical memoryless DPD technique is proposed. It is shown, that this technique can be applied to different types of class-E PAs, such as class-E with finite DC inductance and class-E with shunt capacitance and shunt filter. Lastly, the application of memory polynomial

technique to class-E outphasing PA is demonstrated. Highly linear operation of the outphasing PA presented in Chapter 5 has been achieved on a fully automated testbench.

6.1 Nonlinearity of Chireix power combiner under amplitude imbalance

In Section 5.1 it has been shown, that a Chireix power combiner fed by two ideal voltage sources with equal magnitudes does not introduce any nonlinear distortion into output signal. However, outphasing PAs with non-isolated combiners show significant nonlinear behaviour and phase distortion due to amplitude imbalance between branches [125]. It has been shown that the primary source of this imbalance is load modulation effects in the outphasing PA branches. In this section we present analytical equations that explicitly attribute how amplitude imbalance between combiner branches distorts the AMAM characteristic of an outphasing amplifier. The proposed analytical equations have been compared to both ADS simulations and experimental measurements.

6.1.1 Chireix combiner under amplitude imbalance

In order to analyse the nonlinear behaviour of a Chireix power combiner, first a basic model of the Chireix combiner is developed as shown in Fig. 6.1. This model is a generalization of the model presented in Fig. 5.5 for the case when the branches of the combiner are fed by voltage sources with exciting voltages $\dot{V}_1 = V_1 e^{+j\theta}$ and $\dot{V}_2 = V_2 e^{-j\theta}$. We denote $k_{\mathrm{V}} = V_1/V_2$ and in the case of amplitude imbalance $k_{\mathrm{V}} \neq 1$. Since the sources are connected to the junction point through quarter wavelength transmission lines, the currents next to the load will be $\dot{I}_1 = I_1 e^{j\theta}$ and $\dot{I}_2 = I_2 e^{-j\theta}$ as shown in Fig. 6.2. Therefore, the voltage across the load can be expressed as:

$$\dot{V}_{\mathrm{L}} = \left(I_1 e^{j\theta} + I_2 e^{-j\theta}\right) R_{\mathrm{L}} \tag{6.1}$$

Fig. 6.1 Circuit model of a Chireix combiner excited with two voltage sources with different magnitudes.
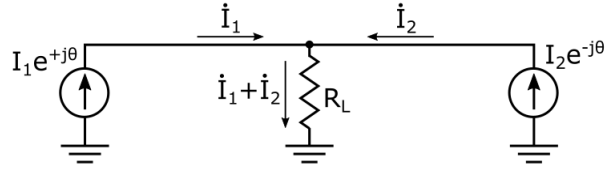
Fig. 6.2 Currents at the junction

and each current source will see impedance:

$$Z_{I1,2} = \frac{\dot{V}_{\mathrm{L}}}{\dot{I}_{1,2}} = R_{\mathrm{L}}\left(1 + \frac{I_{2,1}}{I_{1,2}}e^{\mp 2j\theta}\right) \tag{6.2}$$

Taking into account that transmission lines of the combiner have characteristic impedance Z_{c} and $k_{\mathrm{V}} = V_1/V_2 = I_1/I_2$ we can express the input impedance of the Chireix combiner transmission lines:

$$\frac{1}{Z_{1,2}} = \frac{R_{\mathrm{L}}}{Z_{\mathrm{c}}^2}\left(1 + (k_{\mathrm{V}}e^{2j\theta})^{\mp 1}\right) \tag{6.3}$$

If we assume that the compensating reactive elements C_c and L_c provide the same susceptance $B_{\mathrm{comp}} = \omega C_{\mathrm{c}} = 1/(\omega L_{\mathrm{c}})$ then the input impedance of the Chireix combiner branches will be:

$$\frac{1}{Z_{\mathrm{ch}1,2}} = \frac{R_{\mathrm{L}}}{Z_{\mathrm{c}}^2}\left(1 + (k_{\mathrm{V}}e^{2j\theta})^{\mp 1} \pm jB_{\mathrm{comp}}\right) \tag{6.4}$$

It can be shown that in the particular case when $k_{\mathrm{V}} = 1$ (6.4) gives us the expressions for input impedance of a Chireix combiner (5.18) and (5.19). Having found the

103

input impedance for both branches one can determine the power coming into both branches:

$$P_{\text{in}1,2} = \frac{V_1^2}{2Z_{1,2}} = \frac{V_{1,2}^2 R_{\text{L}}}{2Z_c^2}\left(1 + (k_{\text{V}}e^{2j\theta})^{\mp 1}\right) \tag{6.5}$$

and the power on the load can be found from the energy conservation law:

$$P_{\text{L}} = \text{real}\left\{P_{\text{in}1} + P_{\text{in}2}\right\} = \frac{V_1^2 R_{\text{L}}}{2Z_c^2}\left(1 + \frac{1}{k_{\text{V}}^2} + \frac{2\cos 2\theta}{k_{\text{V}}}\right) \tag{6.6}$$

Therefore, amplitude of voltage across the output load can be expressed as:

$$V_{\text{L}} = \sqrt{2P_{\text{L}}R_{\text{L}}} = \frac{V_1 R_{\text{L}}}{Z_c}\sqrt{1 + \frac{1}{k_{\text{V}}^2} + \frac{2\cos 2\theta}{k_{\text{V}}}} \tag{6.7}$$

From (6.2) it follows that the phase of the output voltage will be distorted relative to the input voltage by a phase shift, which can be expressed as:

$$\Delta\theta = \arctan\left(\frac{k_{\text{V}} - 1}{k_{\text{V}} + 1}\tan\theta\right) \tag{6.8}$$

It should be noted that since the combiner is excited by voltage sources, the compensating reactive components C_{c} and L_{c} do not affect the power coming to the load and, therefore, are not presented in expressions (6.7) and (6.8). However, as it was shown in 5.1, they significantly affect the input impedance of the combiner's branches.

In order to validate the nonlinear behaviour of the Chireix combiner excited by two voltage sources we used ADS Ptolemy cosimulation software tool. To test the combiner, a 16QAM OFDM modulated signal was used. The original signal had 10 MHz bandwidth and 160 Msps sample rate. This signal was generated using MatLab, separated into two outphasing components and exported to ADS simulation software. In ADS, a Ptolemy cosimulation is carried out by importing the two input signals. They are upconverted in the simulation to a carrier frequency of 3.5 GHz and combined using the Chireix combiner. The output impedance values of the IQ

modulators were set to 0.1 ohm. A power imbalance was simulated by additional power added to the $+\theta$ branch, where $\Delta P = 20\log(k_{\mathrm{V}})$.
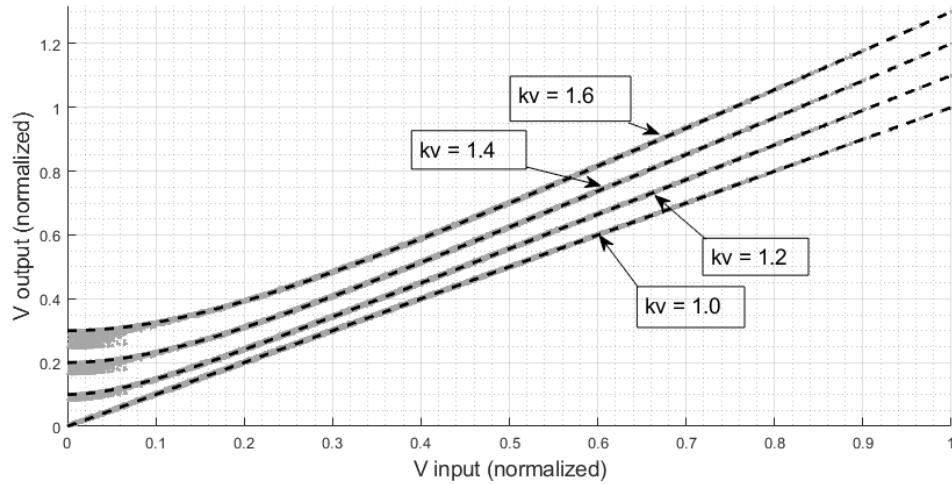
Fig. 6.3   AMAM characteristics of a Chireix combiner for different values of amplitude imbalance: Simulated in ADS (grey dots); predicted by analytical technique (black dashed line)
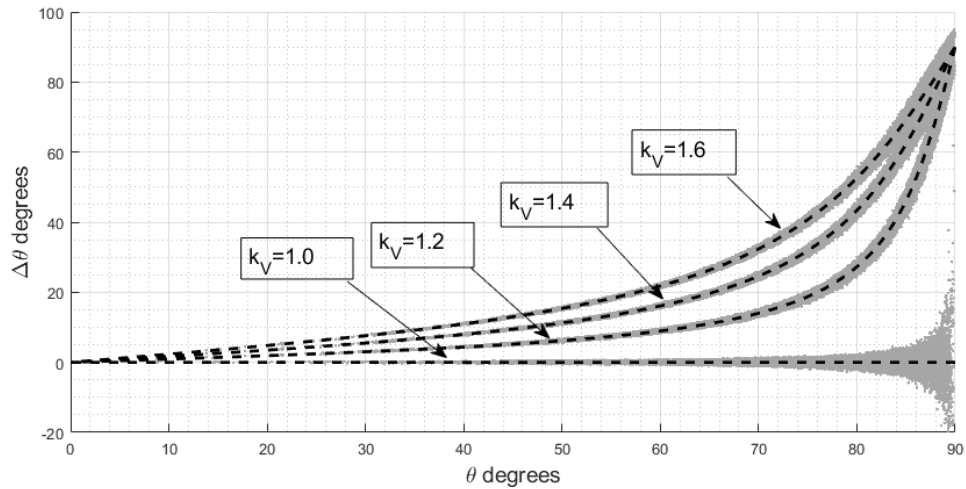
Fig. 6.4   Phase distortion of a Chireix combiner for different values of amplitude imbalance: Simulated in ADS (grey dots); predicted by analytical technique (black dashed line)

The output signal is then captured using a timed sink block. Having the original signal and the signal received from the output of our testbench, one can plot the AMAM characteristic of the system for different values of k_{V}. In Fig. 6.9 and Fig. 6.4 we present AMAM curves and phase distortion. The curves simulated

Table 6.1 MSE and NMSE for different values of amplitude imbalance (voltage source excitation).

k_V	MSE, dB	NMSE, dB
1.0	-42.9	-34.2
1.2	-42.1	-32.3
1.4	-40.7	-31.7
1.6	-39.4	-31.1

using the ADS-Ptolemy cosimulation tool are shown with grey dots and the curves calculated using the proposed model are shown with black dashed lines. The curves are plotted for amplitude imbalance ratios of $k_V = 1.0, 1.2, 1.4, 1.6$. For presentation purposes, all the values are normalised to the maximum output voltage in case of linear response. The values of mean square error (MSE) and normalised mean square error (NMSE) were calculated using expressions (2.36) and (2.37) respectively. The calculated MSE and NMSE values are presented in Table 6.1 as figures of merit for the goodness of fit of the proposed model.

From both the plots and figures of merit, one can see that the results obtained by using the analytical model are in close agreement with the numerical simulations. However, since the proposed model does not take into account memory effects, the results do not match perfectly.

6.1.2 Chireix combiner fed by power sources

Since all real sources have finite impedance, the proposed technique should be adopted to describe Chireix combiner fed by two power sources with output impedance r. In this case each power source will see a parallel connection of transmission lines as the input and compensating reactive element as shown in Fig. 6.5. The rC and rL circuits in the combiner branches operate as voltage dividers. Therefore, voltages $\dot{V}_{11}$ and $\dot{V}_{12}$ across inputs Z_{TL1} and Z_{TL2} respectively will be different from exciting voltages $\dot{V}_1$ and $\dot{V}_2$ in both phases and magnitudes. From ohm's law and equation
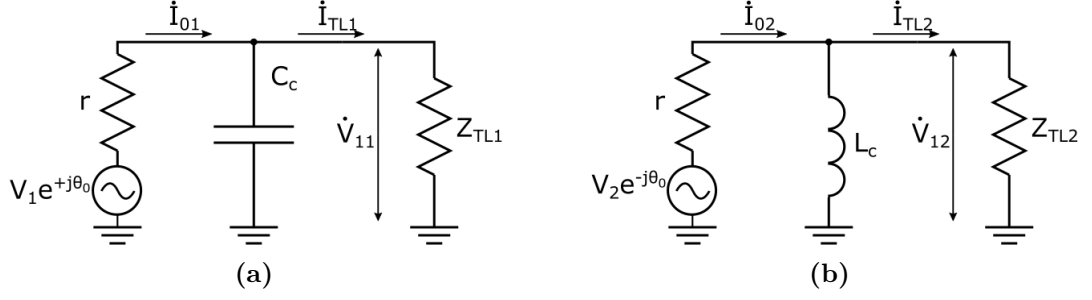
Fig. 6.5   Branches of Chireix combiner excited by power sources: (a) $+\theta$ branch; (b) $-\theta$ branch

(6.3) these voltages can be expressed as:

$$\dot{V}_{11} = \frac{V_1 e^{+j\theta} Z_c^2}{Z_c^2(jr\omega C_{\rm c} + 1) + rR_{\rm L}(1 + \frac{1}{k_{\rm V1}}e^{-j2\theta_1})} \tag{6.9}$$

$$\dot{V}_{12} = \frac{V_2 e^{-j\theta} Z_c^2 j\omega L_{\rm c}}{Z_c^2(j\omega L_{\rm c} + r) + j\omega L_{\rm c} rR_{\rm L}(1 + k_{\rm V1}e^{+j2\theta_1})} \tag{6.10}$$

where $\omega = 2\pi f_c$, f_c is the centre frequency of transmitted signal, $k_{\rm V1} = V_{11}/V_{12}$ is the amplitude ratio at the input of the transmission lines, $2\theta_1$ is the phase difference between voltages $\dot{V}_{11}$ and $\dot{V}_{12}$: $2\theta_1 = \mathrm{phase}(\dot{V}_{11}) - \mathrm{phase}(\dot{V}_{12})$. As well as in the case of voltage source excitation, the compensating reactive components $L_{\rm c}$ and $C_{\rm c}$ provide parallel susceptance $B_{\rm comp}$ defined by (5.15) at the carrier frequency $f_{\rm c}$. Taking into consideration that $V_1 = k_{\rm V} V_2$ we divide both parts of the equations (6.9) and (6.10) and obtain one equation:

$$k_{\rm V1}e^{j2\theta_1} = \frac{k_{\rm V}e^{2j\theta_0}}{j\omega L_c} \cdot \frac{Z_c^2(r + j\omega L_c) + rR_{\rm L}j\omega L_c(1 + k_{\rm V1}e^{j2\theta_1})}{Z_c^2(1 + j\omega rC_c) + rR_{\rm L}(1 + \frac{1}{k_{\rm V1}}e^{-j2\theta_1})} \tag{6.11}$$

Equation (6.11) can be split into two independent equations for real and imaginary parts. One can exclude $k_{\rm V1}$ from the system and solve the system for $2\theta_1$. The final result will be:

$$2\theta_1 = \arctan\left(\frac{A_2 A_3 - A_1}{A_1 A_3 + A_2}\right) + n\pi \tag{6.12}$$

Fig. 6.6   Experimental setup

where A_1, A_2 and A_3 are

$$
\begin{cases}
A_1 = K_1 r R_{\mathrm{L}} - Z_{\mathrm{c}}^2 - r R_{\mathrm{L}} & \text{(6.13a)} \\[2mm]
A_2 = Z_{\mathrm{c}}^2 r X_C - R_{\mathrm{L}} r K_2 & \text{(6.13b)} \\[2mm]
A_3 = \dfrac{X_L r R_{\mathrm{L}} - K_1 X_L (Z_c^2 + r R_{\mathrm{L}}) - K_2 Z_c^2 r}{Z_c^2 X_{\mathrm{L}} K_2 + X_{\mathrm{L}} R_{\mathrm{L}} r K_2 - Z_c^2 r K_1} & \text{(6.13c)}
\end{cases}
$$

where we denoted $X_{\mathrm{c}} = \omega C_c$, $X_L = \omega L_c$, $K_1 = k_{\mathrm{V}} \cos 2\theta_0$ and $K_2 = k_{\mathrm{V}} \sin 2\theta_0$. It should be noted that the outphasing angle defined by (6.12) should fall within the range $[0°...90°]$. Once the outphasing angle at the input of the Chireix combiner is found, one can find the value of magnitude imbalance at this point:

$$
k_{\mathrm{V1}} = \frac{X_L Z_c^2 K_2 + X_L R_{\mathrm{L}} r K_2 - Z_c^2 r K_1}{X_L (D_1 + D_2)} \tag{6.14}
$$

where we denoted:

$$
\begin{cases}
D_1 = (X_c Z_c^2 r - r R_L K_2) \cos(2\theta_1) & \text{(6.15a)} \\[2mm]
D_2 = (Z_c^2 + r R_L - R_L r K_1) \sin(2\theta_1) & \text{(6.15b)}
\end{cases}
$$

Once we have found amplitude and phase imbalance between the two combiner branches we can find voltages across the inputs of the combiner transmission lines using the expressions (6.9) and (6.10). Amplitude and phase of output voltage can be found in turn from (6.7) and (6.8).

Table 6.2 MSE and NMSE for different values of amplitude imbalance (power source excitation).

k_V	MSE, dB	NMSE, dB
1.0	-37.19	-31.25
1.2	-35.2	-29.38
1.4	-33.67	-28.12
1.6	-32.16	-26.88

For an experimental validation of the proposed technique we used a measurement setup consisting of a dual-path digital-to-analogue converter (DAC) board and a high-speed analogue-to-digital converter (ADC) to capture the combined output signal, as shown in Figure 6.6. An OFDM modulated signal with 10 MHz bandwidth was split into two outphasing paths and generated from the DAC board. The two outphasing parts of the signal are recombined with a microstrip Chireix combiner fabricated on RO4350 substrate. The reactive elements of the combiner are optimized for an outphasing angle of 73°. The recombined signal was captured with a high-speed analogue-to-digital converter.

Since the outputs of the DAC board have output impedances of 50 ohm, the results are compared with the theoretical results given by equations presented in this subsection. It should be noted that unlike the ADS testbench simulation in the experimental setup we reduced the power of the $-\theta$ branch. For this reason the bigger the value of k_V the less power that will come to the output load. The MSE and NMSE values for the model compared to the experimentally measured complex envelope responses are listed in Table 6.2. The AMAM distortion of the signal for different values of magnitude imbalance k_V is presented in Figure 6.7.

6.2   Phase-only digital predistortion technique for class-E outphasing PAs

As it was mentioned in Section 6.1, amplitude and phase imbalance between two branches are the two main sources of outphasing PA nonlinearity. In order to address
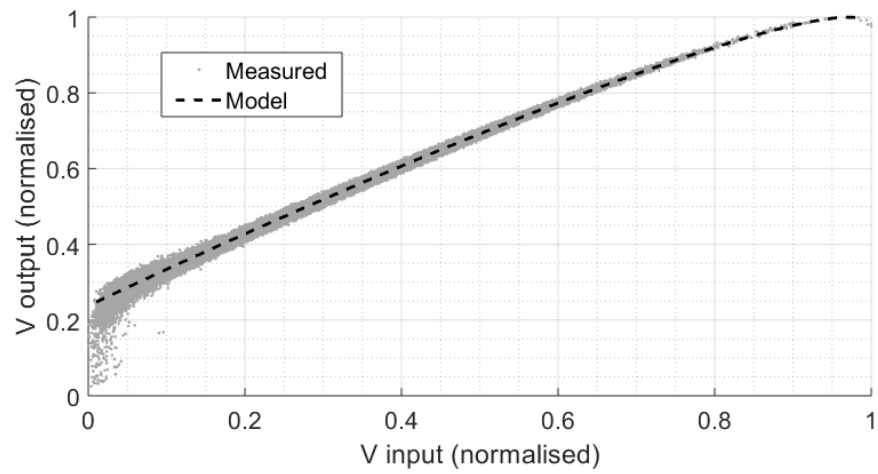
(a)
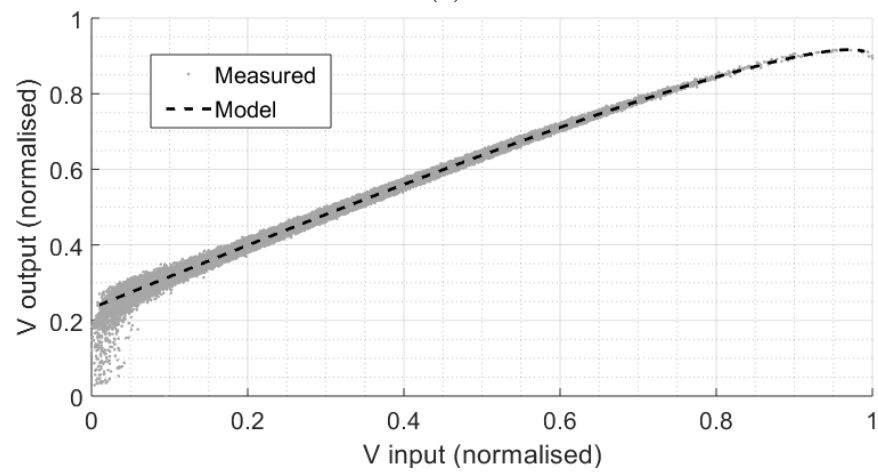
(b)
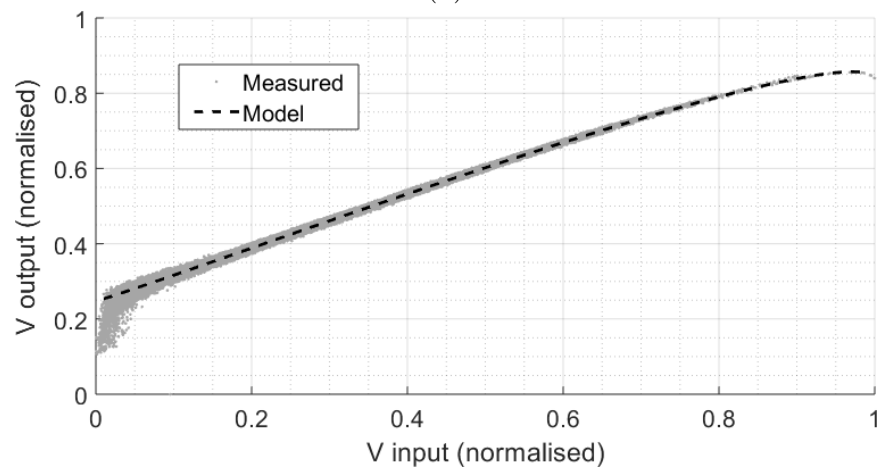
(c)

Fig. 6.7 Measured AMAM characteristics for Chireix combiner excited by two power sources for different values of k_V: (a) $k_V = 1.0$; (b) $k_V = 1.2$; (c) $k_V = 1.4$
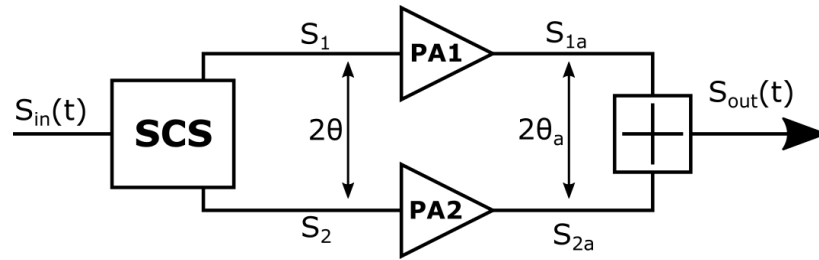
Fig. 6.8 Block-diagram of a LINC transmitter.

these issues various predistortion techniques have been proposed in the literature. In [126] a phase correction technique was applied for a single class-E PA. However, it requires measurement of phase at the output of the PAs and therefore cannot be directly applied to LINC transmitters. In [62] the authors use an iterative procedure in order to estimate magnitude and phase compensation coefficients. The technique presented in [127] is based on representation of branch amplifiers as power sources with constant output impedance. However, since the behaviour of most power amplifiers is closer to the current source rather than to the ideal voltage source, it is difficult to apply this technique to real outphasing PAs. In [128] the authors find phase predistortion coefficients for a class-D outphasing power amplifier solving non-convex optimisation problem.

In this section we propose a phase-only predistortion technique which can be applied to class-E outphasing amplifiers with a nonisolated Chireix combiner. Phase predistortion coefficients are directly extracted from AMAM characteristic of the output signal. The calculation of predistortion coefficients is based on an analytical model of the Chireix combiner and therefore is more computationally efficient compared to the techniques presented previously in the literature. The presented method is proven using simulation of outphasing class-E PA with 16QAM OFDM modulated signal in ADS software.

In order to construct a model describing the nonlinearity of class-E outphasing PA we make the following assumptions:

1. Magnitudes of the gains of the branch amplifiers are identical, constant and equal to G.

111

2. Phases of the gains of the branch amplifiers depend only on the load presented to branch amplifiers.

Later in this section it will be shown, that these assumptions are valid for some types of PAs, particularly, for some types of class-E PA. These assumptions mean that if after the SCS both signals have the same magnitude V_1 and can be expressed as

$$
\begin{cases}
S_1 = V_1 e^{j\theta(t)} & \text{(6.16a)} \\
S_2 = V_1 e^{-j\theta(t)} & \text{(6.16b)}
\end{cases}
$$

then after amplification the signals will be:

$$
\begin{cases}
S_{1a} = GV_1 e^{j(\theta(t)+\Delta\theta_1(t))} & \text{(6.17a)} \\
S_{2a} = GV_1 e^{-j(\theta(t)-\Delta\theta_2(t))} & \text{(6.17b)}
\end{cases}
$$

Two amplified signals are combined together with a nonisolated Chireix combiner discussed in Section 5.1, as shown in Fig. 6.8. Therefore, the outphasing angle at the inputs of the Chireix combiner θ_a can be expressed as:

$$
2\theta_{\mathrm{a}} = 2\theta + \Delta\theta_1 - \Delta\theta_2 = 2\theta + \Delta\theta_{12} \tag{6.18}
$$

where $\Delta\theta_{12} = \Delta\theta_1 - \Delta\theta_2$ is the phase distortion introduced by branch amplifiers.

Since both $\Delta\theta_1$ and $\Delta\theta_2$ depend on the load presented to the respective branch amplifiers they depend on the outphasing angle θ_{a}. Hence, $\Delta\theta_{12}$ is also a function of θ_{a}. This function can be found with load-pull simulation of the amplifier and approximation of the analytical function $\Delta\theta_{12}(\theta_{\mathrm{a}})$.

Once the values θ_a have been found, magnitude of the voltage across the output load can be directly derived from (5.21):

$$
V_{\mathrm{L}} = \frac{2GV_1 R_{\mathrm{L}}}{Z_{\mathrm{c}}} \cos\theta_{\mathrm{a}} \tag{6.19}
$$

where R_L is the output load resistance (e.g. input impedance of transmitter antenna or diplexer), Z_c is the characteristic impedance of the Chireix combiner transformers. From (6.19) it follows that if $\theta_a \neq \theta$ then the input amplitude to output amplitude (AMAM) response of outphasing PA will be nonlinear.

In order to linearize the PA, the initial signal should be predistorted based on an AMAM curve. The output signal of the PA can be captured using an analogue-to-digital converter. Having both input and output signals, the AMAM curve can be plotted. For a narrowband signal it is assumed that the memory effect can be neglected, and AMAM curve can be approximated by the polynomial:

$$\frac{V_L Z_c}{2GV_1 R_L} = a(v) = \sum_{i=0}^{N} a_i v^i \tag{6.20}$$

where $v = V_{in}/V_{in\ max}$ is the normalised input voltage. Having found the expression for the AMAM curve one can find the outphasing angle at the input of the Chireix combiner:

$$\theta_a = \arccos\left(a(v)\right) \tag{6.21}$$

Having found the outphasing angle θ_a for each value $v \in [0, 1]$, the outphasing angle distortion $\Delta\theta_{12}$ can be found using expressions (6.20) and (6.21):

$$\Delta\theta_{12} = 2\theta_a - 2\theta \tag{6.22}$$

It should be noted that, in order to find the predistortion coefficients, $\Delta\theta_{12}$ should be expressed as a function of θ_a. For this reason, θ_{12} can be numerically approximated with a polynomial function.

In order to achieve the linear performance, the initial outphasing angle values θ should be replaced with new values θ' in a way that the angle at the input of the combiner becomes the desired value θ, where θ is defined by (5.3). From (6.22) it follows that these new values can be found as:

$$\theta' = -0.5(\Delta\theta_{12} - 2\theta) \tag{6.23}$$

The proposed predistortion technique can be outlined in the following steps:

1. Capture the output signal and plot the AMAM curve.

2. Approximate the curve with a suitable order polynomial.

3. For each value of output voltage find the distortion of the outphasing angle according to (6.21) and (6.22).

4. Find predistorted outphasing angle values using (6.23).

Once the predistortion angle values that need to be applied are known, the modification of outphasing angle can be carried out in the digital domain along with signal component separation.

The proposed phase-only DPD technique is based on two main assumptions listed in the beginning of this section. The first assumption, that the branch amplifiers have constant gain, is referred to as load insensitivity [44]. This property can be achieved for different types of class-E PAs depending on the structure of the PA and used technology

6.2.1 Implementation of the phase-only DPD for outphasing PA based on class-E PA with finite DC-inductance

As it has been described in Chapter 2, the class-E PA with finite DC inductance can demonstrate high efficiency for wide range of output power levels [42]. Another advantage of this type of class-E PA is the possibility to implement it with CMOS technology due to the absence of bulky RF-choke [129, 130]. The load network of such amplifier consists of DC-feed inductance L_{d}, parallel capacitance C_{p}, series reactance X that can be both inductive and capacitive, and load R as shown in Fig. 2.11.

The input parameters for synthesis of such an amplifier are: output power level P_{out}, supply voltage V_{cc}, carrier frequency f_{c} and mistuning factor of the LC resonator $q = \frac{1}{2\pi f_c \sqrt{LC}}$. It has been shown in [43] that if the mistuning factor is chosen as
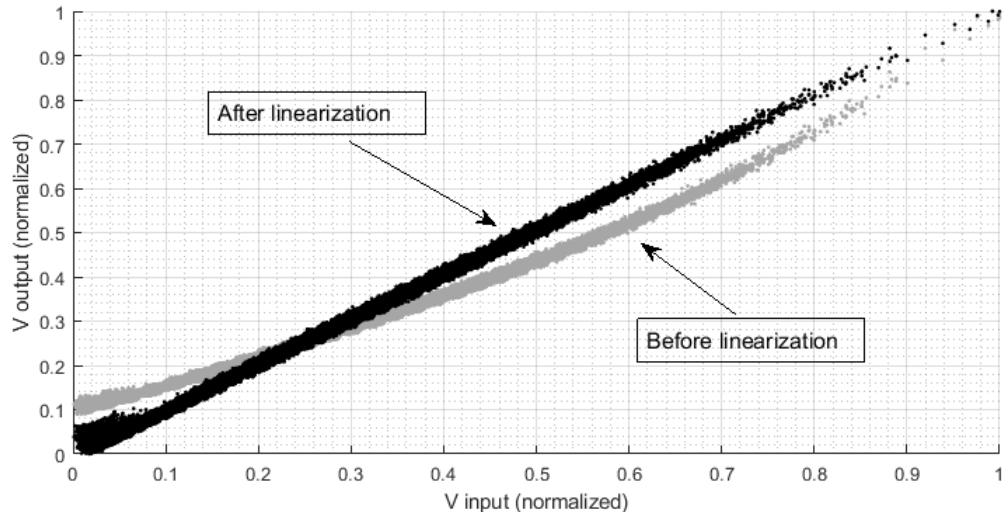
Fig. 6.9 AMAM plot of 20 MHz 16QAM OFDM modulated signal: grey dots - no predistortion applied; black dots - phase predistortion applied.

$q = 1.3$ then efficiency of such a class-E PA will not depend on the output load. It also should be noted that voltage across the output load will not depend on the output load. Therefore,in this situation, the only source of nonlinearity is phase distortion between outphasing amplifier branches.

In the general case, the parameters of the load network for this type of class-E PA can be found from solving a second-order differential equation for the drain voltage in the time domain [19]. However, for practical purposes it is convenient to use approximated analytical expressions presented in [102]. The class-E PA load network is optimized for 10 W output power and 3.5 GHz carrier frequency. In order to achieve load insensitivity, the parameter q was chosen $q = 1.3$. The load network was simulated using lumped components.

In order to prove the concept of the proposed phase-only predistortion technique, a simulation using the ADS-Ptolemy co-simulation tool from Keysight was performed. A 16QAM OFDM modulated signal with bandwidth 20 MHz and a sample rate of 320 Msps was generated and split into two outphasing phase modulated signals. Both phase modulated signals were upconverted to carrier frequency 3.5 GHz and sent to inputs of outphasing PA. The outphasing PA consisted of two identical class-E load-independent amplifiers and a Chireix combiner with compensating reactive elements.
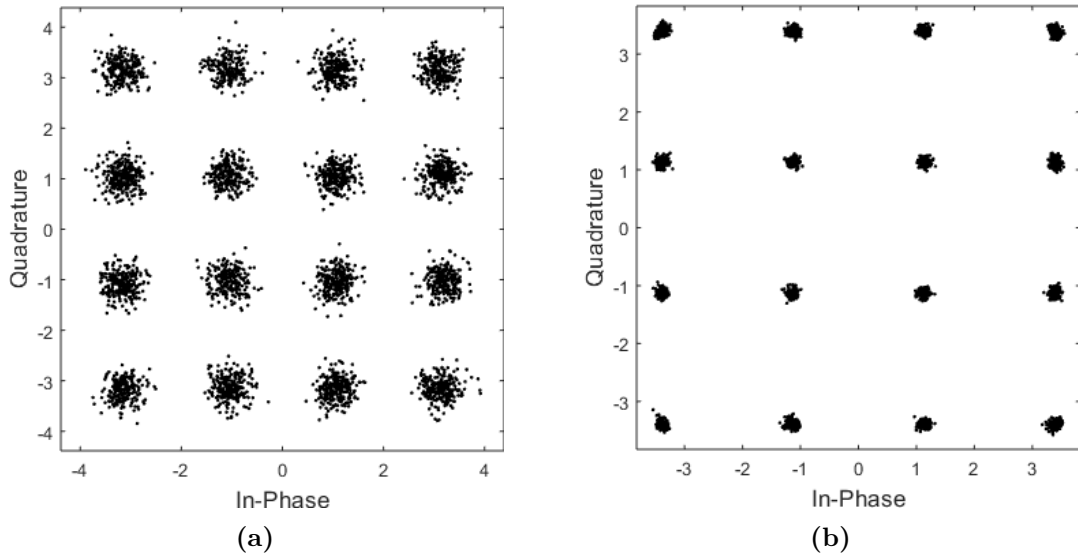
Fig. 6.10   Constellation of a 16QAM OFDM modulated signal: (a) - before DPD (EVM = 10.39%); (b) - after DPD (EVM = 2.43%).

The reactive elements were designed to provide zero susceptance for outphasing angle 73° since the probability density function of outphasing angle for OFDM modulated signal reaches a maximum at this value. For the first simulation an input signal was separated into two outphasing paths without any predistortion and amplified with the outphasing class-E amplifier. As a result, due to the phase imbalance between branches the signal experienced strong nonlinear distortion as shown in Fig. 6.9 and 6.10.

In order to perform the predistortion the AMAM characteristic shown in Fig. 6.9 (the grey curve) was approximated with a fourth-order polynomial function. Phase correction coefficients were calculated according to the equations (6.21) - (6.23). The correction was realised in the simulation set-up as an additional block in the signal component separator. The AMAM plot of the compensated output signal and its constellation are shown in Fig. 6.9 (black) and 6.10(b). From the presented plots one can see that using the proposed technique we managed to reduce the error vector magnitude (EVM) of the amplified signal from 10.39% to 2.43%. It should be noted that since the proposed technique does not take into account memory effect, EVM improvement would be less for signals with wider bandwidth.

6.2.2 Phase-only DPD for outphasing PA based on class-E PA with shunt capacitance and shunt filter

As it has been shown previously, the load insensitivity of a class-E PA with finite DC-inductance can be achieved by adjusting the mistuning factor of $L_\mathrm{d}C_\mathrm{p}$ resonator q. However, when a PA is implemented using microstrip transmission lines and a packaged active device, the parameter q is usually chosen in order to incorporate the device parasitic reactance into the load network. Therefore, a different approach to achieving load insensitivity needs to be used.

In this example a class-E PA is optimized for operation at carrier frequency 3.5 GHz and peak power 10 W. The circuit parameters are chosen in order to achieve purely resistive load at the output of the shunt resonator: $q = 1.607$, $L_\mathrm{s} = 2.26$ nH, $C_\mathrm{p} = 0.353$ pF, the optimum load for the peak power is $Z_\mathrm{L} = 33.6$ ohm. The outputs of the PAs are connected to the quaterwave Chireix combiner using T-shaped transmission lines, as shown in Fig. 6.11. For the sake of simplicity, the shunt capacitance and the series inductance are modelled by lumped components, the shunt filter and the matching network are simulated using ideal transmission lines. The active device is represented using an ideal switch with 4 ohm on-resistance and 10^6 ohm off-resistance. It should be noted that in the ideal case the on-resistance should be chosen as small as possible. However, when the PA is simulated using a harmonic balance simulator, a big difference between on-resistance and off-resistance may cause convergence issues of the simulator. The output Chireix combiner is modelled using ideal transmission lines, and the compensating reactive components are implemented using sections of open and short-circuited transmission lines (see Fig. 6.11).

The length of the output offset lines is chosen in order to eliminate amplitude imbalance between the two branches of the outphasing PA, whereas the characteristic impedance is chosen to be 50 ohm. With the given circuit parameters it has been found, that the optimum length of the offset lines is 75°. As well as in the previous subsection, the algorithm was tested using a 16QAM OFDM modulated signal with 20 MHz bandwidth. The spectrum of the output signal before and after applying
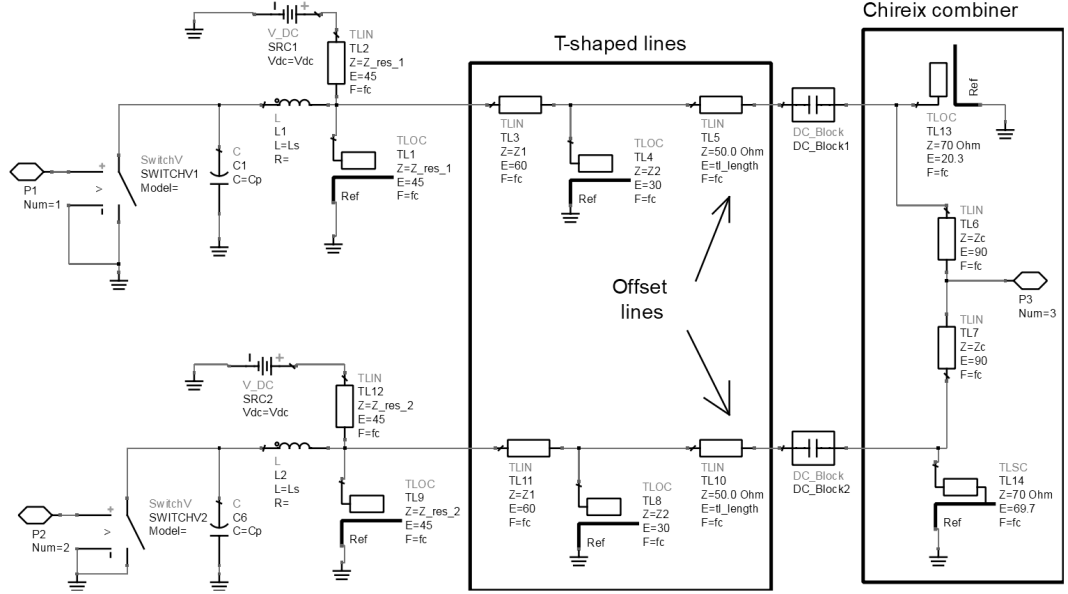
Fig. 6.11 ADS schematic of an outphasing PA based on class-E PAs with shunt capacitances and shunt filters used for phase-only DPD algorithm.

the DPD algorithm is shown in Fig. 6.12. The constellation of the output signal is shown in Fig. 6.13. From these plots one can see, that the proposed linearization algorithm improves the EVM from 12.6% to 1.95%. It should be pointed out, that the length and the characteristic impedance of the offset lines should be adjusted for a particular load network configuration. For example, if the parallel capacitance is chosen to incorporate a packages device parasitics, the load impedance will have reactive part, and therefore, the parameters of the T-shaped lines should be tuned accordingly.

6.3 Linearization of class-E PA using memory polynomials

The technique proposed in Section 6.2 provides a simple and computationally efficient way of improving linearity of outphasing PAs. However, since this technique does not take into account memory effect, the achievable level of linearity will be limited for wideband signals. Memory effect is one of the major sources of distortion in modern
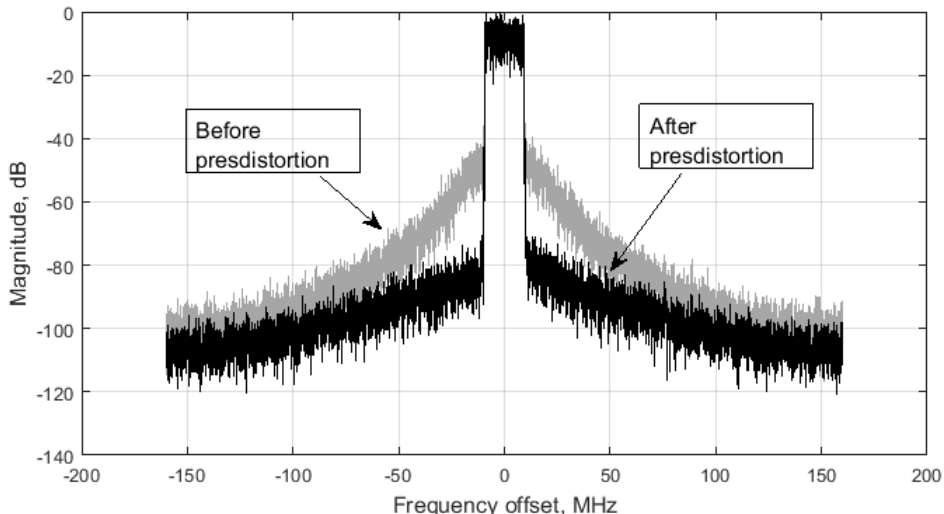
Fig. 6.12 Spectrum of a 20 MHz 16QAM OFDM modulated signal: grey line - no predistortion applied; black line - phase predistortion applied.
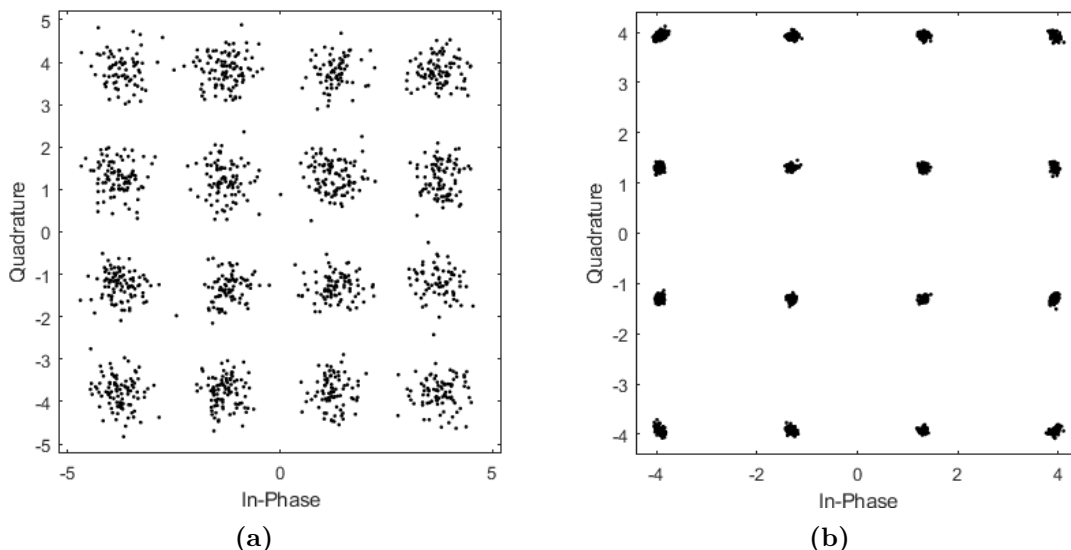
Fig. 6.13 Constellation of a 16QAM OFDM modulated signal: (a) - before DPD (EVM = 12.6%); (b) - after DPD (EVM = 1.95%).

GaN amplifiers [131, 132]. There is a number of models that take into account memory effect, however, they are beyond the scope of this section.

In this section we demonstrate the application of the memory polynomial technique in order to linearize the fabricated outphasing PA presented in Chapter 5. Compared to other algorithms, the memory polynomial technique provides a good trade-off between the precision of PA modelling and computational complexity [95, 133]. A
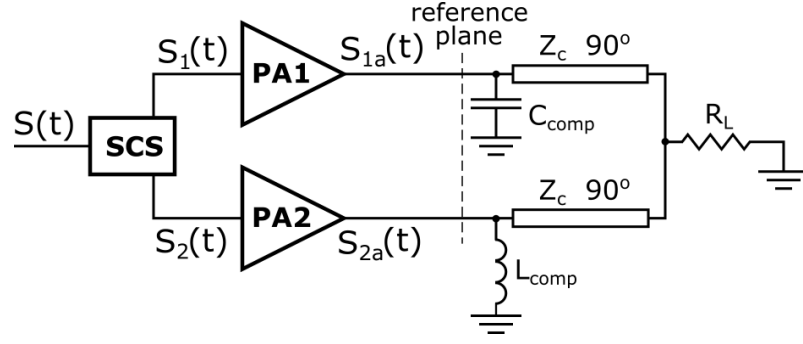
Fig. 6.14 ADS schematic of an outphasing PA based on class-E PAs with shunt capacitances and shunt filters used for phase-only DPD algorithm.

block-diagram of the fabricated outphasing PA is shown in Fig. 6.14. The input amplitude and phase modulated signal can be written in the form:

$$S(t) = A(t)e^{j(\varphi(t)+\omega t)} \tag{6.24}$$

where $A(t)$ is the modulated magnitude of the signal and $\varphi(t)$ is modulated phase, $\omega = 2\pi f_c$ is the carrier angular frequency. The SCS block is implemented in the digital domain using Matlab. Omitting the term representing the carrier wave $e^{j\omega t}$, the signals S_1 and S_2 after the SCS can be written in the form:

$$\begin{cases} S_1(t) = A_0 e^{j(\varphi(t)+\theta(t))} & \text{(6.25a)} \\ S_2(t) = A_0 e^{j(\varphi(t)-\theta(t))} & \text{(6.25b)} \end{cases}$$

After the amplification stage the signals reach the reference plane (see Fig. 6.14). The reference plane is chosen right before the quarterwave combiner, however, in the general case it can be chosen at any point of the output circuit where the angle can be calculated from the output signal. The signal at the reference plane can can be expressed as:

$$\begin{cases} S_{1a}(t) = A_{0a} e^{j(\varphi_a(t)+\theta_a(t))} & \text{(6.26a)} \\ S_{2a}(t) = A_{0a} e^{j(\varphi_a(t)-\theta_a(t))} & \text{(6.26b)} \end{cases}$$

Here we assume that, after the amplification, the signals have the same magnitude that is provided by the structure of the output load circuit of the class-E amplifiers. In expressions (6.26) θ_a represents amplitude modulation distortion and φ_a conveys the distorted phase of the original signal. As it was described in Chapter 2, the relationship between the input and the output signals is modelled using (2.35). In the case of outphasing it is convenient to represent the distorted phases separately using memory polynomial representation:

$$\theta_\mathrm{a}(n) = \sum_{p=1}^{P} \sum_{m=0}^{M} \alpha_{mp}\theta(n-m)|\theta(n-m)|^{2p} \tag{6.27}$$

$$\varphi_\mathrm{a}(n) = \sum_{p=1}^{P} \sum_{m=0}^{M} \beta_{mp}\varphi(n-m)|\varphi(n-m)|^{2p} \tag{6.28}$$

In (6.27) and (6.28) the continuous signals depending upon time t are replaced with sampled signals depending upon the sample number n. The outphasing angle at the reference plane can be found from the output voltage according to (5.21):

$$\theta_\mathrm{a} = \arccos\left(\frac{Z_\mathrm{c}V_\mathrm{out}}{2V_0 R_\mathrm{L}}\right) \tag{6.29}$$

It should be noted that expression (6.29) was derived for a nonisolated Chireix combiner excited with two voltages of equal magnitude. Real outphasing PAs have some amplitude imbalance between the branches due to the load modulation effects. However, expression (6.29) provides a good approximation for the outphasing angle even if a small imbalance between the branches exists. The normalized voltage (V_out/V_0) across the output load can be obtained from measured output signal. Once the signal has been received, the predistorted outphasing angle θ_DPD can be derived using the LMS technique, as described in Chapter 2. Once the amplitude response of the transmitter is linearized, the same technique can be applied in order to predistort the phase $\varphi(t)$.
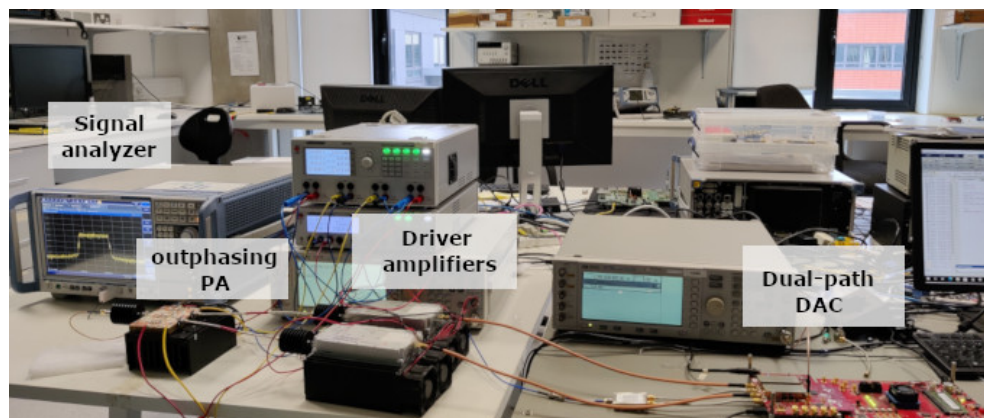
Fig. 6.15   Measurement setup.

6.3.1   Testbench setup

In order to test the linear performance of the PA, a measurement setup was used, as shown in Fig. 6.15. A signal with 64QAM OFDM modulation scheme, 20 MHz bandwidth and 8.8 dB PAPR was separated into two phase modulated signals in the digital domain. The two outphasing signals were generated from a TSW30SH84EVM board at the carrier frequency 2.14 GHz and preamplified using two linear driver amplifiers. The two outphasing signals were amplified using the tested outphasing PA. The output signal was attenuated and captured using a Rohde&Schwarz FSW signal analyzer. This signal analyzer allows for the capture of multiple passes of the transmitted signal. Averaging over 16 captures of the output signal in turn enables reduction of the noise of the received signal and therefore improves the precision of the PA modelling. It should be noted that a band-pass filter needs to be used at the input of the signal analyzer in order to eliminate aliasing. The bandwidth of the signal, however, should be wide enough in order to fully characterize nonlinear distortion of the signal. The postprocessing of the captured signal as well as generation of predistorted signal was implemented using Matlab.

Power spectrum of the output signal before linearization is shown in Fig. 6.16 (gray line). From this plot one can see, that due to phase distortion, the outphasing PA introduces significant spectrum regrowth. After application of the DPD technique, as outlined in this section, the linearity of the output signal was significantly improved
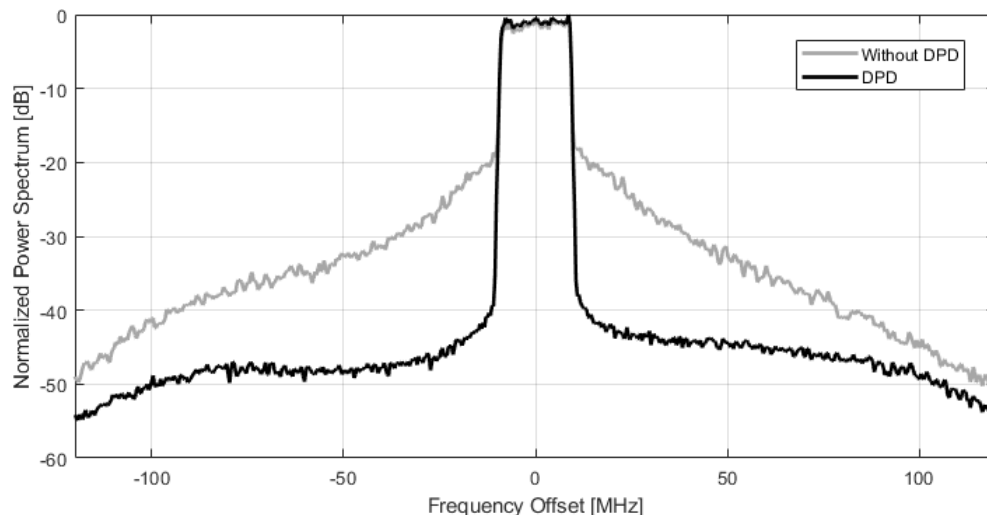
Fig. 6.16 Experimentally measured spectrum of the output signal before and after digital predistortion.

(black line in Fig. 6.16). The measured ACLR of the output signal is -39.5 dB. It should be pointed out, that the achieved ACLR was limited by the dynamic range of the transmitter, and could be further improved by using better equipment. The EVM of the linearized 64QAM OFDM modulated signal is 0.9%. The achieved drain efficiency with modulated signals is 44.3% and PAE is 26%.

It should be pointed out, that presented phase predistortion technique provides sufficient linearity improvement only if an outphasing PA is excited with two constant envelope signals. However, signals with non-constant envelope can be used in order to increase the gain at back-off power level, and therefore improve PAE of the PA [66]. In this case, the linearization techniques that take into account amplitude variation should be used [60]. Since the more advanced linearization methods require additional computational resources, the choice of a particular DPD technique also depends on the affordable complexity of the system.

6.4   Conclusion

In this chapter linear operation of class-E outphasing PAs has been discussed. An analytical description of the behaviour of a Chireix combiner under amplitude
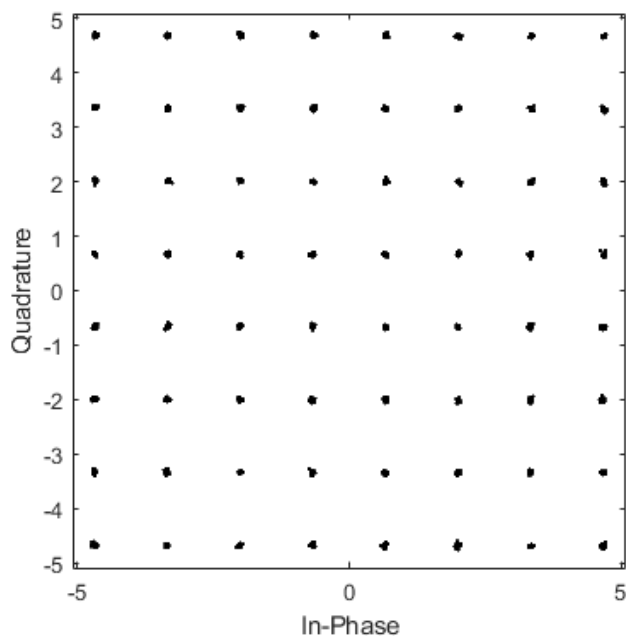
Fig. 6.17 Constellation of the demodulated predistorted signal (EVM = 0.9%).

imbalance has been proposed. It has been shown with numerical simulation and experimental measurement, that the proposed model predicts the AMAM curves of a signal generated from ideal voltage sources or power sources with fixed output impedance. A simple phase-only predistortion technique has been presented, that can be used with a class-E outphasing PA. It has been shown, that this technique can be applied to an outphasing PA based on the different types of class-E amplifiers, such as class-E PA with finite DC-inductance and class-E PA with shunt capacitance and shunt filter. Finally, the application of memory polynomial technique in order to linearize an outphasing PA has been demonstrated. The performance of the fabricated PA was experimentally validated using a 64QAM OFDM modulated signal generated from a dual-path DAC board. After the linearization, ACLR of -39.5 dBc and EVM of 0.9% were achieved. The achieved ACLR is limited by the used hardware, and could be further improved by using transmitter with higher dynamic range.

Chapter 7

Conclusions and future work

Power amplifiers are an essential part of most of wireless communication systems. The PAs have a significant impact on transmitter parameters, such as linearity and energy efficiency. Due to the ever increasing demand for wireless channel capacity, signals with high PAPR are widely used in modern communication systems. Therefore, power amplifiers must maintain high energy efficiency along with low level of nonlinear distortion across wide dynamic range. In order to attain this goal, some advanced transmitter architectures, such as Doherty PA, outphasing PA and envelope tracking technique have lately attracted the attention of industry and academia. These advanced PAs can be built based on different types of single-ended amplifiers. However, using switchmode PAs, such as class-E or class-F, can potentially provide higher efficiency, since the active device is driven into saturation.

In this thesis some issues related to design of load modulation transmitters based on class-E PAs are addressed. Firstly, in Chapter 3 a theoretical analysis of the class-E PA with shunt capacitance and shunt filter for peak and back-off output power has been presented. It has been shown, that the class-E PA with shunt capacitance and shunt filter can maintain high drain efficiency at back-off power level as well as at the peak power. It has also been shown that a back-off power level with a high drain efficiency can be achieved by adjusting the complex output load, which makes this type of PA suitable for load modulation transmitters. An analytical technique

for deriving load network parameters for peak and back-off power has been presented. The proposed technique has been proved using the Keysight ADS simulation tool.

Secondly, in Chapter 4 a wideband class-E PA with shunt capacitance and shunt filter has been proposed. It has been demonstrated, that using an L-shaped output matching circuit one can compensate the variation of the input reactance of the shunt LC-resonator. The proposed broadband class-E PA was optimized in Keysight ADS design tool and implemented using GaN HEMT device from Cree CHG40010F. The input and output circuits have been implemented using mictrostrip transmission lines on Rogers RO4350B substrate. The manufactured PA demonstrated over 65% drain efficiency across 1.7-2.8 GHz frequency band. The variation of the output power across this frequency range is 2 dB.

Thirdly, in Chapter 5 the application of the technique presented in Chapter 3 to outphasing PA design has been demonstrated. Load modulation properties of nonisolated Chireix combiner and isolated Wilkinson combiner have been analytically investigated. Relationships between outphasing angle and the output power for both types of combiners were derived. An outphasing PA based on two class-E amplifiers with shunt capacitances and shunt filters was optimized and fabricated using two GaN HEMT transistors CGH40010F. The performance of the fabricated PA was tested using two single-tone signals. The fabricated PA demonstrated over 60% drain efficiency and over 30% PAE at -8.5 dB back-off power level. It was also shown, that using a non-isolating combiner with lower loaded Q-factor at the back-off power one can improve the wideband performance of the outphasing PA. Simulated results for a Doherty PA based on class-E PA with shunt capacitance and shunt filter have been presented. The simulated PA provides minimum drain efficiency of 50% for back-off output power -7.5 dB.

Finally, in Chapter 6 some issues related to the linear operation of outphasing PAs based on class-E amplifiers have been discussed. An analytical model predicting nonlinear behaviour of a non-isolated Chireix combiner under amplitude imbalance has been proposed. The model was proven using both simulation in Keysight ADS and measurement setup. A phase-only predistortion technique providing memoryless

linearization of class-E outphasing PA has been proposed. It has been demonstrated, that this technique can improve the linearity of outphasing PA based on different types of class-E amplifiers, such as class-E PA with fininte DC inductance and class-E PA with shunt capacitance and shunt filter. In order to linearize the fabricated outphasing PA, a memory polynomial technique has been applied to an OFDM 64QAM modulated signal. The signal was generated from a dual-path DAC board, and the output signal was measured with a signal analyzer. After the linearization the output signal demonstrated ACLR of -39.5 dBc and EVM of 0.9%.

7.1 Future work

In this thesis some issues related to the using of class-E PAs in advanced transmitters are discussed. However, there is a capacity for further research in order to improve the prediction of analytical models, and to achieve better performance of designed transmitters. These research areas are particularly important due to the growing demand for throughput in future 5G and 6G systems, which will introduce more challenges for PA designers.

- The model used for the class-E PA load network parameters estimation uses an idealized representation of an active device as an ideal switch. Therefore, a model that represents some properties of FET transistors, such as finite on-resistance and dependence of drain-source capacitance upon drain voltage may significantly reduce the time required for numerical optimization of PAs.

- In Chapter 5 it has been shown, that the wideband properties of the presented outphasing PA can be improved if a non-isolated Chireix combiner with reduced loaded Q-factor is used. However, the operation was demonstrated using ideal model, when the active devices of outphasing PA are modelled as ideal switches. Implementation of this PA using GaN HEMT transistor could provide a better solution for 5G sub-6GHz frequency range. Besides, the broadband properties of outphasing PA can be explored.

127

- The outphasing PA presented in Chapter 5 was tested using two constant envelope signals in order to drive both branch amplifiers into class-E mode. However, using input signals with non-constant envelope can provide better gain at the back-off power level, which in turn improves PAE of the transmitter. This is particularly important for the transmitters operating with signals with high PAPR.

- The DPD technique presented in Chapter 6 is based on memory polynomial representation of the output signal, and operates with signal phase at the signal component separator. However, using non-constant envelope signals entails an additional source of nonlinearity due to the magnitude distortion. Therefore, the presented linearization technique should be modified in order to account for the signal magnitude nonlinear response.

References

[1] "3GPP The Mobile Broadband Standard," "https://www.3gpp.org/release-16", 2020.

[2] J. G. Andrews, S. Buzzi, W. Choi, S. V. Hanly, A. Lozano, A. C. K. Soong, and J. C. Zhang, "What Will 5G Be?" *IEEE Journal on Selected Areas in Communications*, vol. 32, pp. 1065–1082, 2014.

[3] S. Vishwanath, N. Jindal, and A. Goldsmith, "Duality, achievable rates, and sum-rate capacity of Gaussian MIMO broadcast channels," *IEEE Transactions on Information Theory*, vol. 49, pp. 2658–2668, 2003.

[4] F. Rusek, D. Persson, B. K. Lau, E. G. Larsson, T. L. Marzetta, O. Edfors, and F. Tufvesson, "Scaling Up MIMO: Opportunities and Challenges with Very Large Arrays," *IEEE Signal Processing Magazine*, vol. 30, pp. 40–60, 2013.

[5] R. W. Heath, N. González-Prelcic, S. Rangan, W. Roh, and A. M. Sayeed, "An Overview of Signal Processing Techniques for Millimeter Wave MIMO Systems," *IEEE Journal of Selected Topics in Signal Processing*, vol. 10, pp. 436–453, 2016.

[6] J. G. Proakis and M. Salehi, *Digital communications*. McGraw-hill New York, 2001, vol. 4.

[7] S. B. Weinstein, "The history of orthogonal frequency-division multiplexing [History of Communications]," *IEEE Communications Magazine*, vol. 47, no. 11, pp. 26–35, 2009.

[8] G. Berardinelli, K. I. Pedersen, T. B. Sorensen, and P. Mogensen, "Generalized DFT-spread-OFDM as 5G waveform," *IEEE Communications Magazine*, vol. 54, no. 11, pp. 99–105, 2016.

[9] A. Oswald and J. Schelleng, "Power amplifiers in trans-Atlantic radio telephony," *Proceedings of the Institute of Radio Engineers*, vol. 13, no. 3, pp. 313–361, 1925.

[10] H. Chireix, "High power outphasing modulation," *Proceedings of the Institute of Radio Engineers*, vol. 23, no. 11, pp. 1370–1392, 1935.

[11] W. H. Doherty, "A new high efficiency power amplifier for modulated waves," *Proceedings of the Institute of Radio Engineers*, vol. 24, no. 9, pp. 1163–1182, 1936.

[12] F. Raab, P. Asbeck, S. Cripps, P. Kenington, Z. Popovic, N. Pothecary, J. Sevic, and N. Sokal, "Power amplifiers and transmitters for RF and microwave," *IEEE Transactions on Microwave Theory and Techniques*, vol. 50, pp. 814–826, 2002.

[13] A. Katz, J. Wood, and D. Chokola, "The evolution of PA linearization: From classic feedforward and feedback through analog and digital predistortion," *IEEE Microwave Magazine*, vol. 17, no. 2, pp. 32–40, 2016.

[14] F. M. Ghannouchi and O. Hammi, "Behavioral modeling and predistortion," *IEEE Microwave magazine*, vol. 10, no. 7, pp. 52–64, 2009.

[15] A. Grebennikov, "High-Efficiency Class-E Power Amplifier With Shunt Capacitance and Shunt Filter," *IEEE Transactions on Circuits and Systems I: Regular Papers*, vol. 63, pp. 12–22, 2016.

[16] L. Hallman, "A Fourier Analysis of Radio-Frequency Power Amplifier Wave Forms," *Proceedings of the Institute of Radio Engineers*, vol. 20, pp. 1640–1659, 1932.

[17] B. Miller, "An Analysis of Class B and Class C Amplifiers," *Proceedings of the Institute of Radio Engineers*, vol. 23, pp. 496–509, 1935.

[18] P. Osborn, "A Study of Class B and C Amplifier Tank Circuits," *Proceedings of the Institute of Radio Engineers*, vol. 20, pp. 813–834, 1932.

[19] A. Grebennikov, N. Sokal, and M. Franco, *Switchmode RF and Microwave Power Amplifiers.* Elsevier Science, 2012.

[20] A. Grebennikov, *RF and Microwave Power Amplifier Design.* McGraw-Hill Education, 2004. [Online]. Available: https://books.google.ie/books?id=6oLg-RCx_bMC

[21] J. H. Morecroft and H. T. Friis, "The Vacuum Tube as a Generator of Alternating-Current Power," *Transactions of the American Institute of Electrical Engineers*, vol. XXXVIII, pp. 1415–1444, 1919.

[22] D. Prince, "Vacuum Tubes as Power Oscillators Part I," *Proceedings of the Institute of Radio Engineers*, vol. 11, pp. 275–313, 1923.

[23] S. C. Cripps, *RF power amplifiers for wireless communications.* Artech house Norwood, MA, 2006.

[24] P. Wright, J. Lees, J. Benedikt, P. J. Tasker, and S. C. Cripps, "A Methodology for Realizing High Efficiency Class-J in a Linear and Broadband PA," *IEEE Transactions on Microwave Theory and Techniques*, vol. 57, pp. 3196–3204, 2009.

[25] P. Wright, J. Lees, P. J. Tasker, J. Benedikt, and S. C. Cripps, "An efficient, linear, broadband class-j-mode pa realised using rf waveform engineering," in *2009 IEEE MTT-S International Microwave Symposium Digest*, 2009, pp. 653–656.

[26] P. Baxandall, "Transistor sine-wave LC oscillators. Some general considerations and new developments," *Proceedings of the IEE - Part B: Electronic and Communication Engineering*, vol. 106, pp. 748–758, 1959.

[27] V. Tyler and T. Australia, *A New High-efficiency High-power Amplifier*. Telecom Australia, 1978.

[28] D. Snider, "A theoretical analysis and experimental confirmation of the optimally loaded and overdriven RF power amplifier," *IEEE Transactions on Electron Devices*, vol. 14, pp. 851–857, 1967.

[29] F. Raab, "Class-F power amplifiers with maximally flat waveforms," *IEEE Transactions on Microwave Theory and Techniques*, vol. 45, pp. 2007–2012, 1997.

[30] F. Raab, "Maximum efficiency and output of class-F power amplifiers," *IEEE Transactions on Microwave Theory and Techniques*, vol. 49, pp. 1162–1166, 2001.

[31] P. Richards, "Resistor-transmission-line circuits," *Proceedings of the IRE*, vol. 36, pp. 217–220, 1948.

[32] P. Butterworth, S. Gao, S. F. Ooi, and A. Sambell, "High-efficiency class-F power amplifier with broadband performance," *Microwave and Optical Technology Letters*, vol. 44, no. 3, pp. 243–247, 2005.

[33] V. Carrubba, A. L. Clarke, M. Akmal, J. Lees, J. Benedikt, P. J. Tasker, and S. C. Cripps, "The Continuous Class-F Mode Power Amplifier," in *The 5th European Microwave Integrated Circuits Conference*. IEEE, 2010, pp. 432–435.

[34] N. Tuffy, A. Zhu, and T. J. Brazil, "Novel realisation of a broadband high-efficiency continuous class-F power amplifier," in *2011 6th European Microwave Integrated Circuit Conference*. IEEE, 2011, pp. 120–123.

[35] A. G. Khvilivitsky, "Designing the vacuum-tube generator, operating on detuned load," *Radiotekhnika*, vol. 8, pp. 21–26, 1953, (in Russian).

[36] G. D. Ewing, "High-efficiency radio-frequency power amplifiers," Ph.D. dissertation, Oregon State University, 1965.

[37] N. Sokal and A. Sokal, "Class E-A new class of high-efficiency tuned single-ended switching power amplifiers," *IEEE Journal of Solid-State Circuits*, vol. 10, pp. 168–176, 1975.

[38] F. Raab, "Idealized operation of the class E tuned power amplifier," *IEEE Transactions on Circuits and Systems*, vol. 24, pp. 725–735, 1977.

[39] N. Sokal, "Class E high-efficiency switching-mode tuned power amplifier with only one inductor and one capacitor in load network-approximate analysis," *IEEE Journal of Solid-State Circuits*, vol. 16, pp. 380–384, 1981.

[40] M. Kazimierczuk, "Exact analysis of class E tuned power amplifier with only one inductor and one capacitor in load network," *IEEE Journal of Solid-State Circuits*, vol. 18, pp. 214–221, 1983.

[41] V. I. Degtev, "Switching mode power amplifier with forming circuit," *Radiotekhnika*, vol. 40, pp. 77–80, 1985, (in Russian).

[42] M. Acar, A. J. Annema, and B. Nauta, "Analytical Design Equations for Class-E Power Amplifiers," *IEEE Transactions on Circuits and Systems I: Regular Papers*, vol. 54, pp. 2706–2717, 2007.

[43] M. P. van der Heijden, M. Acar, J. S. Vromans, and D. A. Calvillo-Cortes, "A 19W high-efficiency wide-band CMOS-GaN class-E Chireix RF outphasing power amplifier," in *2011 IEEE MTT-S International Microwave Symposium.* IEEE, 2011, pp. 1–1.

[44] A. Ghahremani, A.-J. Annema, and B. Nauta, "Outphasing Class-E Power Amplifiers: From Theory to Back-Off Efficiency Improvement," *IEEE Journal of Solid-State Circuits*, vol. 53, pp. 1374–1386, May 2018.

[45] M. Kazimierczuk, "Class E tuned power amplifier with shunt inductor," *IEEE Journal of Solid-State Circuits*, vol. 16, pp. 2–7, Feb. 1981.

[46] T. Brabetz and V. Fusco, "Voltage-driven class E amplifier and applications," *IEE Proceedings - Microwaves, Antennas and Propagation*, vol. 152, pp. 373–377, 2005.

[47] M. S. Mugisho, D. G. Makarov, Y. V. Rassokhina, V. G. Krizhanovski, A. Grebennikov, and M. Thian, "Generalized Class-E Power Amplifier With Shunt Capacitance and Shunt Filter," *IEEE Transactions on Microwave Theory and Techniques*, vol. 67, pp. 3464–3474, 2019.

[48] Z. Popovic and J. A. Garcia, "Microwave Class-E Power Amplifiers: A Brief Review of Essential Concepts in High-Frequency Class-E PAs and Related Circuits," *IEEE Microwave Magazine*, vol. 19, pp. 54–66, Jul. 2018.

[49] A. Grebennikov and F. H. Raab, "A History of Switching-Mode Class-E Techniques: The Development of Switching-Mode Class-E Techniques for High-Efficiency Power Amplification," *IEEE Microwave Magazine*, vol. 19, pp. 26–41, Jul. 2018.

[50] D. Cox, "Linear Amplification with Nonlinear Components," *IEEE Transactions on Communications*, vol. 22, pp. 1942–1945, 1974.

[51] C. Conradi, R. Johnston, and J. McRory, "Evaluation of a lossless combiner in a LINC transmitter," in *Engineering Solutions for the Next Millennium. 1999 IEEE Canadian Conference on Electrical and Computer Engineering (Cat. No. 99TH8411)*, vol. 1. IEEE, 1999, pp. 105–110.

[52] X. Zhang, L. E. Larson, P. M. Asbeck, and R. A. Langridge, "Analysis of power recycling techniques for RF and microwave outphasing power amplifiers," *IEEE Transactions on Circuits and Systems II: Analog and Digital Signal Processing*, vol. 49, no. 5, pp. 312–320, 2002.

[53] M. Özen, M. van der Heijden, M. Acar, R. Jos, and C. Fager, "A Generalized Combiner Synthesis Technique for Class-E Outphasing Transmitters," *IEEE Transactions on Circuits and Systems I: Regular Papers*, vol. 64, pp. 1126–1139, May 2017.

[54] S. Moloudi and A. A. Abidi, "The Outphasing RF Power Amplifier: A Comprehensive Analysis and a Class-B CMOS Realization," *IEEE Journal of Solid-State Circuits*, vol. 48, pp. 1357–1369, 2013.

[55] R. Zhang, M. Acar, M. P. van der Heijden, M. Apostolidou, and D. M. W. Leenaerts, "Generalized Semi-Analytical Design Methodology of Class-E Outphasing Power Amplifier," *IEEE Transactions on Circuits and Systems I: Regular Papers*, vol. 61, pp. 2951–2960, Oct. 2014.

[56] D. A. Calvillo-Cortes, M. van der Heijden, M. P, and L. C. de Vreede, "A 70W package-integrated class-E Chireix outphasing RF power amplifier," in *2013 IEEE MTT-S International Microwave Symposium Digest (MTT)*.   IEEE, 2013, pp. 1–3.

[57] R. A. Beltran, "Broadband Outphasing Transmitter using Class-E Power Amplifiers," in *2019 IEEE MTT-S International Microwave Symposium (IMS)*, 2019, pp. 67–70.

[58] K. D. Holzer, W. Yuan, and J. S. Walling, "Wideband Techniques for Outphasing Power Amplifiers," *IEEE Transactions on Circuits and Systems I: Regular Papers*, vol. 65, pp. 2715–2725, 2018.

[59] A. Birafane and A. Kouki, "An analytical approach to LINC power combining efficiency estimation and optimization," in *2003 33rd European Microwave Conference*.   IEEE, 2003, pp. 1227–1229.

[60] K. Finnerty, J. Dooley, R. Wesson, M. P. van der Heijden, M. Acar, and R. Farrell, "Behavioral modeling of outphasing amplification systems," *IEEE Transactions on Microwave Theory and Techniques*, vol. 64, no. 12, pp. 4165–4173, 2016.

[61] P. N. Landin, J. Fritzin, W. V. Moer, M. Isaksson, and A. Alvandpour, "Modeling and Digital Predistortion of Class-D Outphasing RF Power Amplifiers," *IEEE Transactions on Microwave Theory and Techniques*, vol. 60, pp. 1907–1915, 2012.

[62] T. Hwang, K. Azadet, R. S. Wilson, and J. Lin, "Linearization and Imbalance Correction Techniques for Broadband Outphasing Power Amplifiers," *IEEE Transactions on Microwave Theory and Techniques*, vol. 63, pp. 2185–2198, Jul. 2015.

[63] T.-P. Hung, D. K. Choi, L. E. Larson, and P. M. Asbeck, "CMOS outphasing class-D amplifier with Chireix combiner," *IEEE Microwave and Wireless Components Letters*, vol. 17, no. 8, pp. 619–621, 2007.

[64] T. Hwang, K. Azadet, R. S. Wilson, and J. Lin, "Characterization of Class-F Power Amplifier With Wide Amplitude and Phase Bandwidth for Outphasing Architecture," *IEEE Microwave and Wireless Components Letters*, vol. 24, pp. 188–190, Mar. 2014.

[65] T. W. Barton, J. L. Dawson, and D. J. Perreault, "Experimental Validation of a Four-Way Outphasing Combiner for Microwave Power Amplification," *IEEE Microwave and Wireless Components Letters*, vol. 23, pp. 28–30, Jan. 2013.

[66] P. E. de Falco, P. Pednekar, K. Mimis, S. B. Smida, G. Watkins, K. Morris, and T. W. Barton, "Load modulation of harmonically tuned amplifiers and application to outphasing systems," *IEEE Transactions on Microwave Theory and Techniques*, vol. 65, no. 10, pp. 3596–3612, 2017.

[67] T. Cappello, C. Florian, T. W. Barton, M. Litchfield, and Z. Popovic, "Multi-level supply-modulated Chireix outphasing for LTE signals," in *2017 IEEE MTT-S International Microwave Symposium (IMS)*, 2017, pp. 1846–1849.

[68] R. McMorrow, D. Upton, and P. Maloney, "The microwave Doherty amplifier," in *1994 IEEE MTT-S International Microwave Symposium Digest (Cat. No.94CH3389-4)*. IEEE, 1994, pp. 1653–1656 vol.3.

[69] M. Iwamoto, A. Williams, P.-F. Chen, A. Metzger, C. Wang, L. Larson, and P. Asbeck, "An extended Doherty amplifier with high efficiency over a wide power range," in *2001 IEEE MTT-S International Microwave Sympsoium Digest (Cat. No.01CH37157)*, vol. 2. IEEE, 2001, pp. 931–934 vol.2.

[70] W. C. E. Neo, J. Qureshi, M. J. Pelk, J. R. Gajadharsing, and L. C. N. de Vreede, "A Mixed-Signal Approach Towards Linear and Efficient N-Way Doherty Amplifiers," *IEEE Transactions on Microwave Theory and Techniques*, vol. 55, pp. 866–879, 2007.

[71] I. Kim, J. Moon, S. Jee, and B. Kim, "Optimized Design of a Highly Efficient Three-Stage Doherty PA Using Gate Adaptation," *IEEE Transactions on Microwave Theory and Techniques*, vol. 58, pp. 2562–2574, 2010.

[72] D. Y.-T. Wu and S. Boumaiza, "A Modified Doherty Configuration for Broadband Amplification Using Symmetrical Devices," *IEEE Transactions on Microwave Theory and Techniques*, vol. 60, pp. 3201–3213, 2012.

[73] A. Grebennikov and J. Wong, "A Dual-Band Parallel Doherty Power Amplifier for Wireless Applications," *IEEE Transactions on Microwave Theory and Techniques*, vol. 60, pp. 3214–3222, 2012.

[74] D. Gustafsson, C. M. Andersson, and C. Fager, "A Modified Doherty Power Amplifier With Extended Bandwidth and Reconfigurable Efficiency," *IEEE Transactions on Microwave Theory and Techniques*, vol. 61, pp. 533–542, 2013.

[75] P. Saad, R. Hou, R. Hellberg, and B. Berglund, "A 1.8–3.8-GHz Power Amplifier With 40% Efficiency at 8-dB Power Back-Off," *IEEE Transactions on Microwave Theory and Techniques*, vol. 66, pp. 4870–4882, 2018.

[76] Y. Suzuki, T. Hirota, and T. Nojima, "Highly efficient feed-forward amplifier using a Class-F Doherty amplifier," in *IEEE MTT-S International Microwave Symposium Digest, 2003*, vol. 1. IEEE, 2003, pp. 77–80 vol.1.

[77] S. Goto, T. Kunii, A. Inoue, K. Izawa, T. Ishikawa, and Y. Matsuda, "Efficiency enhancement of Doherty amplifier with combination of class-F and inverse class-F schemes for S-band base station application," in *2004 IEEE MTT-S International Microwave Symposium Digest (IEEE Cat. No.04CH37535)*, vol. 2. IEEE, 2004, pp. 839–842 Vol.2.

[78] P. Colantonio, F. Giannini, R. Giofre, and L. Piazzon, "Theory and Experimental Results of a Class F AB-C Doherty Power Amplifier," *IEEE Transactions on Microwave Theory and Techniques*, vol. 57, pp. 1936–1947, 2009.

[79] Y.-S. Lee, M.-W. Lee, and Y.-H. Jeong, "Highly Efficient Doherty Amplifier Based on Class-E Topology for WCDMA Applications," *IEEE Microwave and Wireless Components Letters*, vol. 18, pp. 608–610, 2008.

[80] D. R. Pehlke, "Class E Doherty amplifier topology for high efficiency signal transmitters," May 28 2002, uS Patent 6,396,341.

[81] R. Sperlich, G. C. Copeland, and R. Hoppenstein, "Hybrid Doherty Amplifier System and Method," May 15 2008, uS Patent App. 11/940,096.

[82] R. Darraji, F. M. Ghannouchi, and O. Hammi, "A Dual-Input Digitally Driven Doherty Amplifier Architecture for Performance Enhancement of Doherty Transmitters," *IEEE Transactions on Microwave Theory and Techniques*, vol. 59, pp. 1284–1293, 2011.

[83] M. Hashemi, L. Zhou, Y. Shen, and L. C. N. de Vreede, "A Highly Linear Wideband Polar Class-E CMOS Digital Doherty Power Amplifier," *IEEE Transactions on Microwave Theory and Techniques*, vol. 67, pp. 4232–4245, 2019.

[84] L. R. Kahn, "Single-Sideband Transmission by Envelope Elimination and Restoration," *Proceedings of the IRE*, vol. 40, pp. 803–806, 1952.

[85] D. Tena-Ramos, F. J. Ortega-González, and M. Patiño-Gómez, "Hybrid Envelope Elimination and Restoration Technique for Enhancing the Linearity of Switchmode Envelope Amplifiers," *IEEE Microwave and Wireless Components Letters*, vol. 27, no. 2, pp. 186–188, 2017.

[86] C. Lee and C. Seo, "A High Linearity and Efficiency of Envelope Elimination and Restoration using Photonic Band-gap and Applying Class-F Power Amplifier," in *2007 Asia-Pacific Microwave Conference*. IEEE, 2007, pp. 1–4.

[87] D. Su and W. McFarland, "An IC for linearizing RF power amplifiers using envelope elimination and restoration," *IEEE Journal of Solid-State Circuits*, vol. 33, pp. 2252–2258, 1998.

[88] P. Asbeck and Z. Popovic, "ET Comes of Age: Envelope Tracking for Higher-Efficiency Power Amplifiers," *IEEE Microwave Magazine*, vol. 17, no. 3, pp. 16–25, 2016.

[89] L. E. Barton, "A Plate Modulation Transformer for Radio Stations," *University of Arkansas Bulletin*, May 1930.

[90] A. A. M. Saleh and D. C. Cox, "Improving the Power-Added Efficiency of FET Amplifiers Operating with Varying-Envelope Signals," *IEEE Transactions on Microwave Theory and Techniques*, vol. 31, no. 1, pp. 51–56, 1983.

[91] B. D. Geller, F. T. Assal, R. K. Gupta, and P. K. Cline, "A technique for the maintenance of FET power amplifier efficiency under backoff," in *IEEE MTT-S International Microwave Symposium Digest*, 1989, pp. 949–952 vol.3.

[92] C. E. Shannon, "A mathematical theory of communication," *Bell system technical journal*, vol. 27, no. 3, pp. 379–423, 1948.

[93] F. H. Raab, P. Asbeck, S. Cripps, P. B. Kenington, Z. B. Popovic, N. Pothecary, J. F. Sevic, and N. O. Sokal, "RF and microwave power amplifier and transmitter technologies-Part 1," *high frequency electronics*, vol. 2, no. 3, pp. 22–36, 2003.

[94] M. Schetzen, *The Volterra and Wiener theories of nonlinear systems*, ser. A Wiley - Interscience publication. Wiley, 1980.

[95] J. Kim and K. Konstantinou, "Digital predistortion of wideband signals based on power amplifier model with memory," *Electronics Letters*, vol. 37, no. 23, pp. 1417–1418, 2001.

[96] D. Morgan, Z. Ma, J. Kim, M. Zierdt, and J. Pastalan, "A Generalized Memory Polynomial Model for Digital Predistortion of RF Power Amplifiers," *IEEE Transactions on Signal Processing*, vol. 54, pp. 3852–3860, 2006.

[97] P. N. Landin, T. Eriksson, J. Fritzin, and A. Alvandpour, "Behavioral modeling of outphasing amplifiers considering memory effects," in *2013 IEEE MTT-S International Microwave Symposium Digest (MTT)*. IEEE, 2013, pp. 1–4.

[98] O. Hammi, M. S. Sharawi, and F. M. Ghannouchi, "Generalized twin-nonlinear two-box digital predistorter for GaN based LTE Doherty power amplifiers with strong memory effects," in *2013 IEEE International Wireless Symposium (IWS)*. IEEE, 2013, pp. 1–4.

[99] M. Isaksson, D. Wisell, and D. Ronnow, "A comparative analysis of behavioral models for RF power amplifiers," *IEEE Transactions on Microwave Theory and Techniques*, vol. 54, pp. 348–359, 2006.

[100] S. Amin, E. Zenteno, P. N. Landin, D. Rönnow, M. Isaksson, and P. Händel, "Noise impact on the identification of digital predistorter parameters in the indirect learning architecture," in *2012 Swedish Communication Technologies Workshop (Swe-CTW)*. IEEE, 2012, pp. 36–39.

[101] P. N. Landin, A. E. Mayer, and T. Eriksson, "MILA - A noise mitigation technique for RF power amplifier linearization," in *2014 IEEE 11th International Multi-Conference on Systems, Signals and Devices (SSD14)*. IEEE, 2014, pp. 1–4.

[102] M. Acar, A. J. Annema, and B. Nauta, "Generalized Analytical Design Equations for Variable Slope Class-E Power Amplifiers," in *2006 13th IEEE International Conference on Electronics, Circuits and Systems*. IEEE, 2006, pp. 431–434.

[103] F. J. Ortega-Gonzalez, "Load–Pull Wideband Class-E Amplifier," *IEEE Microwave and Wireless Components Letters*, vol. 17, pp. 235–237, 2007.

[104] K. Shi, D. A. Calvillo-Cortes, L. C. N. de Vreede, and F. van Rijs, "A compact 65W 1.7–2.3GHz class-E GaN power amplifier for base stations," in *2011 41st European Microwave Conference*. IEEE, 2011, pp. 1103–1106.

[105] M. Özen, M. Acar, M. P. van der Heijden, M. Apostolidou, D. M. W. Leenaerts, R. Jos, and C. Fager, "Wideband and efficient watt-level SiGe BiCMOS switching mode power amplifier using continuous class-E modes theory," in *2014 IEEE Radio Frequency Integrated Circuits Symposium*. IEEE, 2014, pp. 243–246.

[106] M. Thian and V. Fusco, "Idealised operation of zero-voltage-switching series-L/parallel-tuned Class-E power amplifier," *IET Circuits, Devices and Systems*, vol. 2, pp. 337–346, 2008.

[107] C. Bowick, *RF circuit design*. Elsevier, 2011.

[108] "Wolfspeed Cree CGH40010 10-W RF Power GaN HEMT," https://www.wolfspeed.com/cgh40010, 2020, [Online; accessed 27-Oct-2020].

[109] Aitchison, C. S. and Davies, R. and Gibson, P. J., "A simple diode parametric amplifier design for use at S, C, and X band," *IEEE Transactions on Microwave Theory and Techniques*, vol. 15, no. 1, pp. 22–31, 1967.

[110] Aitchison, C. S. and Gelsthorpe, R. V., "A circuit technique for broadbanding the electronic tuning range of Gunn oscillators," *IEEE Journal of Solid-State Circuits*, vol. 12, no. 1, pp. 21–28, 1977.

[111] Hongtao Xu and S. Gao and S. Heikman and S. I. Long and U. K. Mishra and R. A. York, "A high-efficiency class-E GaN HEMT power amplifier at 1.9 GHz," *IEEE Microwave and Wireless Components Letters*, vol. 16, no. 1, pp. 22–24, 2006.

[112] M. P. van der Heijden and M. Acar and J. S. Vromans, "A compact 12-watt high-efficiency 2.1-2.7 GHz class-E GaN HEMT power amplifier for base stations," in *2009 IEEE MTT-S International Microwave Symposium Digest*, 2009, pp. 657–660.

[113] K. Chen and D. Peroulis, "Design of Highly Efficient Broadband Class-E Power Amplifier Using Synthesized Low-Pass Matching Networks," *IEEE Transactions on Microwave Theory and Techniques*, vol. 59, no. 12, pp. 3162–3173, 2011.

[114] V. Carrubba, A. L. Clarke, M. Akmal, J. Lees, J. Benedikt, P. J. Tasker, and S. C. Cripps, "The Continuous Class-F Mode Power Amplifier," in *The 5th European Microwave Integrated Circuits Conference*, 2010, pp. 432–435.

[115] R. Soares, *GaAs MESFET Circuit Design.* Artech House, 1988.

[116] A. Grebennikov, "Simple design equations for broadband class E power amplifiers with reactance compensation," in *2001 IEEE MTT-S International Microwave Sympsoium Digest*, vol. 3, 2001, pp. 2143–2146.

[117] N. Kumar and C. Prakash and A. Grebennikov and A. Mediano, "High-Efficiency Broadband Parallel-Circuit Class E RF Power Amplifier With Reactance-Compensation Technique," *IEEE Transactions on Microwave Theory and Techniques*, vol. 56, no. 3, pp. 604–612, 2008.

[118] F. Raab, "Efficiency of outphasing RF power-amplifier systems," *IEEE Transactions on Communications*, vol. 33, no. 10, pp. 1094–1099, 1985.

[119] S. Halder, J. McMacken, N. Craig, and J. Gering, "A hybrid modeling approach for drain-source capacitance of source field plated GaN FET devices for multi-bias application," in *2017 IEEE MTT-S International Microwave Symposium (IMS)*, 2017, pp. 1787–1790.

[120] C. Yin, Y. Li, and Y. Pei, "AlGaN/GaN HEMTs large signal model considering nonlinear Cds," in *2017 International Applied Computational Electromagnetics Society Symposium (ACES)*, 2017, pp. 1–2.

[121] A. Banerjee, R. Hezar, L. Ding, and B. Haroun, "A 29.5 dBm Class-E Outphasing RF Power Amplifier With Efficiency and Output Power Enhancement Circuits in 45nm CMOS," *IEEE Transactions on Circuits and Systems I: Regular Papers*, vol. 64, no. 8, pp. 1977–1988, Aug 2017.

[122] R. Ogasawara, Y. Takayama, R. Ishikawa, and K. Honjo, "A 3.9-GHz-Band Outphasing Power Amplifier with Compact Combiner Based on Dual-Power-Level Design for Wide-Dynamic-Range Operation," in *2020 IEEE/MTT-S International Microwave Symposium (IMS)*, 2020, pp. 111–114.

[123] A. Banerjee, L. Ding, and R. Hezar, "A High Efficiency Multi-Mode Outphasing RF Power Amplifier With 31.6 dBm Peak Output Power in 45nm CMOS," *IEEE Transactions on Circuits and Systems I: Regular Papers*, vol. 67, no. 3, pp. 815–828, 2020.

[124] W. Wang, S. Chen, J. Cai, X. Y. Zhou, W. S. Chan, G. Wang, and Q. Xue, "A Dual-Band Outphasing Power Amplifier Based on Noncommensurate Transmission Line Concept," *IEEE Transactions on Microwave Theory and Techniques*, vol. 68, no. 7, pp. 3079–3089, 2020.

[125] A. Birafane and A. B. Kouki, "On the linearity and efficiency of outphasing microwave amplifiers," *IEEE Transactions on Microwave Theory and Techniques*, vol. 52, no. 7, pp. 1702–1708, 2004.

[126] T. Sowlati, Y. M. Greshishchev, and C. A. T. Salama, "Phase-correcting feedback system for class E power amplifier," *IEEE Journal of Solid-State Circuits*, vol. 32, no. 4, pp. 544–549, 1997.

[127] A. Birafane and A. B. Kouki, "Phase-only predistortion for LINC amplifiers with Chireix-outphasing combiners," *IEEE Transactions on Microwave Theory and Techniques*, vol. 53, no. 6, pp. 2240–2250, 2005.

[128] Y. Jung, J. Fritzin, M. Enqvist, and A. Alvandpour, "Least-Squares Phase Predistortion of a +30 dBm Class-D Outphasing RF PA in 65 nm CMOS," *IEEE Transactions on Circuits and Systems I: Regular Papers*, vol. 60, no. 7, pp. 1915–1928, 2013.

[129] King-Chun Tsai and P. R. Gray, "A 1.9-GHz, 1-W CMOS class-E power amplifier for wireless communications," *IEEE Journal of Solid-State Circuits*, vol. 34, no. 7, pp. 962–970, 1999.

[130] Ka-Wai Ho and H. C. Luong, "A 1-V CMOS power amplifier for Bluetooth applications," *IEEE Transactions on Circuits and Systems II: Analog and Digital Signal Processing*, vol. 50, no. 8, pp. 445–449, 2003.

[131] R. Marante, L. Cabria, P. Cabral, J. C. Pedro, and J. A. García, "Temperature dependent memory effects on a drain modulated GaN HEMT power amplifier," in *2010 Workshop on Integrated Nonlinear Microwave and Millimeter-Wave Circuits*, 2010, pp. 75–78.

[132] F. M. Barradas, L. C. Nunes, T. R. Cunha, P. M. Lavrador, P. M. Cabral, and J. C. Pedro, "Compensation of Long-Term Memory Effects on GaN HEMT-Based Power Amplifiers," *IEEE Transactions on Microwave Theory and Techniques*, vol. 65, no. 9, pp. 3379–3388, 2017.

[133] Lei Ding, G. T. Zhou, D. R. Morgan, Zhengxiang Ma, J. S. Kenney, Jaehyeong Kim, and C. R. Giardina, "A robust digital baseband predistorter constructed using memory polynomials," *IEEE Transactions on Communications*, vol. 52, no. 1, pp. 159–165, 2004.